Acta Biomaterialia 203 (2025) 181–213

Contents lists available at ScienceDirect

Acta Biomaterialia

journal homepage: www.elsevier.com/locate/actbio

Review article

Mechanical characterization of brain tissue: experimental techniques, human testing considerations, and perspectives

Jixin Hou [a], Kun Jiang [a], Arunachalam Ramanathan [a], Abhishek Saji Kumar [b], Wei Zhang [c], Lin Zhao [d], Taotao Wu [e], Ramana Pidaparti [a], Dajiang Zhu [f], Gang Li [g], Kenan Song [a], Tianming Liu [d], Mir Jalil Razavi [h], Ellen Kuhl [i], Xianqiao Wang [a,*]

[a] School of Environmental, Civil, Agricultural and Mechanical Engineering, College of Engineering, University of Georgia, Athens, GA 30602, USA
[b] Department of Material Science, School for Engineering of Matter, Transport and Energy, Ira A. Fulton Schools of Engineering, Arizona State University, Tempe, AZ 85287, USA
[c] School of Computer and Cyber Sciences, Augusta University, GA 30912, USA
[d] School of Computing, The University of Georgia, Athens, GA 30602, USA
[e] School of Chemical, Materials, and Biomedical Engineering, College of Engineering, University of Georgia, Athens, GA 30602, USA
[f] Department of Computer Science and Engineering, The University of Texas at Arlington, Arlington, TX 76019, USA
[g] Department of Radiology and Biomedical Research Imaging Center, The University of North Carolina at Chapel Hill, NC 27599, USA
[h] Department of Mechanical Engineering, SUNY Binghamton University, Binghamton, NY 13902, USA
[i] Department of Mechanical Engineering, Stanford University, Stanford, CA 94305, USA

ARTICLE INFO

Keywords:
Brain tissue mechanical characterization
Invasive testing
Noninvasive elastography
Human brain tissue mechanical properties

ABSTRACT

Understanding the mechanical behavior of brain tissue is crucial for advancing both fundamental neuroscience and clinical applications. Yet, accurately measuring these properties remains challenging due to the brain's unique mechanical attributes and complex anatomical structures. This review provides a comprehensive overview of commonly used techniques for characterizing brain tissue mechanical properties, covering both invasive methods—such as atomic force microscopy, indentation, axial mechanical testing, and oscillatory shear testing—and noninvasive approaches like magnetic resonance elastography and ultrasound elastography. Each technique is evaluated in terms of working principles, applicability, representative studies, and experimental limitations. We further summarize existing publications that have used these techniques to measure human brain tissue mechanical properties. With a primary focus on invasive studies, we systematically compare their sample preparation, testing conditions, reported mechanical parameters, and modeling strategies. Key sensitivity factors influencing testing outcomes (e.g., sample size, anatomical location, strain rate, temperature, conditioning, and post-mortem interval) are also discussed. Additionally, selected noninvasive studies are reviewed to assess their potential for *in vivo* characterization. A comparative discussion between invasive and noninvasive methods, as well as *in vivo versus ex vivo* testing, is included. This review aims to offer practical guidance for researchers and clinicians in selecting appropriate mechanical testing approaches and contributes a curated dataset to support constitutive modeling of human brain tissue.

Statement of significance: Accurate characterization of brain tissue mechanics is essential for both neurological research and the development of predictive biomechanical models. This review synthesizes current experimental approaches used in **brain mechanical testing**—spanning both invasive and noninvasive methods—with a focus on their principles, applications, and limitations. We further systematically compile and analyze a comprehensive set of invasive studies—supplemented by representative noninvasive reports—on **human brain tissue mechanical properties**. The collected dataset offers valuable support for constitutive modeling. Additionally, we discuss key factors affecting testing outcomes, offering practical insights to guide the design and interpretation of future brain mechanical research.

* Corresponding author.
E-mail address: xqwang@uga.edu (X. Wang).

https://doi.org/10.1016/j.actbio.2025.07.046
Received 21 April 2025; Received in revised form 10 July 2025; Accepted 21 July 2025
Available online 22 July 2025

1. Introduction

As the central regulator of the human body, the brain orchestrates a wide range of vital physiological and cognitive functions. Accordingly, brain research spans multiple disciplines, including molecular biology, cellular neuroscience, bioelectrical signaling, and functional imaging. Among these, biomechanics plays a critical yet often underappreciated role. Understanding the brain's mechanical behavior is essential for uncovering fundamental physiological and pathological processes, such as cortical folding during brain development [1–6], traumatic brain injury (TBI) [7,8], and neurological disease progression [9,10]. For example, studies have shown that cortical folding arises from mechanical buckling, driven by compressive forces generated through differential growth between gray and white matter [11–13]. In the case of TBI, external impacts induce rapid and excessive shear deformation, leading to immediate tissue damage and long-term degeneration [14–16]. Similarly, neurodegenerative diseases such as Alzheimer's disease (AD) involve progressive tissue degradation, often initiated by aging-related mechanical changes or the spread of toxic proteins [10,17]. Beyond its role in mechanical understanding, biomechanics also holds increasing promise in brain disorders diagnosis. Variations in tissue stiffness have been correlated with pathological conditions such as brain tumors [10,17], epilepsy [18,19], and dementia [20], which offers opportunities for noninvasive disease detection and monitoring. Accurate characterization of brain mechanical properties is therefore indispensable for effectively analyzing the underlying mechanics of these complex phenomena and supporting clinical applications.

Mechanical testing of brain tissue, however, presents significant challenges due to the tissue's complex mechanical characteristics. Brain tissue is ultrasoft, fragile, biphasic, and exhibits pronounced anatomical and microstructural heterogeneity [21]. These attributes complicate both sample preparation and experimental execution. For instance, its fragility constrains the range of applicable deformation to preserve tissue integrity during tests [22,23]. Anatomical variability restricts consistent sampling, while the ultrasoft nature and potential dehydration of fluidic components can cause dimensional change under the tissue's weight [24–26]. Over the past decades, a variety of testing techniques have been developed to assess brain mechanics at different spatial and temporal scales. These techniques ensure diverse characterizations in brain tissue tailored to specific research objectives. Atomic force microscopy (AFM), for example, enables the measurement of cellular and subcellular mechanical properties, thereby facilitating the investigation of the microstructural relevance to macroscale brain properties [27]. Indentation (IND) offers a versatile platform for probing brain mechanical properties, enabling the assessment of spatially resolved modulus and time-dependent viscoelastic behaviors [28]. Oscillatory shear testing (OST) allows for the evaluation of frequency-dependent viscoelastic properties, aiding the study of the underlying biomechanism in TBI [29]. Meanwhile, continuous stress-strain data collected through axial mechanical testing (AMT) support the development of hyperelastic constitutive models [30], which are essential for simulating convoluted physiological phenomena such as cortical folding during brain development [12,31,32]. Despite these achievements, reported mechanical parameters vary widely across studies—often differing by several orders of magnitude—posing significant barriers to both inter- and intra-study comparisons of brain tissue mechanics.

Due to ethical limitations and logistical constraints on human brain experimentation, animal models have been extensively employed to study brain mechanics [33]. Brains from species such as rodents [34,35], pigs [36,37], and bovines [38,39] are often employed as surrogates for the human brain. However, growing evidence indicates notable interspecies differences, not only in anatomical structure but also in mechanical behavior [40]. Variations in the mechanical properties of gray and white matter, strain-rate sensitivity, and regional stiffness patterns can differ remarkably across species [41,42]. These unignorable discrepancies raise important concerns about the validity of directly translating findings from animal models to humans. The emergence of noninvasive techniques such as magnetic resonance elastography (MRE) and ultrasound elastography (USE) has enabled direct measurement of human brain mechanical properties *in vivo* [43]. These approaches support population-level studies and facilitate statistically robust investigations into how mechanical properties vary with age, gender, and disease [43]. Their noninvasive nature also allows for repeated and continuous measurements of the same individuals over time [44]. Despite these advantages, current noninvasive methods are limited to capturing relatively simple mechanical quantities—such as shear stiffness, storage, and loss moduli—within small deformation ranges to ensure participant safety and comfort. In addition, the shear-related properties derived from these techniques often show noticeable discrepancies compared to those obtained through invasive approaches. This inconsistency naturally raises concerns regarding the comparability and reliability of the reported mechanical data. More broadly, it points to a longstanding issue in brain testing: the divergence of testing outcomes obtained under different experimental conditions, including *in vivo, ex vivo, in vitro*, and *in situ* settings [45].

In this review, we aim to provide a comprehensive summary of the current state of brain tissue mechanical testing. We begin by introducing six widely used experimental techniques, including AFM, IND, AMT, OST, MRE, and USE. Each method is summarized in terms of its working principles, measurable mechanical parameters, advantages, and limitations, as well as representative studies. Next, we collect and analyze existing data on human brain mechanics from peer-reviewed studies, categorizing them based on whether the methods are invasive or noninvasive, and discussing key sensitivity factors that influence the testing outcomes. Finally, we provide a comparative discussion between invasive and noninvasive techniques, as well as *in vivo versus ex vivo* testing. The review is structured as follows: Section 2 introduces the experimental techniques; Section 3 summarizes human brain tissue mechanical data from the literature; and Section 4 concludes with key insights and perspectives for future research on brain tissue mechanical testing and characterization.

2. Established techniques for quantifying brain tissue mechanical properties

In this section, we introduce various testing techniques commonly used for characterizing the mechanical properties of soft tissue, with a focus on brain tissue. These include invasive methods such as AFM, IND, AMT, OST, and noninvasive approaches like MRE and USE. In addition to these six primary techniques, other methods—such as pipette aspiration [46,47], needle-induced cavitation [48–50], and optical-based diffusion correlation spectroscopy [51]—have also been employed to characterize the mechanical properties of brain tissue. Although these approaches show promise in capturing various aspects of brain mechanics, they have yet to gain widespread attention in the field. Each of the six techniques considered operates based on distinct principles and is suited for measuring various mechanical properties across different length scales (from the cellular to organ level) and time scales (from quasistatic to high-rate dynamics), as shown in Fig. 1. However, their testing outputs may be biased due to varied sensitivity factors, thereby requiring careful consideration during testing. As a result, each technique has specific advantages and limitations in measuring the mechanical properties of brain tissue. To provide context, we briefly review these aspects based on existing literature. Since this review focuses on brain tissue mechanics, readers interested in a broader review of these techniques for other tissues may refer to Bejgam, et al. [52], Song, et al. [53], and Navindaran, et al. [54].

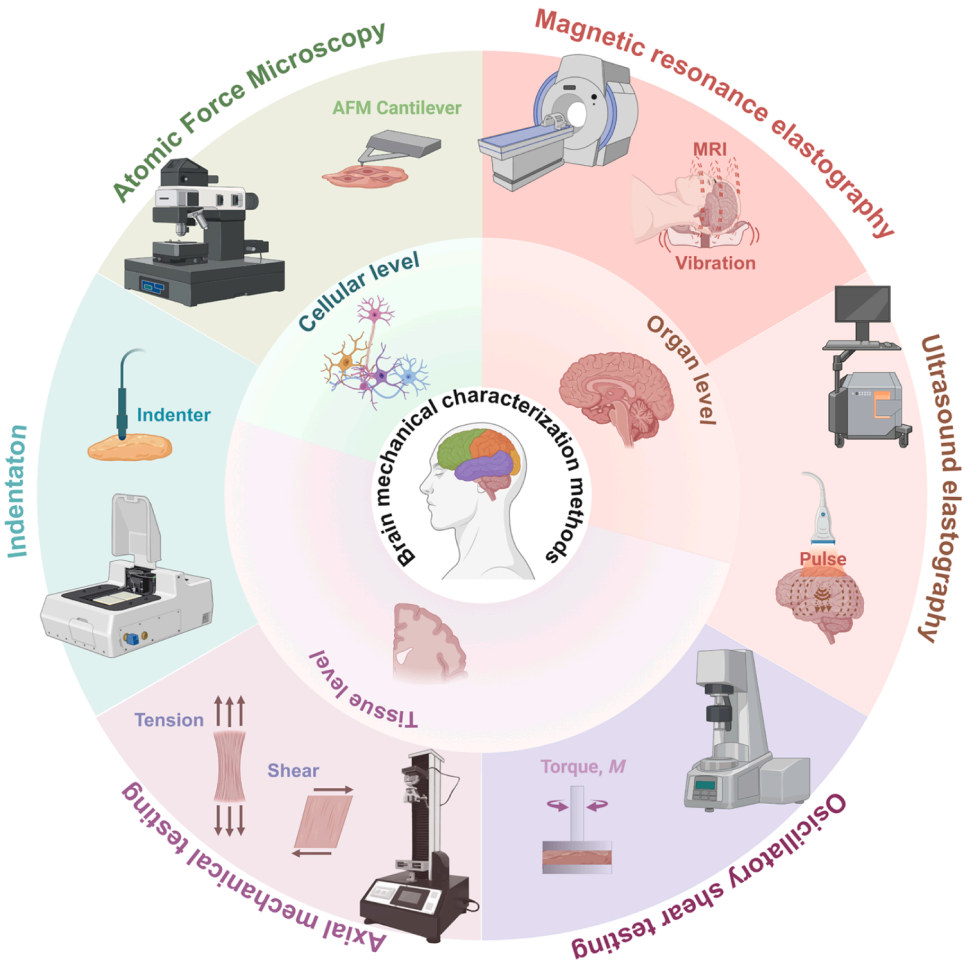

Fig. 1. Common mechanical characterization techniques for brain tissue. Each method applies to distinct spatial scales. Figure created with BioRender.com.

2.1. Atomic force microscopy: brain characterization at cellular and subcellular scale

AFM is a powerful technique for measuring the mechanical properties of brain tissue at the micro- and nanoscale. It operates by detecting the contact interaction between an indenter tip and the tissue surface. As illustrated in Fig. 2, an AFM system consists of four main components: a cantilever with an integrated indenter tip to establish contact; a laser beam directed onto the cantilever tip; a position-sensitive photodiode that detects the reflected laser beam to measure cantilever deflection; and a piezo scanner that controls sample movement [27]. Through precise feedback control, AFM functions not only as an imaging tool to generate high-resolution topology images [55,56], but also as a highly sensitive mechanical measurement system, capable of recording force-displacement curves with piconewton-scale sensitivity [57]. These capabilities have made AFM a widely used technique for characterizing brain tissue mechanics across tissue, cell, and even molecular scales [58, 59]. For example, Morr, et al. [60] used AFM to assess the microscopic mechanical properties of murine hippocampal subregions, and their results revealed that areas with high neurogenic activity exhibited nearly 40 % lower stiffness than less active regions. Similarly, AFM measurements by Urbanski, et al. [61] on demyelinated mice and human brain tissue demonstrated that acute demyelination reduces stiffness, whereas chronic demyelination leads to increased stiffness.

Beyond mechanical characterization, AFM has been instrumental in elucidating pathogenic mechanisms of brain disorders from biomechanical perspectives [57,62,63]. De, et al. [64] conducted a comparative analysis using AFM to analyze amyloid-β protein aggregates in human cerebrospinal fluid, their observations support a correlation between the aggregate morphology and progression of AD. Lobanova, et al. [56] harnessed AFM's high-resolution capability to examine the size distribution of α-synuclein aggregates in cerebrospinal fluid and serum from Parkinson's disease (PD) patients, identifying a greater proportion of larger protein aggregates (exceeding 150 nm) in affected individuals. Additionally, Bahwini, et al. [55] employed AFM to compare the mechanical properties of cancerous and normal brain cells, observing significantly lower Young's modulus in cancer cells.

AFM can detect small variations in mechanical properties, making it a versatile tool for assessing tissue mechanical heterogeneity [65]. For instance, Elkin, et al. [66] used AFM to individually measure the elastic modulus of five subregions within the rat hippocampus and found significant regional variations in terms of the modulus value, highlighting the inherent mechanical heterogeneity of hippocampus tissue. Beyond elastic properties, AFM's versatility also allows it to characterize viscoelastic behavior. In addition to quasistatic indentation, AFM is well-suited for dynamic testing, including stress relaxation, strain creep, and oscillatory loading tests [67]. Due to its requirement for direct contact, AFM is primarily operated in *ex vivo* settings, such as on brain slices or isolated cells. A notable advancement came from Thompson, et al. [68], who developed time-lapse *in vivo* AFM (tiv-AFM) to measure changes in brain stiffness over time within a live embryo. Using this approach, they observed the stiffness-gradient-driven neuronal migration during early embryonic development in frogs. While AFM is effective for measuring brain mechanical properties, the testing outcome is influenced by the choice of tip geometry. Commonly used shapes include pyramidal, conical, and spherical indenters, each requiring different

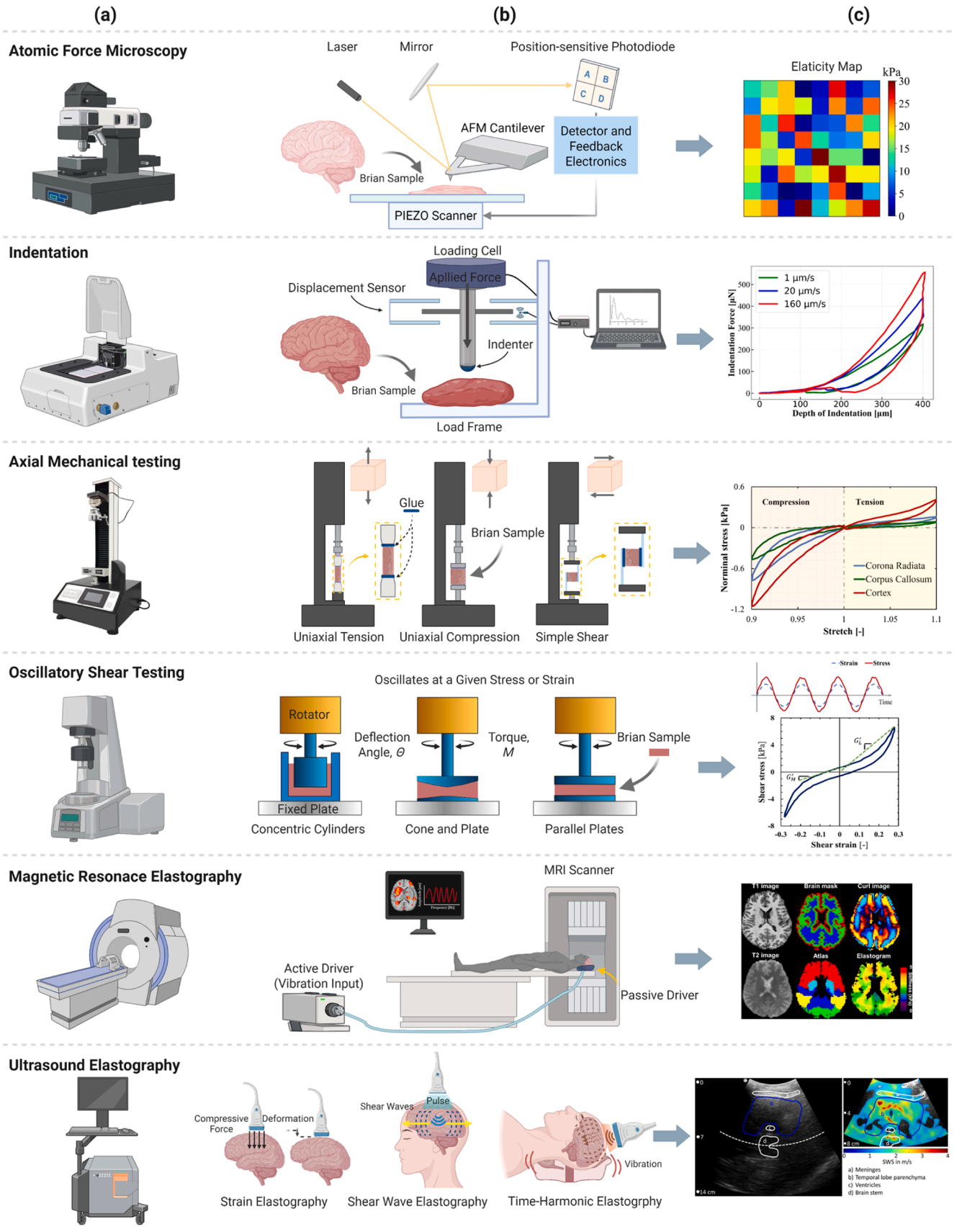

Fig. 2. Schematic representation showing the fundamental working principles of various testing techniques. (a) Conceptual diagrams of testing apparatus; (b) Overview of the working mechanisms and special treatments applied during testing; (c) Key outcomes from each testing technique [98] Reproduced with permission [99] Reproduced with permission. Figure created with BioRender.com.

mechanical models for data interpretation. The Hertz model is typically applied for spherical indenters, the Sneddon model for conical indenters, and an extended Sneddon model for pyramidal indenters [27]. However, these models assume small deformation, and their accuracy may degrade when indentation exceeds these prerequisite limits. To address this limitation, alternative approaches such as the hyperelastic material model like the Ogden model [69] or the parameter reverse engineer approach [70] could be endeavored to improve parameter characterization accuracy. Additionally, as the tissue samples are excited from their native biological environment—despite being preserved in supporting medium such as artificial cerebrospinal fluid—the measured properties may deviate from their *in vivo* state [27]. This limitation is also encountered in other invasive testing techniques to be introduced later.

2.2. Indentation: scalable and versatile measurement of brain tissue mechanics

IND is a frequently used technique for characterizing the mechanical properties of brain tissue. Similar to AFM, IND also works by measuring the contact behaviors between an indenter tip and the tissue surface. From a broader perspective, AFM can be treated as a scaled-down version of the indentation method [54]. As exemplified in Fig. 2, a custom IND system is constructed by two main components: a loading cell equipped with a probe that applies the indentation force, and a displacement sensor that records the resulting deformation. With minimal sample preparation requirements, IND offers flexibility in measuring tissue mechanical properties at scales ranging from the microscale to the macroscale simply by adjusting the indenter size [71]. IND is frequently employed to assess the brain's regional stiffness within the elastic regime [28,72,73]. For instance, Weickenmeier, et al. [38] conducted 116 IND tests on bovine brain using a 1.5 mm diameter flat punch indenter, revealing that white matter is nearly twice as stiff as gray matter, with stiffness values of 1.330 ± 0.630 kPa and 0.680 ± 0.200 kPa, respectively. Expanding on this, Weickenmeier, et al. [74] used the same approach to measure stiffness in demyelination brain tissues. Combined with histological characterization, their findings indicated a positive correlation between white matter stiffness and myelin content, suggesting that brain tissue stiffness could serve as an effective biomarker for multiple sclerosis and other demyelinating brain disorders. More recently, Bailly, et al. [75] applied a smaller flat punch indenter (0.5 mm diameter) to characterize the elastic modulus of various spinal cord subregions. Their study identified significant heterogeneity in the elastic modulus of gray matter regions, while white matter regions exhibited more uniform stiffness.

In addition to healthy brain tissue, IND has been widely used to assess mechanical abnormalities in diseased brain tissue, including conditions such as brain tumors [76,77], epilepsy [19], and AD [78]. Notably, Qian, et al. [79] took a step further in exploring the effects of electric fields—commonly introduced during brain disorder treatments—on brain mechanical properties. Using a flat punch indenter (8 mm diameter), they conducted IDN tests on porcine brain tissue exposed to current electric field ranging from 0 to 50 V. Their results indicated that brain tissue softens and responds more rapidly at higher electric field intensities, contributing to potential refinements in therapeutic protocols. Beyond the elasticity measurements, IND has been employed to characterize the viscoelastic properties of brain tissue through stress relaxation and oscillatory loading tests [80–83]. Qiu, et al. [84] investigated changes in mouse brain viscoelasticity following controlled cortical impact, systematically varying both the velocity and direction of the impact. Their findings revealed that the instantaneous shear modulus within the impacted region varied significantly with impact angle, whereas the long-term shear modulus remained largely unaffected by different impact configurations. Due to its simple tissue preparation and operational flexibility, IND can be performed not only *in vitro* but also *in situ* and even *in vivo* [85]. Prevost, et al. [86] conducted IND tests using a 12.65 mm diameter hemispherical indenter on the frontal and parietal lobes of living and deceased porcine brains after craniotomy, as well as on excited specimens, to measure various brain mechanical properties *in vivo, in situ*, and *in vitro*, respectively. Through testing, they found a significantly stiffer indentation response *in situ* than *in vivo*, implying a post-mortem stiffening effect [87]. In contrast, indentation responses *in vitro* exhibit greater compliance compared to *in situ* measurements.

Analogous to AFM, IND results are reliant on the choice of indenter tip geometry. Various shapes, including cylindrical [23], conical [85], spherical [83], rectangular [88], and square [73] indenter, have been used in existing studies. Notably, Budday, et al. [23] suggested a circular flat punch to minimize adhesion effects by maintaining a constant contact area between the indenter and tested samples, while Feng, et al. [89] recommending a rectangular indenter due to its asymmetric nature, which is beneficial for characterizing anisotropic mechanical properties. Additionally, indenter tip size also affects the testing outcomes. Budday, et al. [23] compared punch indenter with varying diameters ranging from 0.75 mm to 1.5 mm when measuring the bovine brain properties, finding that the elastic modulus decreased as the punch diameter increased. A similar trend was observed by Li, et al. [90], who reported that larger indenters significantly reduced the storage and loss stiffness of porcine brain tissue. Moreover, excessive indentation depth can introduce biases due to boundary effects from the substrates [91]. To minimize these effects and ensure accurate measurements, it is suggested that tissue thickness be at least 3–5 times greater than the indenter diameter [92] and that indentation depth not exceed 10 % of the tissue's thickness [93]. Also, the accuracy and reliability of IND-based brain mechanical characterization are influenced by factors such as assumptions of incompressibility, isotropy, and frictionless contact, as well as the choice of mechanical models [71]. To improve these assessments, reverse engineering approaches using finite element method (FEM) can be employed to systematically evaluate and mitigate potential errors, ensuring a more precise representation of brain tissue mechanics [88,94,95].

2.3. Axial mechanical testing: mode-specific evaluation of brain tissue mechanics

During IND testing, the applied indentation force leads to nonuniform deformation within the brain tissue. The area directly beneath the indenter undergoes compression, while the surrounding tissue experiences tensile and shear forces to preserve structural integrity [73]. This interaction produces a complex stress state that blends brain tissue's response across different loading modes such as tension-compression asymmetry [30,37]. An alternative approach, AMT—a well-established method in mechanical research—has been widely employed to obtain the mechanical properties of brain tissue under individual loading modes, including uniaxial tension, uniaxial compression, simple shear, and pure shear [45,96]. AMT is performed by controlling the specimen holder to apply specific forms of displacement, thus the tissue requires to be securely attached to the holder during testing. Due to the fragile nature of brain tissue, glue adhesives are commonly adopted instead of traditional clamps [21]. In some cases, sandpaper is added to increase the adhesive surface area and ensure a more stable fixation [30]. Unlike IND testing, AMT engages the entire tissue in the loading process, resulting in nearly uniform force distribution across each cross-section. This uniformity allows for direct recording of stress-strain relationships, which significantly facilitates post-processing and ensures accurate characterizations of various mechanical properties, such as elastic modulus, yield strength, and failure strength [54]. Moreover, the consistent deformation patterns enable the investigation of brain mechanical anisotropy, which potentially arises from axonal fiber alignment or other structural factors [30,41,97]. This capability enriches the exploration of bridging the brain structural organization to its functions from a biomechanical perspective. However,

to achieve these advantages, the tissue needs to be prepared in regular shapes, such as hexahedral or cylindrical forms with consistent cross sections, which inevitably complicates the preparation process. Additionally, this requirement makes it challenging to characterize regional material properties, particularly in small structures such as the hippocampus.

Extensive research has used AMT to characterize the mechanical properties of brain tissue under various loading conditions. For example, Miller, et al. [22] first conducted tension testing on swine brain tissue under finite deformation (< 20 % strain) at two strain rates (0.64 and 0.0064 s^{-1}). Their findings demonstrated that brain tissue exhibits strain-rate dependence, stiffening with increased loading rates. Comparing these results with their previous compression test, they observed significantly softer behavior in tension and proposed an Ogden hyperelastic model to describe this asymmetry. A similar conclusion was derived by Rashid and his colleagues, who performed a series of tensile tests on porcine brain tissue up to 30 % strain at higher strain rates ranging from 30 s^{-1} to 90 s^{-1} [100–102]. Notably, while Franceschini, et al. [24] recorded tensile failure in human brain tissue at about 90 % strain, interior damage may initiate at much smaller strain (around 18 %) [21]. This suggests that careful consideration of strain limits is essential when conducting tensile tests on brain tissue. Additionally, to minimize boundary effects caused by adhesion during testing, sampling preparation should ensure a suitable aspect ratio. For cylindrical samples, the diameter-to-thickness ratio should ideally not exceed 1 [100], while for hexahedral samples, an equivalent dimensional balance should be considered. Ensuring an appropriate sample size helps prevent artifactual anisotropy caused by dimensional effect in mechanical characterization [30].

Although compression follows the opposite loading trend of tension, it is more versatile for measuring brain mechanical properties [45]. Given the biphasic nature of brain tissue (fluid *vs* solid about 4:1), compression test typically involves two modes: confined and unconfined compression. In confined compression, the fluid remains largely trapped within the solid matrix and contributes to tissue stiffness. In contrast, unconfined compression allows fluid to escape during the test, leaving the solid matrix to sustain the primary load [21]. Cheng, et al. [103] conducted unconfined compression tests on calf brain, revealing that the rheological response of white matter is primarily governed by the viscoelastic properties of the solid phase. A similar effect was observed by Su, et al. [104], who performed unconfined compression on the porcine brain and noted that this influence becomes more pronounced at low strain rates. In contrast, Haslach, et al. [105] performed confined compression test on rat brain tissue to isolate the contributions of the solid and fluid phases to brain mechanics. By forcing extracellular fluid to flow in the direction of deformation, they observed peak stress at about 11 % strain, indicating that extracellular fluid plays a key role in load resistance until tissue damage permits pathological fluid flow. Their findings were further supported by magnetic resonance imaging, which revealed significant changes in tissue microstructure during confined compression. In confined compression, the tissue is radially constrained within a rigid, impermeable chamber to prevent outward movement. This requires bonding the tissue to the specimen holder, typically using surgical glue [105]. In unconfined compression, however, the tissue expands freely in the lateral direction without restraint. To facilitate this movement, lubricants like silicone grease are usually applied between the tissue and the holder to allow finite slippage [106]. For accurate modeling, Rashid, et al. [107] recommended dynamic friction coefficient values of 0.09 and 0.18 for strain rates of 1 s^{-1} and 30 s^{-1}, respectively.

The simple shear test stands out for brain mechanical measurements due to its ability to better replicate physiological deformation compared to tension and compression. Shear tests distribute stress more evenly, thus reducing unwanted premature failure during testing. Rashid, et al. [108] conducted a simple shear test on porcine brain tissue at various loading rates and observed homogeneous deformation, which is further validated by the independence check of shear stress magnitude from specimen thickness. Similarly, Destrade, et al. [109] performed quasi-static simple shear tests on porcine brain tissues and compared their deformation behaviors to silicone gels. Their results indicated that brain tissue behaves as an extremely soft solid under shear force (at least 30 times softer than a silicone gel). Moreover, they identified a significant positive Poynting effect, meaning the brain tissue tends to "spread apart" perpendicular to the shear plane, generating compressive normal stress. This phenomenon was also observed in the torsional measurement of brain tissue [110]. To accurately capture this effect, Destrade, et al. [109] successfully modeled it using a two-term Mooney-Rivlin hyperelastic model. Additionally, Kuhl, et al. [111] suggested incorporating a second invariant of the deformation gradient into the strain energy function to improve the representation of this behavior.

Beyond pure uniaxial mechanical testing, many studies have employed multiple loading modes to better capture brain tissue mechanics. These include combinations of tension and compression [24,94,112], compression and shear [37,42,113,114], or all three loading modes [26,30,97,115]. These "multi-modal" tests provide a more comprehensive characterization of brain mechanical properties and greatly enhance the generalizability of calibrated models [21,116,117]. Additionally, multiaxial testing has been used to assess brain tissue anisotropy, though less frequently than in artery or skin studies. One of the few investigations was carried out by Labus and his colleagues, who performed biaxial tensile tests on Ovine brain tissue [118,119]. In their studies, corona radiata and corpus callosum were extracted from white matter and subjected to biaxial tension to examine the role of axonal structure in brain mechanics. Using histology and transmission electron microscopy, they found a positive correlation between mechanical anisotropy and axon volume fraction. Furthermore, their findings suggest that combining both biaxial and uniaxial tests can significantly improve the accuracy of model predictions.

2.4. *Oscillatory shear testing: frequency-dependent insights into brain tissue mechanics*

Brain tissue primarily undergoes shear deformations under physiological and pathological conditions, such as during impact trauma. This makes shear testing a more relevant method for assessing brain mechanics compared to tension and compression. In addition to the quasistatic shear test, OST has been widely used to characterize the viscoelastic behaviors of brain tissue. As illustrated in Fig. 2, OST operates by using a rotating component to apply oscillatory motion, which is transmitted to the adhesive tissue sample [120]. Unlike shear tests in AMT, where tissue is subjected to continuous monotonic shear at constant strain rates, OST oscillates tissue back and forth by applying cyclic shear, typically in the form of sinusoidal strain or stress [120,121]. Depending on how the sinusoidal input is configured, OST can be categorized into amplitude sweep tests (AST) and frequency sweep tests (FST). In AST, the maximal shear is systematically varied over a predefined range at a fixed frequency. In contrast, FST keeps the shear amplitude constant while varying the frequency of oscillation [122]. These tests enable direct quantification of the brain tissue's viscoelastic properties, including the storage modulus (elastic response) and loss modulus (viscous response). The ratio between them, known as the loss tangent, reflects the balance between elastic and viscous behavior, indicating whether the tissue behaves more like a solid or a fluid [42].

Shuck, et al. [123] were among the first to systematically conduct FST on human brain tissue, applying shear strain at 3.5 % across a frequency range of up to 350 Hz. Using a four-parameter linear viscoelastic model to calibrate their results, they derived a set of frequency-dependent storage and loss moduli and observed a frequency-stiffening trend for both. More recently, Xue, et al. [122] employed AST to investigate the age-dependent viscoelastic properties in rat brain tissues across developmental stages, from postnatal day 4 to 4 months of age. They first conducted AST at 0.16 Hz with strain

amplitude sweeping from 0.01 % to 100 % to determine the linear viscoelastic range. A 1 % shear strain threshold was identified as the upper limit of this range and subsequently used for FST over a frequency span from 0.016 Hz to 19.1 Hz. Results showed that both storage and loss moduli increased with age. However, the ratio of the two moduli remained constant at low frequencies (<1.6 Hz) and began to decline in the mid-frequency range (1.6–16 Hz). In a related study, Qing, et al. [124] applied a similar approach to assess frequency-dependent shear moduli in both healthy and autism spectrum disorders (ASD) rat brain tissues. AST was first performed at 0.16 Hz and 1.6 Hz to determine a linear viscoelastic limit between 1 and 3 % shear strain. FST was then carried out at 1 % strain across frequencies from 0.016 Hz to 6.4 Hz. Their findings revealed no significant differences in the loss and storage moduli of ASD brain tissue, in spite of significant changes observed in cellular organization.

Most OSTs on brain tissue have been conducted at small strain amplitudes to minimize damage to this fragile material. These conditions correspond to the linear viscoelastic range, where linear models such as the Kelvin-Voigt model can be effectively applied to characterize material properties [58,93,113,121,125]. However, brain tissue exhibits inherent nonlinear behavior, suggesting that its viscoelastic response under large deformation may differ significantly from that observed under small deformation [41,126]. In scenarios such as automotive crashes, the brain can experience large shear deformations (often exceeding 10–20 % strain) within milliseconds. Under such conditions, viscoelastic properties characterized using linear models may fail in accurately capturing brain behaviors [127]. To address this discrepancy, Darvish, et al. [128] conducted FST on bovine brain tissue across a frequency range of 0.5 to 200 Hz at a shear strain of up to 20 %. A quasilinear viscoelastic model was employed to account for nonlinear behaviors at large strains. Their results exhibited a pronounced strain-hardening effect beyond 10 % strain and identified a non-recoverable strain conditioning behavior in measured moduli, which may explain discrepancies reported across different studies. Analogously, Boudjema, et al. [29] performed larger-deformation shear tests on lamb and bovine brain tissue, measuring storage and loss moduli over a frequency range of 1 to 100 Hz and at shear strains up to 50 %. Their findings also revealed clear strain-dependence behavior and a notable stiffening effect in both moduli. This observation, however, contrasts with traditional views that brain tissue softens at large deformations due to tissue damage or degradation [113,129]. These contradictory findings may stem from differences in the viscoelastic models used to interpret the data, as Boudjema, et al. [29] did not explicitly report the constitutive models applied in their analysis. In addition to shear testing, oscillatory methods have also been applied in other loading modes, such as compression [39,130], which further demonstrates the versatility of oscillatory testing in characterizing brain tissue mechanics.

2.5. *Magnetic resonance elastography: in vivo measurement of brain tissue mechanical properties*

MRE is a phase-contrast MRI technique that allows for the noninvasive assessment of brain tissue mechanics *in vivo* [20,44,131]. The process typically involves three components: a mechanical actuator that generates a shear wave within the brain, an MRI scanner that captures tissue deformations, and a post-processing system that estimates mechanical properties based on imaging data [132]. As illustrated in Fig. 2, shear waves are commonly produced using a passive mechanical actuator, such as a soft pillow. During testing, the pillow is placed beneath the head and continuously vibrates at predefined frequencies controlled by an external active pneumatic driver [133,134]. Alternative actuator designs include a head cradle for human applications [135], a bit-bar system for animal experiments [136], customized piezoelectric soft actuators [137] and electromagnetic actuators [138,139]. In contrast to these external actuators, a pilot study by Weaver, et al. [140] proposed an intrinsic activation approach that uses natural cardiac pulsations. By capturing blood flow oscillations via MR angiography and converting them into harmonic deformations through Fourier transformation, this method skillfully circumvented the issue of wave attenuation or delay caused by the cranium and meninges [141]. As a result, it offers more consistent and reproducible measurements of brain mechanical properties [142,143]. Building on this concept, Qiu, et al. [139] recently developed an alternative indirect actuation strategy that generates shear waves with minimal alteration of cerebral blood flow. Notably, their results demonstrated that the mechanical property measurements obtained using this indirect actuator were comparable to those acquired with conventional external actuators, supporting its validity for brain stiffness quantification. For external actuation, the actuation frequency is often controlled within a range of 10–100 Hz [144], typically around 50–60 Hz considering the balance between penetration and attenuation attributes of indued shear waves [145]. Intrinsic actuation, on the other hand, enables much lower frequencies (around 1 Hz), which significantly benefits for probing deep brain regions. Because lower frequencies correspond to longer wavelengths that experience less attenuation, thereby improving signal penetration and reducing imaging noise [146]. However, it should be noted that at very low frequencies (*e.g.*, below ~5 Hz), the resulting wavelengths may exceed the imaging field of view, which can complicate wavelength estimation and increase the susceptibility to noise in reconstructed stiffness maps. To address this challenge, recent advances such as the nonlinear inversion MRE framework proposed by Zeng, et al. [147] have demonstrated robust recovery of both spatial distributions and magnitude of mechanical properties measured under low-frequency actuation, even at noise levels up to 5 %. In parallel, significant progress has been made in both imaging and inversion techniques, including motion encoding (as part of the acquisition process) [148,149], phase image preprocessing [150], and advanced model-based inversion algorithms [151]. These topics will not be elaborated here as they fall beyond the scope of this review. Readers interested in these technical advancements are referred to the comprehensive reviews by Hiscox, et al. [146], Johnson, et al. [132], and Sack [152].

In brain MRE, various mechanical properties, such as Young's modulus, storage and loss moduli, as well as bulk modulus, can be characterized based on the underlying material model assumptions, including elasticity [153,154], viscoelasticity [155,156], and poroelasticity [140,145] (see Table 1). Thanks to its noninvasive nature and modeling versatility, MRE has been widely employed in both fundamental and clinical brain research. For example, Sack, et al. [157] used MRE to investigate the effects of aging and gender on brain viscoelastic properties in a cohort of 55 healthy participants (23 females) aged 18 to 88 years. Their study for the first time revealed a notable decline in brain shear stiffness with age, approximately 0.8 % per year. Interestingly, they also found that female brains were, on average, 9 % stiffer than male brains, implying that women may be mechanically a decade "younger" than men. Similar age-related trends have been reported in other studies [135,154,158,159]. With the incorporation of brain parcellation atlas, MRE has been further used in examining the regional mechanical difference across brain structures, from broad distinctions between gray and white matter [133,135,160,161] to more detailed explorations of functionally diverse regions [148,156,162,163]. Clinically, MRE holds great promise for facilitating the diagnosis of brain disorders [164]. It has been applied to characterize mechanical changes in conditions such as brain tumors [153,165–167], neurodegenerative disease like AD [144,168] and PD [169], brain injury [44], dementia [170], normal pressure hydrocephalus [171], and epilepsy [172]. In addition, advanced techniques such as multi-excitation MRE combined with a nonlinear FEM-based inversion algorithm have shown promise in estimating anisotropic mechanical properties—particularly in white matter—by leveraging fiber tractography data [173–175]. Building on these advancements, recent developments have integrated machine learning with traveling wave expansion methods in MRE, yielding

Table 1
Comparison of techniques in measuring mechanical properties of brain tissue. Testing methods: AFM: atomic force microscopy, IND: indentation, AMT: axial mechanical test, OST: oscillatory shear test, MRE: magnetic resonance elastography, USE: ultrasound elastography; **Testing modes:** QSIT: quasi-static indentation test, UT: uniaxial tension, UC: uniaxial compression, SS: simple shear, CT: creep test, SRT: stress relaxation test, CSRT: constant strain rate test, OLT: oscillatory loading test, CLT: cyclic loading test, FST: frequency sweep test, AST: amplitude sweep test, AT: adhesion test, MALT: multi-axial loading test, SWE: shear wave elastography, SE: strain elastography; **Measurable Mechanical Properties:** CL: cellular level, TL: tissue level, OL: organ level.

Testing Methods	Referenced Literatures & Brain Tissue	Experimental Settings		Measurable Mechanical Properties	Sample Preparation Requirement	Accuracy-Sensitive Factors
		Testing Condition	Testing Modes			
AFM	Elkin, et al. [66] rat Canovic, et al. [58] mouse Yue, et al. [186] human Bahwini, et al. [55] human Qing, et al. [124] mouse De, et al. [64] human Thompson, et al. [68] frog Urbanski, et al. [61] mouse & human Eberle, et al. [187] mouse Ong, et al. [188] rat Iwashita, et al. [189] mouse Hall, et al. [190] rat Lobanova, et al. [56] human Morr, et al. [60] murine Jamal, et al. [70] ovine Chuang, et al. [67] rat Najera, et al. [62] rat Runke, et al. [59] mouse	*in vitro* *ex vivo*	QSIT, CT, SRT, OLT, AT, CLT	Young's modulus (CL) Shear modulus (CL) Viscoelasticity (CL) Hysteresis (CL) Surface adhesion (CL) Poisson's ratio (CL) Elasticity map (TL) Heterogeneity (TL)	Cut fresh tissue into thin sections for easy handling and indentation Ensure a flat sample surface Keep sample hydrated to prevent dehydration and mechanical variation Control temperature Immobilize tissue to minimize movement during measurement	Probe tip geometry Surface roughness Substrate effects Indentation depth Tip/sample adhesion Mechanical model assumptions
IND	Elkin, et al. [72] porcine Finan, et al. [80] rat Elkin, et al. [81] rat Feng, et al. [89] lamb Sridharan, et al. [85] rat Budday, et al. [23] bovine MacManus, et al. [73] mouse Weickenmeier, et al. [38] bovine Feng, et al. [88] porcine Stewart, et al. [76] human Weickenmeier, et al. [74] bovine MacManus, et al. [191] human Qian, et al. [91] porcine Qian, et al. [79] porcine Li, et al. [90] porcine Menichetti, et al. [28] human Qiu, et al. [84] mouse	*ex vivo,* *in vitro,* *in situ,* *in vivo*	QSIT, CT, SRT, OLT, CLT, MALT	Young's modulus (TL) Shear modulus (TL) Viscoelasticity (TL) Hysteresis (TL) Hardness (TL) Poisson's ratio (TL) Heterogeneity (TL)	Select bulk tissue samples with proper thickness to mitigate substrate effects Ensure a flat and smooth tissue surface Maintain tissue hydration Control temperature Secure the sample to prevent movement during measurement	Indenter shape and size Indentation depth Surface roughness Preconditioning effects Mechanical assumptions Boundary effects and constraints
IND	Antonovaite, et al. [78] mouse Greiner, et al. [94] human Sundaresh, et al. [82] porcine Pan, et al. [19] human Basilio, et al. [95] human Skambath, et al. [77] human Bailly, et al. [75] porcine	*ex vivo,* *in vitro,* *in situ,* *in vivo*	QSIT, CT, SRT, OLT, CLT, MALT	Young's modulus (TL) Shear modulus (TL) Viscoelasticity (TL) Hysteresis (TL) Hardness (TL) Poisson's ratio (TL) Heterogeneity (TL)	Select bulk tissue samples with proper thickness to mitigate substrate effects Ensure a flat and smooth tissue surface Maintain tissue hydration Control temperature Secure the sample to prevent movement during measurement	Indenter shape and size Indentation depth Surface roughness Preconditioning effects Mechanical assumptions Boundary effects and constraints
AMT	Miller, et al. [22] porcine Prange, et al. [192] human Franceschini, et al. [24] human Cheng, et al. [103] bovine	*in vitro,* *ex vivo*	UT, UC, SS, CT, SRT, CLT, CSRT, MALT	Young's modulus (TL) Shear modulus (TL) Tissue strength (TL) Viscoelasticity (TL) Hyperelasticity (TL) Hysteresis (TL)	Select uniform tissue samples to ensure consistent mechanical properties Cut samples into standardized dimensions, ensuring parallel and smooth loading surfaces Control temperature Fix the sample securely to prevent slippage or uneven loading	Preconditioning effects Clamping artifacts Sample slippage Hydration loss Sample misalignment

(*continued on next page*)

Table 1 (*continued*)

Testing Methods	Referenced Literatures & Brain Tissue	Experimental Settings		Measurable Mechanical Properties	Sample Preparation Requirement	Accuracy-Sensitive Factors
		Testing Condition	Testing Modes			
	Hrapko, et al. [114] porcine Rashid, et al. [100] porcine Rashid, et al. [107] porcine Rashid, et al. [101] porcine Rashid, et al. [193] porcine Jin, et al. [97] human Rashid, et al. [108] porcine Haslach, et al. [105] rat Rashid, et al. [102] porcine Destrade, et al. [109] porcine Budday, et al. [30] human Budday, et al. [194] human Budday, et al. [126] human Balbi, et al. [110] porcine Hosseini-Farid, et al. [195] porcine Budday, et al. [115] human Hosseini-Farid, et al. [196] porcine Eskandari, et al. [112] bovine Greiner, et al. [94] human Su, et al. [197] human Boiczyk, et al. [37] porcine Hinrichsen, et al. [26] human Su, et al. [104] Porcine Reiter, et al. [198] human			Fatigue resistance (TL) Poisson's ratio (TL) Heterogeneity (TL) Anisotropy (TL)	Ensure alignment of the sample along the loading axis Measure initial dimensions (length and cross-sectional area) to ensure accurate stress-strain calculations	Mechanical model assumptions
OST	Fallenstein, et al. [199] human Shuck, et al. [123] human Arbogast, et al. [125] porcine Darvish, et al. [128] bovine Nicolle, et al. [200] porcine & human Hrapko, et al. [129] porcine Garo, et al. [93] porcine Chatelin, et al. [120] human Canovic, et al. [58] mouse Forte, et al. [42] human Li, et al. [121] porcine Boudjema, et al. [29] lamb & cow Qing, et al. [124] mouse Xue, et al. [122] rat	*in vitro, ex vivo*	OLT, FST, AST, CT, SRT	Viscoelasticity (TL) Storage modulus (TL) Loss modulus (TL) Damping factor (TL) Yield strain (TL)	Select uniform tissue samples to ensure consistent mechanical properties. Trim samples into a well-defined shape for uniform shear strain distribution Ensure consistent sample thickness to minimize boundary effects Maintain physiological hydration Control temperature Fix the sample securely to prevent slippage or uneven loading Measure the sample's initial dimensions (diameter, thickness) for accurate shear stress calculations	Preconditioning effects Non-uniform tissue thickness Sample slippage Plate surface properties Sample off-center placement Strain amplitude selection Mechanical model assumptions
MRE	Xu, et al. [153] human Kruse, et al. [135] human Sack, et al. [157] human Sack, et al. [155] human Weaver, et al. [140] human Murphy, et al. [98]	*in vivo, in situ*	OLT, FST	Shear modulus (OL) Bulk modulus (OL) Viscoelasticity (OL) Stiffness map (OL) Heterogeneity (OL) Anisotropy (OL)	No samples preparation required	MRI scanner capability Compressive wave interference Shear wave frequency Imaging resolution Motion artifacts

(*continued on next page*)

Table 1 (*continued*)

Testing Methods	Referenced Literatures & Brain Tissue	Experimental Settings		Measurable Mechanical Properties	Sample Preparation Requirement	Accuracy-Sensitive Factors
		Testing Condition	Testing Modes			
	human Braun, et al. [161] human McGarry, et al. [145] human Zorgani, et al. [142] human Huston III, et al. [170] human Murphy, et al. [168] human Johnson, et al. [132] human Weickenmeier, et al. [201] human & porcine Huang, et al. [133] human Yeung, et al. [158] human Smith, et al. [173] human Ozkaya, et al. [159] human					
MRE	Qiu, et al. [138] human Troelstra, et al. [143] human Smith, et al. [174] human McIlvain, et al. [154] human Burman Ingeberg, et al. [148] human Ma, et al. [151] human Wang, et al. [175] porcine Karki, et al. [171] human Triolo, et al. [163] human Qiu, et al. [139] human Ma, et al. [176] human Wang, et al. [149] human	*in vivo, in situ*	OLT, FST	Shear modulus (OL) Bulk modulus (OL) Viscoelasticity (OL) Stiffness map (OL) Heterogeneity (OL) Anisotropy (OL)	No samples preparation required	MRI scanner capability Compressive wave interference Shear wave frequency Imaging resolution Motion artifacts
USE	Xu, et al. [202] human Xu, et al. [203] mouse & rat Jiang, et al. [204] porcine Su, et al. [205] human Chauvet, et al. [206] human Kim, et al. [207] human Liu, et al. [208] porcine Albayrak, et al. [209] human Tzschätzsch, et al. [99] human Liu, et al. [210] human Dirrichs, et al. [211] human Lay, et al. [212] mouse Garcés Iñigo, et al. [213] human Blackwell [214] ovine Klemmer Chandía, et al. [215] human Yu, et al. [216] human	*in vivo, in situ, ex vivo*	SWE, SE	Shear modulus (TL&OL) Viscoelasticity (TL&OL) Viscosity (TL&OL) Stiffness map (TL&TL) Heterogeneity (TL&OL)	No samples preparation required for *in vivo* or *in situ* testing. If used *ex vivo*, critical requirements are as follows: Keep samples hydrated during testing Apply ultrasound coupling gel evenly to ensure proper wave transmission Ensure flat and even contact between the transducer and tissue	Shear wave frequency Transducer positioning Skull Attenuation effects Boundary reflection

enhanced inversion performance for both viscoelastic and anisotropic property estimation [151,176].

While MRE is a powerful modality for measuring *in vivo* brain mechanical properties, several challenges remain that can affect its accuracy and interpretability. One persistent challenge is spatial resolution, which—despite recent advances enabling sub-2 mm isotropic imaging [177]—may still be insufficient for resolving fine-scale anatomical structures and capturing microstructural heterogeneity, particularly in small or complex regions such as hippocampal subfields, which typically have volumes of 200–600 mm^3 [178]. To address this, the use of higher magnetic field strengths (*e.g.*, 7T) to improve the signal-to-noise ratio [148,163], optimized motion encoding gradients [179], and advanced

imaging sequences like spin-echo-planar imaging [180] may enhance imaging spatial fidelity. Additionally, inversion-recovery MRE (IR-MRE) has emerged as a valuable refinement by suppressing cerebrospinal fluid (CSF) oscillation signals, thereby improving the delineation of tissue–CSF boundaries. This approach has been shown to yield approximately 10 % higher cortical stiffness values and more accurate ventricle segmentation, without compromising the accuracy of parenchymal measurements [181]. Another major challenge is the inverse problem of MRE, namely deriving mechanical properties from the measured wave fields. This problem, however, is mathematically ill-posed and highly sensitive to noise, boundary conditions, and model assumptions, such as tissue homogeneity and linear viscoelasticity [146]. To tackle this issue, nonlinear inversion algorithms implemented using FEM may significantly enhance the physical rigor of the results [182]. Nonetheless, FEM-based approaches require iterative simulations that can lead to long reconstruction times—often on the order of several hours—which may be suitable in research contexts but are limited for real-time clinical applications [183]. Recent advances in machine learning (ML)-based methods offer a promising alternative by accelerating the inversion process while maintaining or even boosting effective accuracy [184]. For example, neural network-based models such as the image-to-geometry learning inversion (ILI) framework can reconstruct stiffness maps in under 10 min, following an initial training phase spanning several days [185]. More notably, the TWENN method achieves full 3D multi-frequency brain inversions in under 15 s after a training phase of only a few minutes [151]. These developments highlight the promise of ML-based inversion to deliver substantial time savings in clinical workflows, making them highly attractive despite the upfront computational investment required during training

2.6. *Ultrasound elastography: real-time assessment of brain tissue mechanics*

Another widely used elastography technique is USE, which utilizes ultrasound imaging to track mechanically induced tissue displacements, from which stiffness-related properties can be inferred through appropriate inversion algorithms [217,218]. Compared to MRE, USE is capable of providing real-time imaging of tissue mechanical properties using a cost-effective system with greater portability and accessibility, making it well-suited for bedside diagnostic applications. Because the skull impedes ultrasound transmission and hinders effective imaging of intracranial structures, USE has not been as widely used to assess the mechanical properties of brain tissue compared to other organs such as the liver, breast, and kidney [214]. Despite this challenge, significant efforts have been dedicated to advancing transcranial USE techniques to enable reliable and clinically relevant assessment of brain mechanics [219].

The technical details of USE for measuring brain mechanical properties have been documented in several studies [214,217,220]. Based on the operational principles, brain-focused USE techniques are generally divided into two categories: quasistatic strain elastography (SE) and dynamic shear wave elastography (SWE) [220], as shown in Fig. 2. In SE, axial brain deformation, induced either by external compressive forces or internal physiological stimuli such as cardiac pulsation, is captured by ultrasound to estimate tissue mechanical properties [221]. This approach typically produces a 2D strain map derived from B-mode ultrasound images, offering relative comparisons of tissue stiffness rather than absolute mechanical values. For example, Kim, et al. [207] used SE to assess 21 healthy neonates between 28 and 40 gestational weeks. Using semi-quantitative color scale assessment, they compared the relative stiffness of various brain regions, including ventricle, periventricular white matter, caudate, subcortical, cortical gray matter, and subdural space. Their results showed notable stiffness variation across brain regions, with cortical gray matter being the stiffest region, and found a positive correlation between tissue stiffness and gestational age. Despite these insights, the qualitative nature of SE and its inability to provide absolute stiffness values restrict its broader applicability in scientific and clinical contexts.

In contrast to SE, SWE enables quantitative assessment of tissue mechanical properties such as shear modulus [209], viscoelasticity [99], and hyperelasticity [204] (see Table 1). Like MRE, SWE relies on the generation of shear waves within brain tissue to infer material properties. These waves can be generated either mechanically or through acoustic radiation force (ARF). One mechanical approach is transtemporal time-harmonic elastography (THE), which uses externally induced harmonic vibrations along with ultrasound-based motion tracking to image brain properties [216]. Klemmer Chandía, et al. [215] conducted a comparative study using both multifrequency MRE (20–35 Hz) and THE (27–56 Hz). Their findings indicated that THE can provide brain stiffness measurements consistent with MRE. Moreover, they suggested an optimal THE measurement depth of 40–60 mm, balancing ultrasound attenuation and near-field effects. The acoustic radiation force (ARF)-based method uses high-intensity focused ultrasound (typically in the MHz range) to generate localized tissue displacement primarily in the axial direction. This displacement induces both localized compression and the generation of laterally propagating shear waves. In acoustic radiation force impulse imaging (ARFI), tissue stiffness is inferred by measuring the magnitude, peak displacement, or recovery time of the axial displacement using a separate set of low-intensity tracking ultrasound pulses, without explicitly tracking shear wave propagation [222]. ARFI can be applied noninvasively in neonates, taking the advantage of the open fontanelle as an acoustic window [205]. However, after fontanelle closure, its use becomes limited due to skull-induced attenuation and is typically restricted to intraoperative or open-skull settings. Beyond ARFI, the laterally propagating shear waves generated by the ARF push can be leveraged in advanced modalities such as shear wave elasticity imaging (SWEI) and SWE. These methods track the shear wave front at multiple lateral positions using high-frame-rate ultrasound sequences, enabling the estimation of shear wave velocity through time-of-flight or phase-based algorithms [223]. Given that shear wave speed is directly related to tissue shear modulus under linear elastic assumptions, these techniques allow for real-time quantitative assessment of tissue stiffness [224]. A key distinction between THE and ARFI-based methods lies in their excitation frequencies. THE uses low-frequency mechanical vibrations (typically 20–100 Hz), allowing deep penetration through the skull and enabling global brain stiffness assessment. In contrast, ARFI-based techniques use focused ultrasound to generate localized tissue displacements, producing shear wave with center frequency typically around 100–300 Hz [225,226]. This relatively higher shear wave offers high spatial resolution but limits penetration depth due to stronger attenuation.

Compared to MRE, USE offers greater portability, lower cost, and the real-time imaging capabilities, making it well-suited for point-of-care and bedside applications. Its measurement is also less susceptible to variations in signal-to-noise ratio, enhancing its practicality and accessibility for characterizing brain tissue mechanical properties—especially in pediatric populations [205,207,212,213,220]. Moreover, USE has shown promise in the diagnosis and monitoring of various brain conditions, including brain tumors [206,227], ischemic stroke [202], TBI [203,228], and hydrocephalus [211], due to its sensitivity in detecting stiffness alterations associated with pathological processes. The versatility of USE also extends to *ex vivo* applications, particularly on animal brains. Liu, et al. [210] performed both *in vivo* and *ex vivo* SWE measurement on rabbit brains. *In vivo* tests were conducted after removing the skin and skull over the frontal lobe, while *ex vivo* measurements were taken on dissected brain tissue immersed in artificial cerebrospinal fluid at body temperature. Their results exhibited an average 47 % increase in shear modulus *in vivo* compared to *ex vivo* measurements, although this difference became negligible when *ex vivo* tests were taken within 60 min of tissue extraction. Despite its advantages, USE faces several limitations. In addition to skull-induced acoustic impedance and scattering,

ultrasound experiences significant attenuation within brain tissue, limiting its ability to probe deep brain structures under standard *in vivo* conditions. However, in *ex vivo* or open-skull scenarios, these barriers are largely removed, allowing high penetration depths to be achieved with improved image quality [206]. Moreover, such as THE has demonstrated the ability to achieve penetration depths of up to 12 cm through the intact skull when conducted under optimized conditions [215], suggesting that depth limitations are context-dependent and can be mitigated by appropriate methodological choices. Additionally, ultrasound measurement is also operator-dependent, which can affect measurement accuracy and reproducibility. For example, Blackwell [214] demonstrated that stiffness measurements in bovine brains were highly sensitive to the angle of the transducer application.

3. Discussions of human brain mechanical testing

Accurate mechanical characterization of human brain tissue is essential for understanding the complex biomechanical behaviors of the brain under both physiological and pathological conditions. Such testing, however, is inherently challenging due to ethical considerations and the limited availability of suitable human samples [21]. These constraints have led researchers to explore the use of animal brain tissue as an experimental surrogate, with species such as porcine and bovine commonly employed based on reported similarities in gross anatomy or mechanical response [38,86,102,196]. Despite their widespread use, there still remains no clear consensus regarding the appropriateness of animal models for replicating human brain tissue mechanics. For example, MacManus, et al. [33] advocated for the use of pig and rat brains based on a comparative analysis of dynamic mechanical properties among mouse, rat, pig, and human brains. In contrast, Prange, et al. [41] found that human brain tissue exhibited significantly greater stiffness than porcine brain, with an average 29 % higher shear modulus. Variabilities in genetic backgrounds, anatomical structures, and cellular compositions between animals and humans can further contribute to substantial deviations in mechanical behaviors [40]. An illustrative example is found in the contrasting regional stiffness trends reported by Budday and her colleagues. In their bovine brain study, white matter (average modulus of 1.895 ± 0.592 kPa) was found to be approximately 39 % stiffer than gray matter (average modulus of 1.389 ± 0.289 kPa) [23]. However, their subsequent study on human brain tissue revealed the opposite pattern, with gray matter regions (average modulus of 1.065 kPa) exhibiting nearly double the stiffness of white matter regions (average modulus of 0.505 kPa) [30]. In addition, animal brain models often fall short in fully capturing the complex, anisotropic, and region-specific mechanical characteristics intrinsic to the human brain [229,230]. These limitations are particularly problematic in the context of computational modeling and constitutive model characterization [231,232], where accurate mechanical data from human brain tissue are vital for developing realistic computational models to simulate fundamental brain mechanisms [4,5,233], injury biomechanics [8], surgical interventions [18], and disease progression [234] with high fidelity.

Given the challenges pertinent to human brain tissue mechanical measurement, each related study represents a valuable contribution toward unraveling the complexity and inherent elegance of human brain biomechanics. In what follows, we reviewed the body of literature dedicated to mechanical testing of human brain tissue, aiming to provide a comprehensive and comparative overview of its mechanical characteristics. While various mechanical properties—such as viscosity, nonlinearity and fracture behavior—have been reported across different studies, this review focuses on the shear modulus due to its importance in characterizing brain tissue and its widespread availability in the literature. To structure our analysis, we categorized the testing methods into two main groups: invasive and noninvasive approaches. The invasive category includes AFM, IND, AMT, and OST, while the noninvasive category comprises USE and MRE. It is important to note, however, that this classification is not absolute. For instance, techniques such as MRE and USE have also been applied in *ex vivo* contexts [210,235,236]. Our classification is therefore grounded in the most commonly reported use cases within the literature. Relevant publications were identified through an extensive literature search using widely accessed academic databases, including Google Scholar, PubMed, and Web of Science. The search strategy included broad keywords such as “human brain”, “mechanical testing”, “mechanical properties”, and “material characterization”. To ensure inclusion of studies employing specific experimental methods, we also included method-specific terms like “elastography”, “tension”, “compression”, “shear”, “AFM” and “indentation”. Boolean operators and filtering criteria were applied to restrict the search exclusively to peer-reviewed studies involving human brain tissue. Notably, the following review primarily focuses on invasive testing methods, as they directly probe the material response of brain tissue and offer more robust quantitative data for constitutive modeling and validation of computational simulations.

3.1. Invasive mechanical testing: direct, informative, and high-fidelity characterization

Through our literature search, we identified 35 peer-reviewed studies that employed invasive mechanical testing on human brain tissue, spanning from the earliest work by Fallenstein, et al. [199] to the recent advancements reported by Greiner, et al. [237]. The details of these studies are presented in Table 2, where we summarize key experimental parameters, including sampling regions; tissue freshness (indicated by post-mortem interval or durations after surgical resection); subject age distribution; specimen geometry; measurement techniques; loading modes performed in testing; environmental testing temperature; frequencies or strain rates chosen for dynamic test and predefined strain range. Additionally, we documented the reported material properties and constitutive models used for data interpretation, as well as the parameter calibration methods, whether through conventional least squares fitting or inverse FEM-based indentation approaches. Based on this comprehensive dataset, we analyzed the distribution of key experimental attributes to find common trends across studies. We further discussed the primary factors that contribute to variabilities in reported properties, such as differences in specimen preparation, experimental protocols, and modeling assumptions. To facilitate a comparative overview, we also summarized the mechanical properties extracted from these studies, including various moduli (e.g., shear, storage, loss, and relaxation modulus) and representative stress-strain curves. Through these analyses, we aim to address the following two questions: (1) what factors contribute to the huge variability in reported mechanical properties of the human brain? (2) what insights can we infer from existing experimental efforts regarding the mechanical behaviors of human brain tissue?

Fig. 3 illustrates a statistical summary of several key aspects observed across the reviewed studies, including testing regions (Fig. 3a), testing methods (Fig. 3b), fitted material models (Fig. 3c), and primary loading modes (Fig. 3d). As shown, the cortex (C) is the most frequently tested human brain region, likely due to its anatomical location as the outermost layer of the brain, which makes it more accessible for sample collection during surgical resections or post-mortem dissections. The corona radiata (CR) and corpus callosum (CC) are also commonly selected, owing to their well-defined structure as major white matter tracts—ideal candidates for investigating the anisotropic mechanical properties of the brain. Notably, the category labeled cerebrum (Cb) refers to samples containing both gray and white matter, typically used in earlier studies where tissues were undissected or only roughly separated without clear anatomical differentiation [199,238–240]. Specimens classified as diseased brain (DB) primarily include brain tumors, though some studies have also examined the biomechanical implications of neurological conditions such as epilepsy [19,241] and AD [242]. Among the various testing methods, AMT and IND stand out as frequently used methods due to their experimental versatility and ability

Table 2

Literature summary of human brain tissue testing. **Regions**: Cb: cerebrum (white and gray), C: cortex, T: thalamus, H: Hippocampus, CR: corona radiata, CC: corpus callosum, BG: basal ganglia, Mb: midbrain, BS: brain stem, CB: cerebellum, WB: whole brain, BT: brain tumor; **PMI** (*Post-mortem* Interval), * indicates the time after post-operative resection; **Testing Methods**: AFM: atomic force microscopy, IND: indentation, AMT: axial mechanical test, OST: oscillatory shear test, MRE: magnetic resonance elastography, USE: ultrasound elastography, PA: pipette aspiration; **Loading Modes:** QSIT: quasi-static indentation test, UT: uniaxial tension, UC: uniaxial compression, SS: simple shear, TS: torsional shear, PS: pure shear, CT: creep test, SRT: stress relaxation test, CSRT: constant strain rate test, OLT: oscillatory loading test, CLT: cyclic loading test (large strain), FST: frequency sweep test, AST: amplitude sweep test, AT: adhesion test, MALT: multi-axial loading test, SWE: shear wave elastography, SE: strain elastography; **Specimen**: W: width, L: length, H: height, R:radius; **Temp** (temperature); **Fitted Material Models**: Hyperelastic: NH: neoHookean model, D: Demiray model, G: Gent model, MR: Mooney-Rivlin model, O: Ogden model; Viscoelastic: Zn: Zener model (standard linear solid model), Mw: Maxwell model, Sp: springpot model, KV: Kelvin-Voigt model, Bg: Burgers model (four-parameter fluid model), PS: Prony series, LEV: linear viscoelastic model (linear), QLV: quasi-linear viscoelastic model (non-linear), GRV: Green-Rivlin viscoelastic model (non-linear), MD: multiplicative decomposition; Poroelastic: TC: Terzaghi's Consolidation, BTP: Boit's theory of poroelasticity, DL: Darcy's law. **PIM** (Parameter Identification Method): LsF: Least-square Fit, IFEM: inverse identification using finite element modeling.

Literatures	Regions	PMI (hours)	Ages (years)	Testing Methods	Loading Modes	Specimen (cm)	Temp (°C)	Frequency/strain/ strain rate range	Measured Material Properties	Fitted Material Models			PIM
										Hyperelastic	Viscoelastic	Poroelastic	
Fallenstein, et al. [199]	Cb	10–62	44–92	OST	OLT, SS	Rectangular W2 × L3 × H0.4–0.7	37	9–10 [Hz], 7–24.5 % [-]	Storage modulus, Loss modulus		KV		LsF
Galford, et al. [238]	Cb	6–12	–	AMT	CT, SRT, OLT	Cylindrical R0.318 × H0.635	37	10–40 [Hz]	Storage modulus, Loss modulus, Creep compliance, Relaxation modulus, Viscoelasticity		Bg		LsF
Estes, et al. [245]	CR	7–12	52–84	AMT	UC, CSRT	Cylindrical: R0.635 × H0.635	37	0–170 % [-] 0.08–40 [s^{-1}]	Stress-strain curves				LsF
Shuck, et al. [123]	CR, T	–	–	OST	FST,PS, OLT	Cylindrical: R0.635 × H1.27	37	5–350 [Hz], 1.3–3.5 % [-]	Storage modulus, Loss modulus, Viscoelasticity, Limited strains & strain rates, Heterogeneity, Anisotropy		Bg		LsF
McElhaney, et al. [239]	Cb,	6–10	–	IND	CSRT, QSIT	Cylindrical: R0.635 × H2.54	37	9–10 [Hz]	Bulk modulus, Viscosity				LsF
Donnelly, et al. [240]	CC, Mb	< 48	44–92	AMT	CSRT, SS	Cylindrical: R0.615–0.953 × H0.53–2.64	22	0–45 % [-] 30–180 [s^{-1}]	Storage modulus, Viscosity, Viscoelasticity, Stress-strain curves, Heterogeneity,		Zn		LsF
Prange, et al. [246]	C	< 3*	–	AMT	SS, SRT, UC	Rectangular: W0.5 × L1 × H0.1	–	2.5–50 % [-] 0.42–8.3 [s^{-1}]	Shear modulus, Anisotropy, Hyperelasticity, Heterogeneity, Viscoelasticity	O	PS		LsF
Prange, et al. [41]	C	< 3*	–	AMT	SS, SRT, UC	Rectangular: W0.5 × L1 × H0.1	–	2.5–50 % [-] 0.42–8.3 [s^{-1}]	Hyperelasticity, Shear modulus, Anisotropy, Heterogeneity, Viscoelasticity	O	PS		LsF
Takhounts, et al. [247]	Cb	< 24	–	AMT	SS, SRT, UC	Cylindrical: R2 × H0.9–1.8	22	12.5–50 % [-] 3.125, 6.25 [s^{-1}]	Viscoelasticity		LVE, QLV, GRV		LsF
Nicolle, et al. [113]	CR, T	> 72	–	OST	SRT,TS, OLT	Cylindrical: R0.5 × H0.015–0.085; R1 × H0.225	37	0.1–10,000 [Hz], 0.001 % [-]	Hyperelasticity, Storage modulus, Loss modulus, Viscoelasticity, Anisotropy, Heterogeneity	O	Mw		LsF
Franceschini, et al. [24]	C,CC,T	< 12	–	AMT	CSRT, UC, UT, CLT	Cylindrical: R0.7–0.75 × H0.8–0.98; Rectangular: W0.8 × L1.3 × H0.8	22	0–270 % [-] 5.5–9.3e^{-3} [s^{-1}]	Hyperelasticity, Hysteresis, Fracture & Damage, Viscoelasticity, Poroelasticity, Stress-strain curves	O	KV	TC	LsF
Schiavone, et al. [47]	C	–	–	PA	QSIT	–	37	–	Hyperelasticity	MR			IFEM
Zhu, et al. [25]	CC,T	>168	45	AMT	UC	Rectangular: W1.5 × L1.5 × H0.8	37	0.5,5,35[s^{-1}]	Young's modulus, Shear modulus, Viscoelasticity, Heterogeneity, Stress-strain curves		Zn		IFEM
Chatelin, et al. [120]	CR, T, BS	24–48	0.2 – 55	OST	FST,TS, OLT	Cylindrical: R1cm × H0.2–0.5 cm	37	0.1–10 Hz, 0.5 % [-]	Storage modulus, Loss modulus, Heterogeneity		LVE		LsF

(*continued on next page*)

Table 2 (*continued*)

Literatures	Regions	PMI (hours)	Ages (years)	Testing Methods	Loading Modes	Specimen (cm)	Temp (°C)	Frequency/strain/ strain rate range	Measured Material Properties	Fitted Material Models			PIM
										Hyperelastic	Viscoelastic	Poroelastic	
Jin, et al. [97]	C,T, CC,CR	~96	45–94	AMT	UT,UC,SS	Rectangular: W1.4 × L1.4 × H0.5	37	0–50 % [-], 0.5–30 [s^{-1}]	Heterogeneity, Anisotropy, Stress-strain curves				LsF
Forte, et al. [42]	Cb	26–48	65–88	OST, AMT	FST, OLT, SRT, UC, TS	Cylindrical: R1.25 × H0.2–0.8; R0.6 × H0.8	24; 37	0.01–25 Hz, 1 % [-]; 0–35.6 %, 1e–$^{-4}$–1 [s^{-1}]	Storage modulus, Loss modulus, Hyperelasticity, Viscoelasticity, Poroelasticity	O	PS	DL	LsF
Budday, et al. [30]	CC,CR,BG, C	< 60	54–81	AMT	UT,UC,S, CLT,SRT, MALT	Rectangular: W0.5 cm × L0.5 cm × H0.5 cm	22	0–10 % [-]; 0–10 % [-]; 0–20 % [-];	Hyperelasticity, Hysteresis, Anisotropy, Heterogeneity, Stress-strain curves	O,NH,MR,D, G			LsF
Budday, et al. [194]	CC,CR,BG, C	< 60	54–81	AMT	UT,UC,SS, CLT,SRT, MALT	Rectangular: W0.5 × L0.5 × H0.5	22	0–10 % [-]; 0–10 % [-]; 0–20 % [-];	Viscoelasticity, Hyperelasticity, Hysteresis, Heterogeneity, Stress-strain curves	O	Zn		LsF
Budday, et al. [126]	CC,CR,BG, C	< 60	54–81	AMT	UT,UC,SS, CLT,SRT, MALT	Rectangular: W0.5 × L0.5 × H0.5	22	0–10 % [-]; 0–10 % [-]; 0–20 % [-];	Viscoelasticity, Hyperelasticity, Hysteresis, Heterogeneity, Stress-strain curves	O	PS, Zn		LsF
Finan, et al. [241]	C, H	< 6*	4–58	IND	SRT	H0.1	22	0–10 % [-],5e–$^{-3}$–5 [s^{-1}]	Shear modulus, Viscosity, Viscoelasticity, Heterogeneity		PS		LsF
Stewart, et al. [76]	BT	3–4*	–	IND	SRT	H0.3	37	0–10 % [-]	Shear modulus, Viscoelasticity		Zn		LsF
Karimi, et al. [243]	CB	<10	60–80	AMT	UC, CLT	Proper size	37	0–50 % [-], 1[s^{-1}]	Young's modulus, Failure stress, Stress strain curve				LsF
Park, et al. [242]	C	2.5–14.5	61–75	AFM	FS, QSIT	H0.0008	21	0.01–10 Hz, 0–2 % [-],	Young's modulus, Storage modulus, Loss modulus, Hysteresis, Surface roughness, Viscosity, Stress-strain curve		KV		LsF
Budday, et al. [115]	CC,CR,BG, C	24–60	55–68	AMT	SS, SRT, UC, UT, CLT	Rectangular: W0.5 × L0.5 × H0.5	22	0–20 % [-], 0.0067 [s^{-1}]; 20 % [-], 0.33 [s^{-1}]; 0–10 % [-]; 0–10 % [-]	Viscoelasticity, Viscosity, Hyperelasticity, Hysteresis, Heterogeneity, Stress-strain curves	O	PS		LsF
MacManus, et al. [33]	C, CB, BS	<96	64–94	IND	SRT	Cylindrical: R0.125 × H0.125	22	0–30 % [-], 10 [s^{-1}]	Shear modulus, Viscoelasticity, Hyperelasticity, Heterogeneity	NH	PS		IFEM
Menichetti, et al. [28]	CC,CR,BG, C,BS,	<96	64–94	IND	SRT	H2	37	0–35 % [-]; 10 [s^{-1}]	Shear modulus, Relaxation modulus, Viscoelasticity, Hyperelasticity, Heterogeneity, Heterogeneity	NH	PS		IFEM
Greiner, et al. [94]	C, CR	–	77	IND, AMT	QSIT, UT, UC, SRT, CLT	Cylindrical: R0.4 × H0.4	37	0–15 % [-]	Hyperelasticity, Viscoelasticity, Poroelasticity, Stress-strain curve	O	MD	DL	
Pan, et al. [19]	C	<3*	35–52	IND	SRT	H0.6	22	0–17 % [-]	Shear modulus, Viscoelasticity		QLV		LsF
Sundaresh, et al. [248]	C, H	< 6*	4–58	IND	SRT	H0.1	–	0–30 % [-], 1.9 [s^{-1}]	Shear modulus, Hyperelasticity, Viscoelasticity, Heterogeneity	NH, MR, O	QLV		LsF
Hinrichsen, et al. [26]	CC, CR, C, BGH, Mb, BS, T, CB	<72	62–92	AMT	UT,UC,TS, SRT,FS, CLT	Cylindrical: R0.4 × H0.27–0.72	37	0–15 % [-], 0–30 % [-], 1 e^{-2} [s^{-1}]	Shear modulus, Bulk modulus Hyperelasticity, Hysteresis, Heterogeneity, Stress-strain curves	O			IFEM
Su, et al. [197]	BT	<12	72	AMT	UC,SRT	Cylindrical: R0.5 × H0.46	22	0–10 % [-],1 [s^{-1}]	Young's modulus, Relaxation modulus, Poisson's ratio, Hydraulic permeability, Viscoelasticity, Poroelasticity		PS	BTP	LsF
Basilio, et al. [95]	C,H	<6*	4–58	IND	SRT	H0.1	22	0–30 % [-], 0.79–3.57 [s^{-1}]	Hyperelasticity, Viscoelasticity, Heterogeneity	NH, MR, O	QLV		IFEM
Skambath, et al. [77]	BT,C	< 0.1	–	IND	QSIT	H0.2–1	20	0–10 % [-]	Young's modulus				LsF

(*continued on next page*)

Table 2 (*continued*)

Literatures	Regions	PMI (hours)	Ages (years)	Testing Methods	Loading Modes	Specimen (cm)	Temp (°C)	Frequency/strain/ strain rate range	Measured Material Properties	Fitted Material Models			PIM
										Hyperelastic	Viscoelastic	Poroelastic	
Greiner, et al. [237]	C,CR		57–71	AMT	UT,UC, SRT,CLT	Cylindrical: R0.4 × H0.27–0.72	37	0–15 % [-], 1e $^{-2}$[s $^{-1}$]	Viscoelasticity, Heterogeneity, Poroelasticity		MD	DL	IFEM
Reiter, et al. [198]	CC, CR, BS, CB, MB	< 98	62–92	AMT	UC,UT,SS, SRT	Cylindrical: R0.4 × H0.27–0.72	37	0–15 % [-], 0–30 % [-], 8 e^{-3} [s $^{-1}$]	Stress-strain curves				LsF

to characterize localized mechanical response (see Sections 2.2 and 2.3). OST has been widely utilized to capture the frequency-dependent viscoelastic behavior of brain tissue, which is particularly relevant for injury biomechanics such as automotive impact modeling [42,113,120,123,199]. Only one study by Park, et al. [242] employed AFM to assess viscoelastic properties of autopsy brain tissue in the context of AD. In terms of mechanical parameters calibration, the human brain is commonly represented as viscoelastic or hyperelastic, reflecting its nonlinear and time-dependent response. Only a few studies have assumed linear elasticity, primarily to estimate basic elasticity properties such as Young's modulus [77,243]. Additionally, the poroelasticity of the brain has been explored to account for its biphasic features and fluid-solid interactions [24,42,94,197]. A variety of loading modes have been implemented in human brain tissue testing. Among them, stress relaxation tests are commonly used due to their suitability for capturing the viscoelastic response of brain tissue. In addition, compression and shear tests are more frequently performed compared to tension tests, likely because of the highly fragile and easily damaged nature of brain tissue, which poses significant challenges for tensile loading [96].

Despite extensive efforts that have been made to characterize the mechanical properties of human brain tissue, the reported parameters show substantial variability, often spanning several orders of magnitude, and in some cases, even present contradictory findings across studies [71]. Fig. 4 compares various shear-related moduli, including shear modulus, instantaneous modulus, relaxation modulus, and long-term modulus, between gray and white matter, based on existing literature focused on human brain tissue. For studies that investigated multiple brain regions, shear modulus values were averaged across gray and white matter regions to facilitate comparison. Additionally, for studies reporting only storage and loss moduli, the magnitude of the complex modulus was calculated to represent an equivalent shear modulus. Since Shuck, et al. [123] and Chatelin, et al. [120] reported frequency-dependent complex shear moduli, we present only the values measured at the lowest frequencies used in their studies—5 Hz and 0.1 Hz, respectively. Only studies that reported mechanical properties for both gray and white matter are included to enable direct inter-group comparisons. In this analysis, the relaxation modulus is defined as the difference between the instantaneous and long-term shear modulus, reflecting the gradual reduction in shear resistance due to viscous dissipation. As seen in Fig. 4, reported values of shear modulus vary in multiple orders of magnitude, from tens of Pascals to several kilopascals, especially for the instantaneous and long-term components. Moreover, conflicting trends between gray and white matter properties are also evident. For example, Zhu, et al. [25] reported that gray matter is softer than white matter, with stiffness values of 3100 Pa and 4100 Pa, respectively (Fig. 4a). This finding is supported by Pan, et al. [19], who found gray matter (653.36 ± 155.81 Pa) only to be slightly softer than white matter (684.58 ± 101.61 Pa). In contrast, studies by Budday and her colleagues reported the opposite trend, indicating a significantly higher stiffness value for gray matter compared to white matter [26,30,115]. Similar inconsistencies in the relative stiffness of gray and white matter are also observed for the other shear moduli shown in Fig. 4b-d Notably, the figure is intended to illustrate the reported range and variability of values across the literature, rather than to define absolute or standardized reference value. This interpretation similarly applies to the subsequent figures, where appropriate.

In addition to the global comparison between gray and white matter, we also summarized the specific shear stiffness values reported for individual brain regions, as illustrated in Fig. 5. Here, only commonly dissected regions were included, and for studies that measured multiple anatomical subregions, values were averaged again across regions corresponding to the broader parcellation stated here. For example, Menichetti, et al. [28] reported viscoelastic properties for 12 distinct anatomical regions of the human brain, including six subregions within the cortex and two within the brain stem. Another study by Hinrichsen, et al. [26] measured the mechanical properties of 19 anatomical human

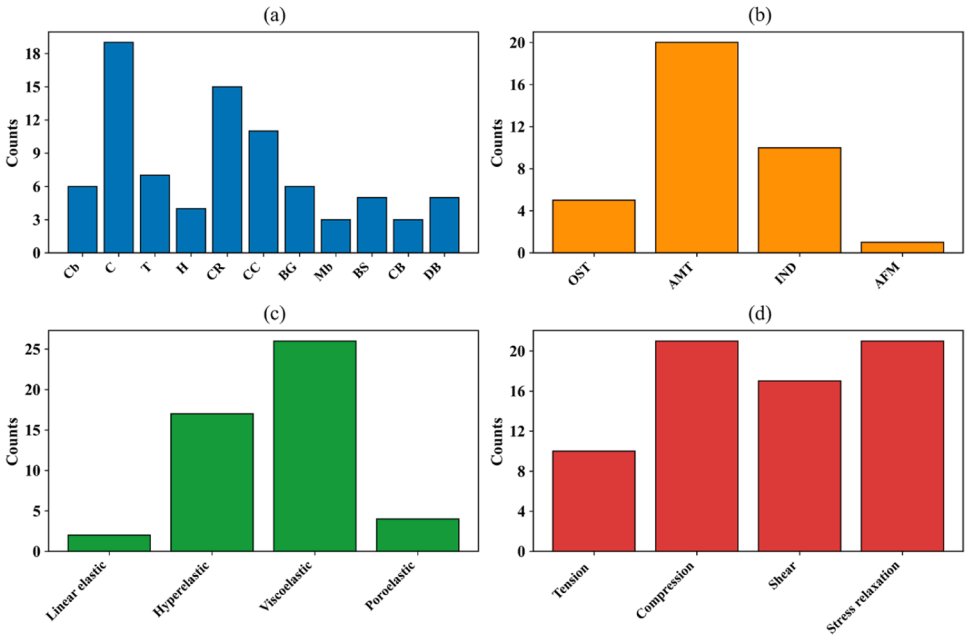

Fig. 3. Summary of publications on human brain tissue mechanical testing. (a). Distribution of tested brain regions; (b). Distribution of testing methods used for measuring human brain tissue mechanical properties; (c). Model assumptions applied in characterizing brain tissue mechanical properties; (d). Loading modes performed in human brain tissue mechanical testing. Abbreviations in (a) and (b) follow those in the caption of Table 1.

brain regions, including five cortex subregions, three basal ganglia subregions, and two subregions each from brain stem, corona radiata, cerebellum, and midbrain, respectively. As shown in Fig. 5, considerable variability exists even within these localized anatomical regions, particularly for the cerebellum, corona radiata, corpus callosum, basal ganglia, and cortex. For other regions, smaller deviations are observed, however, this is likely attributed to the limited number of studies rather than consistency in the mechanical properties. Further investigation is needed to determine whether these smaller deviations are representative or simply the result of insufficient data.

The substantial variability observed in reported brain tissue mechanical properties arises from a combination of factors. As discussed in Section 2, these include differences in subject-specific variables such as age and gender, tissue sample preparation (e.g., post-mortem time, sampling size, hydration level, anatomical location, and sampling direction), experimental conditions (e.g., temperature, preconditioning, and loading rate or frequency for dynamic tests), and the choice of constitutive model (e.g., linear, hyperelastic, viscoelastic, or poroelastic), all of which may affect the testing outcomes and data interpretation. To visualize the scope of these influences, we compiled the potential effects reported in each study into Fig. 6. In this figure, each factor is marked as "1″ if considered influential and "0" if deemed negligible. While these effects have been comprehensively reviewed in prior literature [21,45,71,244], here we provide a brief discussion based on the summary of human brain tissue testing studies.

3.1.1. Age and gender effects on human brain mechanics

Throughout development, maturation, and aging, the brain undergoes significant structural and compositional changes, implying that age may influence its mechanical properties. This effect has been well-documented in animal studies, where mechanical testing has shown clear age-dependent trends [34,41,122]. However, in human brain tissue, aging appears to have a minor influence on mechanical properties [28,30,95,97,241,248]. Most of these studies focused on adult brain tissue, with small age variations across limited samples. A notable exception is the study by Finan, et al. [241], who conducted an IND test on 11 human brains ranging from 4 to 58 years of age, covering children, adolescents, and adults. Despite this age range, no significant correlation was found between age and the shear modulus of cortical gray or white matter. Only one study by Chatelin, et al. [120] reported a notable age-related effect. They performed OST on both human child brains (five subjects aged 5 to 22 months) and adult brains (two subjects aged 50 to 55 years). Their results identified a significant increase in both storage and loss moduli with age in the pediatric group and found adult brain tissue to be three to four times stiffer than the younger brains. It is worth noting that the conclusion made on the aging effect may lack statistical robustness, as the small sample size used in their studies due to the inherent challenges of acquiring human brain tissue across a broad age range. In contrast, the noninvasive approach like MRE offers a more practical and ethical approach for assessing the aging effect *in vivo*, and several studies have consistently reported age-related stiffening in the human brain using MRE [154,157,158]. Similar challenges exist in investigating the influence of gender on brain mechanics. Among limited evidence, Finan, et al. [241] reported a significant gender difference in the stress relaxation behaviors of cortical white matter. Specifically, male brain tissue exhibited greater modulus decay during stress relaxation, although long-term shear modulus values seem consistent between genders.

3.1.2. Consistent regional heterogeneity versus conflicting anisotropy in human brain mechanics

Given the intricate anatomical structure of the human brain, sample preparation has a non-negligible impact on tissue mechanical testing outcomes. Numerous studies have consistently reported mechanical heterogeneity across different human brain regions. However, findings regarding the anisotropy of brain tissue—i.e., its direction-dependent mechanical behavior—remain inconsistent. Some studies suggest that human brain tissue exhibits only minor anisotropy, even within highly organized white matter structures such as corpus callosum, which contains densely aligned axonal fiber tract [30,113,123]. For instance, Budday, et al. [30] investigated the directional mechanical response of the corona radiata and corpus callosum. In their tests, compression and tension tests were conducted both along and perpendicular to fiber orientation, while simple shear tests in three distinct directions relative to the fiber alignments. Their results showed minimal directional dependence, although the tissue was slightly softer in compression and

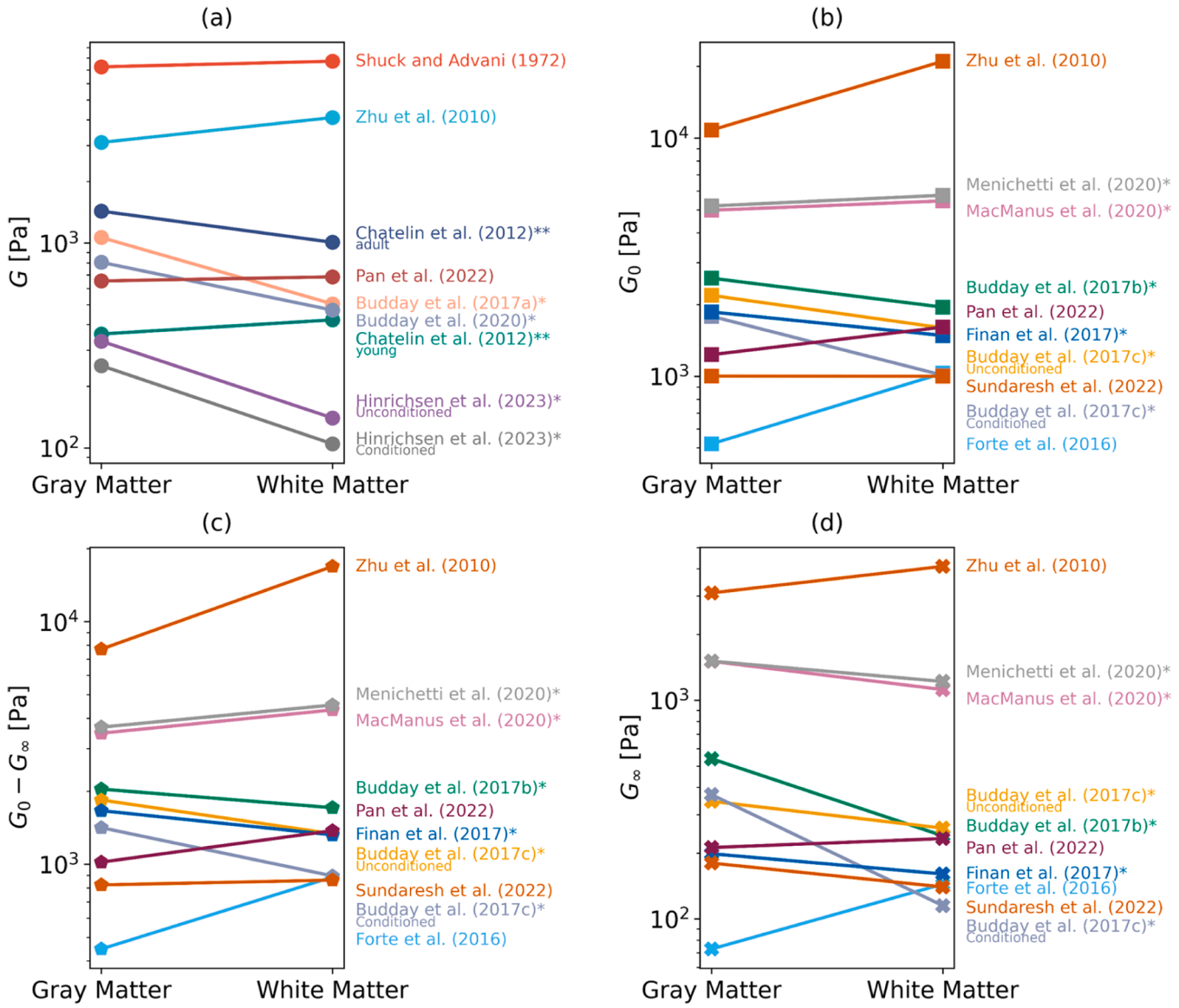

Fig. 4. Gray matter *vs* white matter in measured mechanical properties. (a) Comparisons of shear modulus (G); (b-d). Comparisons of instantaneous shear modulus (G_0), relaxation shear modulus ($G_0 - G_\infty$), and long-term shear modulus (G_∞). Only invasive studies are included, as collected in Table 2. For studies that measure multiple gray or white matter regions (marked with *), modulus values are averaged across regions. For studies reporting multiple regions within gray or white matter (marked with *), modulus values are averaged across regions. The magnitude of complex modulus was calculated for studies only reporting loss and storage modulus (marked with **). In the study by Zhu, et al. [25], shear modulus was derived using the standard linear elastic relationship $G = E/(2(1+\nu))$, assuming incompressibility. In study by Budday, et al. [30], the shear modulus was chosen from simultaneous fit using a modified one-term Ogden model. In the study by Chatelin, et al. [120], the stiffness value measured under lowest frequency was selected. Note: The values presented in this figure are drawn from studies employing diverse experimental setups, measurement modalities, and tissue conditions. As such, direct quantitative comparisons should be interpreted with caution.

marginally stiffer in tension when tested along the fiber. However, in a more recent study, they revised their earlier conclusion, reporting pronounced anisotropic mechanical behavior in the corpus callosum based on cyclic compression-tension and simple shear tests [198]. Supporting this, Jin, et al. [97] observed significantly higher shear stress when loading was applied along the fiber direction compared to transverse loading in white matter. Interestingly, they did not observe such anisotropy in tension and compression tests. It is worth noting that the apparent anisotropy in Jin's study might have been influenced by geometric effects, as the rectangular specimens used (14 × 14 × 5 mm) had unequal lateral dimensions, potentially affecting the measured responses [30]. These conflicting findings underscore the need for further systematic investigations to resolve the debate surrounding the anisotropic mechanical properties of brain tissue.

3.1.3. *Difference caused by sample size and post-mortem interval*

To facilitate mechanical testing, brain tissue samples are often prepared in either rectangular or cylindrical shapes, with their dimensions ranging from a few millimeters to several centimeters, especially in studies utilizing OST and AMT (see Table 2). However, sample size has not been found to significantly influence mechanical outcomes in the two existing human brain studies on this topic [42,113]. Both studies used cylindrical specimens of varying thickness for OST and reported that thickness has little to no effect on the result, once the samples were securely affixed to the testing plates. While this suggests that OST measurements are size-independent within small deformation ranges, further investigation is warranted to determine whether varying sample dimensions introduce bias in larger deformation tests such as AMT, which potentially leads to artificial anisotropy artifacts. Another concern related to the size effect is the inconsistency between the

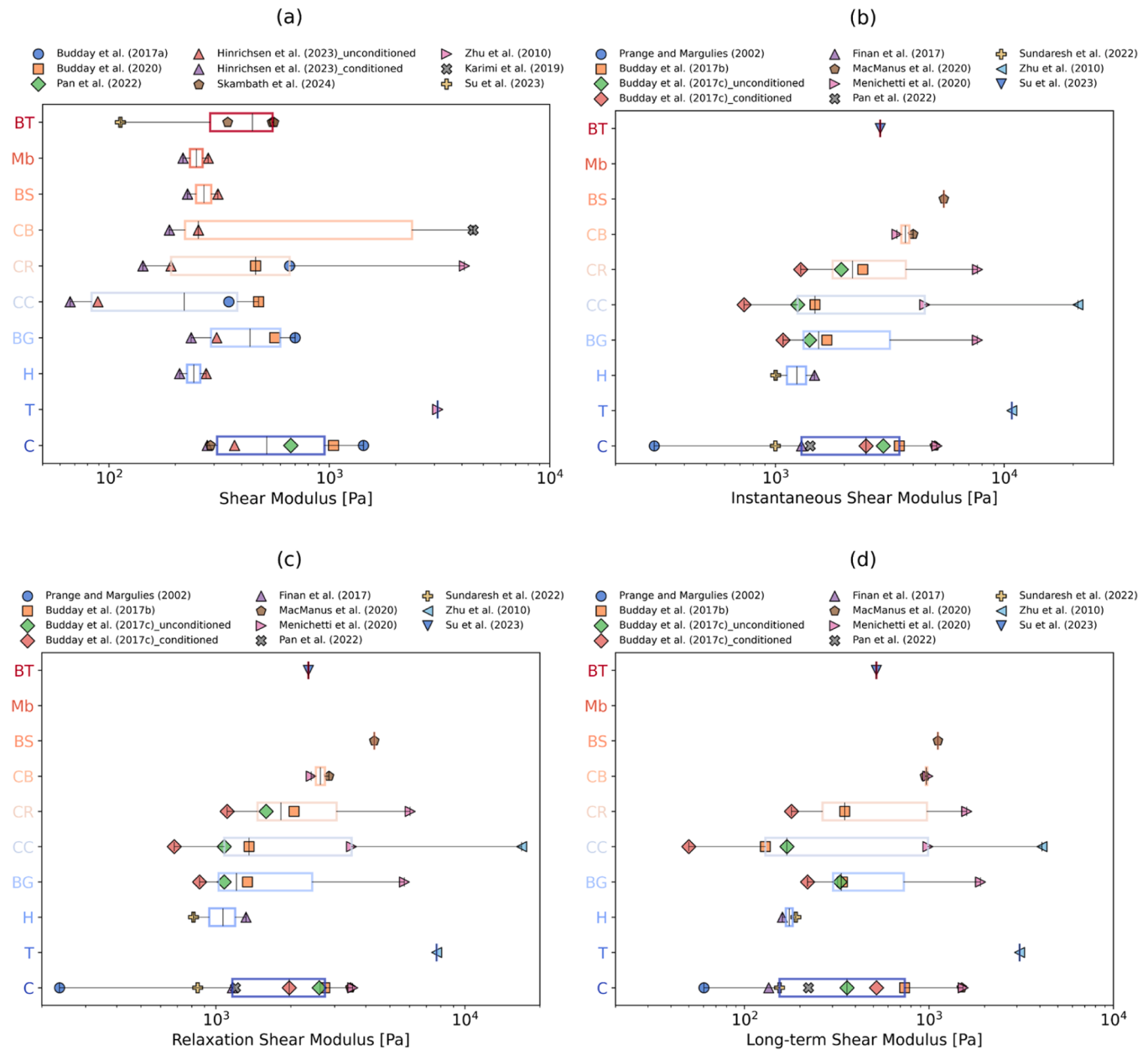

Fig. 5. Summary of various shear moduli for human brain regions. Box plot and data points illustrate the distribution of regional shear modulus (a), instantaneous shear modulus (b), relaxation shear modulus (c), and long-term shear modulus (d) based on collected in-vitro or ex-vivo studies, as presented in Tabel 2. C: cortex, T: thalamus, H: Hippocampus, BG: basal ganglia, CC: corpus callosum, CR: corona radiate, CB: cerebellum, BS: brain stem, Mb: midbrain, BT: brain tumor. In the study by Zhu, et al. [25], shear modulus was derived using the standard linear elastic relationship $G = E/(2(1+\nu))$, assuming incompressibility. In study by Budday, et al. [30], the shear modulus was chosen from simultaneous fit using a modified one-term Ogden model. Note: The values presented in this figure are drawn from studies employing diverse experimental setups, measurement modalities, and tissue conditions. As such, direct quantitative comparisons should be interpreted with caution.

sample's intended size during preparation and its actual size during testing, particularly for large samples. Due to the brain's ultrasoft nature, significant deformation can occur under gravitational loading alone [21]. One approach to address this issue is inverse parameter identification via FEM. A more precise strategy was proposed by Zhu, et al. [25], who employed a laser scanning system in conjunction with a 3D surface reconstruction algorithm to capture the realistic geometry of each brain sample prior to testing and FEM simulation. Post-mortem interval is another critical factor to consider in invasive mechanical tests. Although brain tissue experiences structural variations due to biochemical degradation, enzymatic activity, and water content rapidly after death, several studies have reported that the effect of post-mortem appears to be negligible when tissue is appropriately preserved [21,113,199,239]. For example, Menichetti, et al. [28] found no significant impact of post-mortem delay on inter-regional mechanical difference, and Forte, et al. [42] similarly concluded that varying post-mortem durations between 26 and 48 h did not affect mechanical outcomes in their study population.

3.1.4. *Undervalued effects of temperature and humidity*

Humidity and temperature controls are also important for human brain tissue mechanical testing, especially during long-duration experiments such as OST or quasistatic AMT. Forte, et al. [42] systematically examined the influence of both factors on OST results. They evaluated humidity effects by testing brain tissue under three conditions: continuous water misting for full humidity control, no moisture regulation,

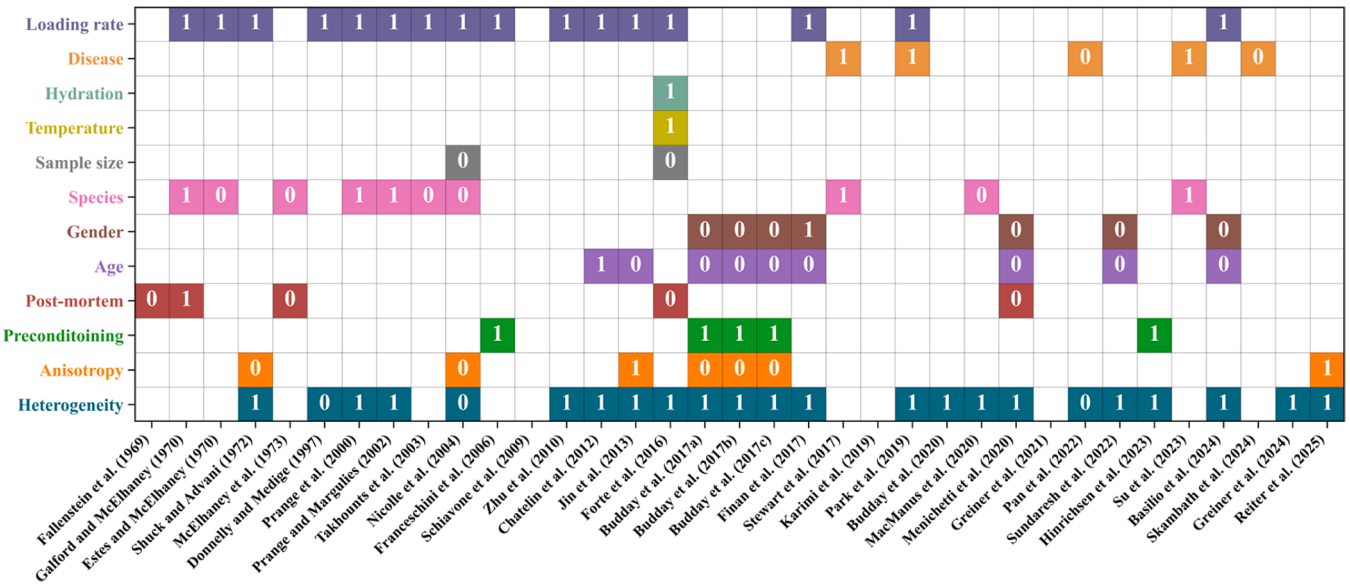

Fig. 6. Overview of considered factors in human brain tissue mechanical testing across various studies. The colored blocks represent the effects investigated and discussed in each publication. The in-block text "1″ indicates that the effect may significantly influence testing results, while "0" suggests minimal impact.

and periodic rehydration using saline. These tests were conducted at controlled temperatures of 24 °C and 37 °C. For temperature effects, a sweep from 22 °C to 37 °C was performed, both with and without humidity control. Their findings revealed that in the absence of humidity control, tissue dehydrates rapidly and stiffens significantly. This phenomenon is more notable at higher temperatures (37 °C), where the measured storage modulus increased by up to 21.9 times. Partial recovery of stiffness was observed after rehydration. In temperature sweep analysis, a strong stiffening trend emerged when no moisture control was applied, whereas the opposite trend was observed under full humidity control, with both storage and loss moduli decreasing by 1.4 and 1.6 times at 37 °C compared to 22 °C, respectively. Despite these findings, many studies on human brain tissue mechanics have been conducted at room temperature (22 or 24 °C, see Table 2) rather than at physiological temperature (37 °C), often overlooking the effects of temperature [30,33,95,197,241]. This oversight is likely based on early evidence derived from animal brain tests [107], though these were based only on discrete comparisons at 22 °C and 37 °C, not a continuous temperature sweep like in the study of Forte, et al. [42]. Therefore, to reduce potential artifacts introduced by temperature variability, it is recommended to maintain environmental temperature close to physiological conditions (37 °C) during mechanical testing of human brain tissue.

3.1.5. *Loading rate–dependent behavior of human brain tissue*

In dynamic testing of the human brain tissue, viscoelasticity-related measures such as storage and loss modulus, are commonly found to be frequency dependent, as shown in Fig. 7(a)-(b). Regardless of differences in testing methods, loading modes, or deformation levels, a consistent trend was observed that both the elastic (storage) and viscous (loss) resistance of the brain increased with frequency, reflecting enhanced stiffness and energy dissipation at higher loading rates. Analogously, as demonstrated in Fig. 7(c)-(d), the human brain exhibits pronounced compression or shear softening under prolonged loading, underscoring its time-dependent mechanical behavior. These viscoelastic attributes highlight the strong sensitivity of the brain mechanical response to the rate of applied loading. Fig. 8 further illustrate this rate dependence by collecting stress-strain data reported from various AMT studies on the human brain, with Fig. 8(a)-(c) focusing on small deformation cases ($\epsilon_{max} < 0.25$) and Fig. 8(d)-(f) on large deformation range ($\epsilon_{max} > 0.25$). The tested brain regions and corresponding loading rates are also present in the figure legend for inter- and intra-study comparison. As seen in the Fig. 8, the human brain exhibits a pronounced strain rate stiffening behavior. For example, in the study by Zhu, et al. [25], the maximum stress in the corona radiata at 65 % strain was nearly 2.5 times higher when the strain rate increased from 0.8 s^{-1} to 40 s^{-1}, emphasizing the importance of loading rate control in accurately characterizing brain mechanics.

3.1.6. *Conditioning effects on human brain mechanics*

The preconditioning effect is also evident in human brain tissue mechanical testing. After conditioning, brain tissue responses tend to become more stable and repeatable. Therefore, the data recorded during post-conditioning cycles—typically the second or third—are frequently used for calibrating constitutive models [24,30,41]. The conditioning effects is generally attributed to microstructural adjustments or minor damage occurring during the initial loading cycles.

Interestingly, preconditioning behavior appears to be recoverable under small deformations. For instance, Budday, et al. [30] observed that brain tissue, after resting for one hour, could fully recover and display a similar preconditioning response as in the initial test. Based on this, they attributed this effect to reversible changes in tissue state—such as interstitial fluid redistribution or recoverable intracellular interactions—rather than the irreversible microstructural damage like microstructural reorganization, owing to the porous and fluid-saturated nature of brain tissue. Moreover, Budday, et al. [126] emphasized that data collected during the preconditioning phase are also valuable as reflections of *in vivo* physiological conditions, while the conditioned data can serve as reproducible baseline for *ex vivo* mechanical testing. Similarly, all of the reported stress-strain data, as depicted in Fig. 8, are valuable regarding different research and clinical objectives. Data obtained under quasistatic scenarios within the small deformation range are suitable for representing long-term brain behaviors, such as those associated with brain development, aging, or disease progression. In contrast, stress-strain data measured under large deformation and high loading rate are critical for capturing the brain's mechanical response over shorter timescales, as encountered in scenarios such as TBI.

3.1.7. *Modeling assumptions in human brain mechanics*

Human brain tissue mechanical characterizations are also influenced by the assumptions embedded in the constitutive models used to calibrate material parameters. Assumptions such as isotropy versus

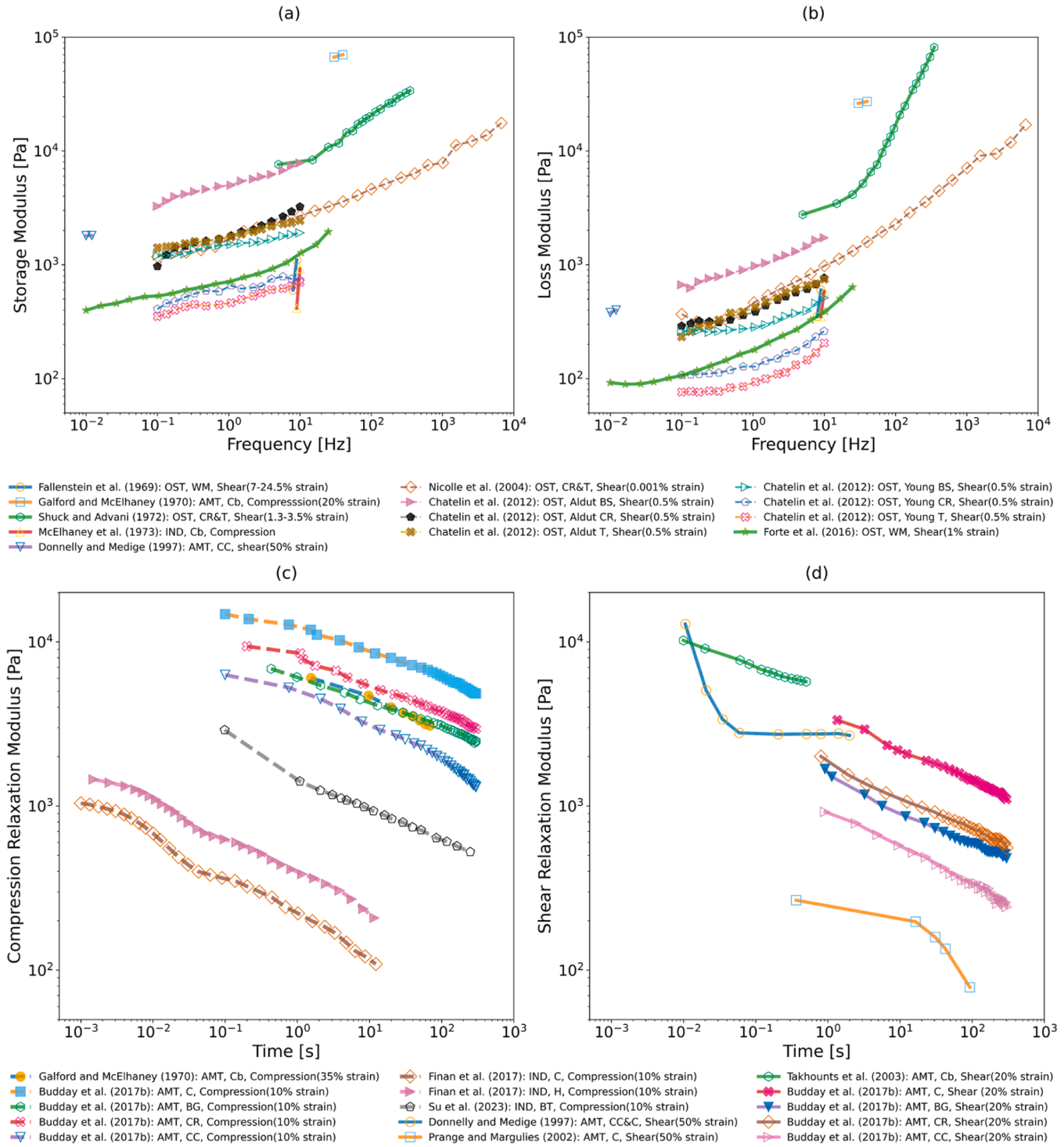

Fig. 7. Summary of various moduli reported in the literature for human brain tissue. Frequency-dependent storage modulus (a) and loss modulus (b); time-dependent compressive relaxation modulus (c) and shear relaxation modulus (d). The data references are provided along with the details on the testing methods, tested regions, loading modes, and the applied strains.

anisotropy, incompressibility versus compressibility, and the selection of material type—elastic, hyperelastic, viscoelastic, or poroelastic—can all lead to different interpretations of the same experimental data [26]. As summarized in Table 2, various constitutive models have been applied in current studies to capture the brain's complex mechanical responses. For long biological timescales, such as those involved in modeling brain development or growth, hyperelastic models—particularly the Ogden-type models—are well-suited for capturing nonlinear elastic behavior [26,30]. In such scenarios, where the timescale of loading significantly exceeds the tissue's characteristic relaxation time, viscoelastic effects become negligible, and a purely elastic approximation is appropriate. Conversely, at shorter timescales where the time-dependent effects become dominant, viscoelastic or poro-viscoelastic constitutive models provide a more accurate representation [24,42]. For example, Greiner, et al. [94] modeled brain tissue as a poro-viscoelastic medium, where the solid matrix—including the

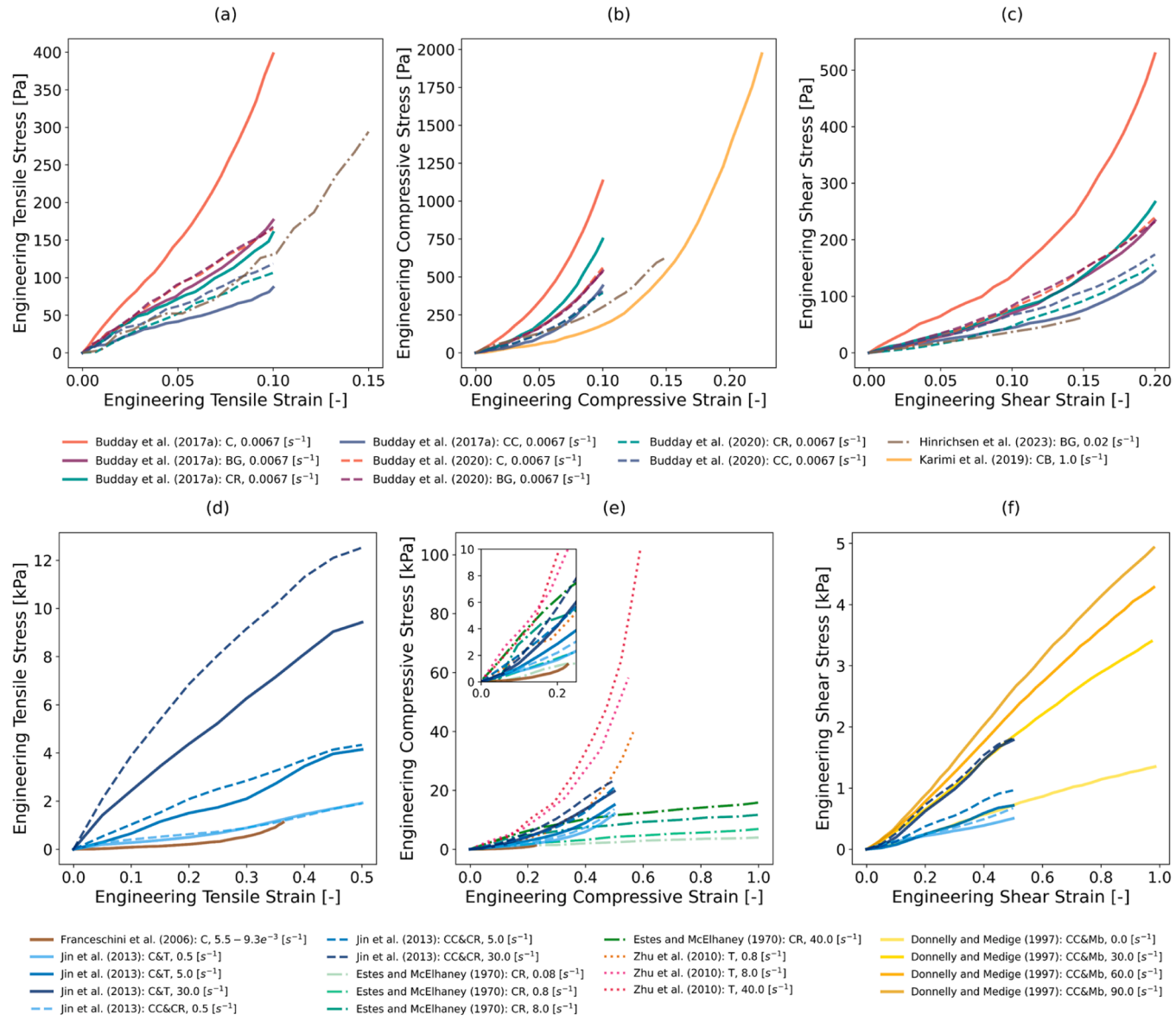

Fig. 8. Stress-strain curves of the human brain tissue under small and large deformation. (a)-(c) represent the tension, compression, and shear data measured within small deformation range. (d)-(f) represent the tension, compression, and shear data measured within large deformation range. The inset in (e) provides a zoom-in view of recorded curves for the first 20 % strain. All testing data were obtained through axial mechanical testing. The data references including details on the tested brain regions and applied strain rates are present at the bottom of the figure.

network of cells embedded within the extracellular matrix—accounts for the viscoelastic contribution, and the free-flowing interstitial fluid contributes to the poroelastic effect. Through parameter studies, they emphasized that the brain's nonlinear behaviors cannot be captured by a single effective modulus, as derived from simple indentation tests. Instead, a combination of cyclic and stress relaxation experiments across multiple loading modes is necessary for reliable calibration of viscoelastic parameters. They further attributed discrepancies between compression and indentation results to the intricate interplay of poroelastic and viscous effects with inherent material nonlinearities. In a follow-up study, Greiner, et al. [237] proposed a six-parameter poro--viscoelastic framework based on multiplicative decomposition, which successfully captured the brain's combined responses to cyclic tension, compression, and relaxation. Additionally, a pilot study by Su, et al. [197] proposed a novel scaling approach to separate poroelastic and viscoelastic contributions across time scale. By scaling the relaxation force and time with the square of the sample length, they revealed a clear transition point between the viscoelasticity-dominated short-time regime and the poroelasticity-dominated long-time regime.

3.2. *Noninvasive mechanical testing: in vivo, accessible, and diagnostic characterization*

For the noninvasive studies, we primarily focused on two techniques: MRE and USE. Given the substantial body of literature in this field, we selectively reviewed representative studies that offer meaningful insight into the potential of noninvasive methods for estimating brain mechanical properties. These studies are summarized in Table 3, which includes key details such as the number of subjects, age and gender distribution, interested brain regions, testing methods, frequencies used, reported shear modulus values, and the factors considered like the age, gender, and pathological conditions. In the following section, we briefly discuss the findings from these noninvasive studies, with a primary focus on their comparison to invasive testing results presented in Section 3.1. This comparison serves as the basis for a broader discussion on the difference between *in vivo* and *ex vivo* assessments of brain tissue

Table 3
Literature summary on non-invasive testing. **N**: subject number, female and male number are also presented; **Regions**: WB: whole brain, G: gray matter, W: white matter, C: cortex, T: thalamus, H: Hippocampus, CC: corpus callosum, BS: brain stem, CB: cerebellum, BT: brain tumor; **Testing Methods**: MRE: magnetic resonance elastography, USE: ultrasound elastography; **Glo/Dis**: shear modulus of the global brain tissue or diseased brain tissue, *f25* indicates the modulus measured at the frequency of 25 Hz; **Age**: effect of age considered in the study,"0": no significant effect, "-": negative correlation (decrease with age), "+": positive correlation; **Gender**: gender effect considered in the study, ($F > M$): shear stiffness of female brain greater than male brain; "0": no significant gender difference; Disease: diseased brain tissue been tested, BT: brain tumor, AD: Alzheimer's disease, E: Epilepsy, PD: Parkinson's disease, D: Dementia, NPH: Normal pressure hydrocephalus.

Literature	N (F/M)	Age (years)	Regions	Testing Methods	Frequency (Hz)	Shear Modulus [kPa]			Effects		
						Glo/Dis	Gray	White	Age	Gender	Disease
Kruse, et al. [135]	25 (–/–)	23–79	G,W	MRE	100		5.22	13.6	√(0)		
Sack, et al. [157]	55 (24/31)	18–88	WB	MRE	25–62.5	*f25*: 1.21 *f37.5*: 1.43 *f50*: 1.63 *f62.5*: 2.16			√(-)	√($F > M$)	
Sack, et al. [155]	66 (35/31)	18–72	WB	MRE	25–62.5	*f25*: 1.82 *f37.5*: 2.18 *f50*: 2.39 *f62.5*: 2.89			√(-)	√($F > M$)	
Weaver, et al. [140]	6 (2/4)	25–55	WB,W,G	MRE	100	2.34	2.14	2.40			
Guo, et al. [257]	23 (–/–)	22–72	W,CC,T	MRE	30–60		1.06	1.25			
Johnson, et al. [160]	7 (0/7)	24–53	CC,CR	MRE	50		2.27**	3.07**			
Murphy, et al. [98]	10 (2/8)	23–55	C,CB	MRE	60	2.99	3.10*				
Simon, et al. [165]	16 (11/5)	26–78	BT	MRE	45	1.40*		1.83*			√(BT)
Braun, et al. [161]	5 (0/5)	26–55	G,W	MRE	40–60		0.89	1.08			
McGarry, et al. [145]	2 (0/2)	24,51	G,W	MRE	1,50		2.20	2.80			
Su, et al. [205]	41 (19/22)	neonates	W,T,CB	USE	3.5e6				√(+)		
Huston III, et al. [170]	5 (0/5)	53–65	WB, C, CB	MRE	60	2.77/2.59	2.91*				√(D)
Chauvet, et al. [206]	63 (–/–)	24–85	BT	USE	9e6	11.01,7.9,3.82,5.57					√(BT)
Anderson, et al. [250]	1 (1/0)	28	WB,CC,CR	MRE	50	2.67**		2.94**			
Murphy, et al. [168]	48 (22/26)	–	WB, C, CB	MRE	60	2.51/2.40	2.65*				√(AD)
Kim, et al. [207]	21 (–/–)	neonates	G,W	USE	3–16e6				√(+)		
Lipp, et al. [169]	59 (24/35)	49–82	WB,C,T	MRE	30–60	1.04/0.96	1.06*				√(PD)
Hiscox, et al. [258]	24 (12/12)	19–30 66–73	G	MRE				2.82*	√(-)	√(0)	
Albayrak, et al. [209]	83 (42/41)	neonates	G,W,T	USE	1–6e6		8.58	6.81	√(+)	√(0)	
Tzschätzsch, et al. [99]	26 (9/17)	21–86	WB	USE	27–56	2.44					
Huang, et al. [133]	10 (4/6)	24–38	WB,G,W	MRE	40–60	*f40*: 2.57 *f50*: 3.04 *f60*: 3.27	*f40*: 2.24 *f50*: 2.82 *f60*: 3.33	*f40*: 3.36 *f50*: 3.78 *f60*: 3.85			
Dirrichs, et al. [211]	184 (–/–)	neonates		USE	1.5e7						√(NPH)
Yeung, et al. [158]	36 (–/–)	7–44	GW	MRE	30–60		*f30*: 1.07 *f40*: 1.50 *f60*: 2.21	*f30*: 1.12 *f40*: 1.54 *f60*: 2.24	√(0)		

(*continued on next page*)

Table 3 (*continued*)

Literature	N (F/M)	Age (years)	Regions	Testing Methods	Frequency (Hz)	Shear Modulus [kPa]			Effects		
						Glo/Dis	Gray	White	Age	Gender	Disease
Kalra, et al. [253]	28 (17/11)	18–62	WB,G,CB,T,CC	MRE	60	1.51*	1.47*	1.48*	√(-)	√(0)	
Lv, et al. [255]	46 (22/24)	26–76	G,W	MRE	40–90				√(-)		
Schrank, et al. [259]	12 (0/12)	23–58	WB	MRE	20–40				√(-)		
Hiscox, et al. [260]	134 (56/78)	18–35	WB,G,W,H,T,CC,CR	MRE	50	2.62	2.37	2.95		√(*F* < *M*)	
Huesmann, et al. [172]	12 (10/2)	26–61	H	MRE	50						√(E)
Smith, et al. [173]	4 (1/3)	2–32	CC	MRE	50			3.78			
Takamura, et al. [261]	50 (25/25)	20–69	WB,G,CB	MRE	60	2.34	2.32*		√(-)	√(0)	
Ozkaya, et al. [159]	26 (13/13)	7–17	WB,G,W	MRE	40–80	*f40*: 1.69 *f60*: 2.37 *f80*: 2.75	*f40*: 1.65 *f60*: 2.35 *f80*: 2.74	*f40*: 1.83 *f60*: 2.45 *f80*: 2.76	√(0)	√(*F* > *M*)	
Chan, et al. [227]	35 (20/15)	1–62	BT	USE	3–15e6						√(BT)
Garcés Iñigo, et al. [213]	57 (25/32)	neonates	T,CC	USE	4–9e6		1.17	1.60	√(0)	√(0)	
Qiu, et al. [138]	3 (–/–)	23–25	WB,G,W	MRE	30–60	*f30*: 1.03 *f40*: 1.47 *f50*: 2.35 *f60*: 3.13	*f30*: 0.94 *f40*: 1.28 *f50*: 2.01 *f60*: 2.74	*f30*: 1.15 *f40*: 1.66 *f50*: 2.67 *f60*: 3.53			
Smith, et al. [174]	17 (7/10)	22–30	G,W,CC,CR	MRE	50		2.68	2.79			
McIlvain, et al. [154]	125 (62/63)	5–35	WB,G,W,H,T	MRE	50	3.17	3.20	3.22	√(-)		
Burman Ingeberg, et al. [148]	8 (3/5)	21–33	G,W	MRE	50	0.21	0.20	0.22			
Parker, et al. [256]	28 (8/20)	22–79	WB,G,W	MRE	50				√(-)		
Qiu, et al. [139]	15 (8/7)	22–28	WB,G,T	MRE	50	2.40*	2.64*				
Karki, et al. [171]	137 (–/–)			MRE	60						√(NPH)
Klemmer Chandía, et al. [215]	10 (9/1)	25–40	C	USE	27–56		1.30		√(-)		
Triolo, et al. [163]	18 (9/9)	24–31	WB,G,W,C,H,T,CC	MRE	50	2.73	2.70	2.84			
Yu, et al. [216]	1 (1/0)	–	BT	USE	180–300	1.47/2.37					√(BT)
Ma, et al. [176]	11 (–/–)	23–29	WB,G,W	MRE	30	1.95**	1.85**	2.14**			
Wang, et al. [149]	9 (7/2)	21–24	WB,G,W	MRE	20	2.01	1.98	2.16			

* values averaged across subregions or multiple scans,.
** values converted from complex modulus.

mechanical properties.

Compared to invasive testing, noninvasive testing generally includes more participants, often including dozens or hundreds of participants (see Table 3). This is primarily due to the key advantages of noninvasive, which can assess brain mechanical properties *in vivo* without the need for surgical intervention or tissue extraction. As a result, these methods pose minimal risk and discomfort to participants, making recruitment easier and more ethically feasible, particularly in healthy populations. The availability of large datasets enables more robust statistical analyses, thereby improving the reliability and generalizability of findings

across various populations and conditions. Additionally, noninvasive testing is capable of characterizing regional brain properties. Using an accurate anatomical atlas, techniques such as MRE are able to quantify material properties in small or deep-located brain structures, which are significantly challenging in sample preparation for *ex vivo* testing. For example, McIlvain, et al. [154] utilized high-resolution MRE to investigate regional mechanical properties in both pediatric and adult brains across an age range of five to 35 years. Through anatomical parcellation, they successfully mapped age-related trajectories of stiffness and damping ratio in multiple brain regions, including finely parcellated cortical areas and deep structures such as the Hippocampus, Caudate, and Amygdala. Their findings highlighted distinct maturation patterns in mechanical properties across different regions.

Though the presence of anisotropy in human brain tissue remains debated in invasive mechanical testing, noninvasive techniques—particularly MRE—have increasingly reported evidence of anisotropic mechanical behavior, especially in white matters structures [173,182,249–251]. For instance, Romano, et al. [252] developed a waveguide elastography (WGE) method that integrates MRE, diffusion tension imaging (DTI), and anisotropic inversion to estimate direction-dependent elastic properties of white matter. Their findings revealed reduced anisotropic shear moduli—both parallel and perpendicular to the corticospinal tracts—in patients with amyotrophic lateral sclerosis (ALS) compared to healthy controls. In parallel, Kalra, et al. [253] used similar techniques to investigate the effects of aging on brain anisotropic stiffness in healthy individuals. They observed distinct age-related trends across different components of the elasticity stiffness tensor ($C_{11},\ C_{22},\ldots,C_{66}$) in various anatomical regions. Notably, while gray matter exhibited a generalized decline in all elasticity components with age, the thalamus showed a pronounced decrease specifically in C_{33}. To improve the accuracy of anisotropic parameter estimation, McGarry, et al. [254] developed a finite element-based transverse isotropic nonlinear inversion (TI-NLI) algorithm. This method reconstructs detailed maps of brain anisotropic properties using multi-excitation MRE displacement data and fiber orientation derived from DTI, with validation through realistic simulation datasets. Using this framework, Smith, et al. [174] quantified the potential anisotropy for various brain structures, reporting the highest levels in coronal radiata, where tensile anisotropy reached 1.049 ± 0.144 and shear anisotropy 0.164 ± 0.047. Notably, even within the same anatomical structure—such as corpus callosum—the anisotropic mechanical properties varied substantially among its subregions (genu, body, and splenium). These differences are expected considering the distinct fiber densities and alignments characteristic within each subregion. More recently, Ma, et al. [176] introduced a traveling wave expansion (TWE)-based inversion framework that analytically decomposes complex MRE displacement fields into slow and fast shear wave components. By incorporating physically meaningful differential operators and multi-frequency data fusion, this method enables rapid and direct estimation of viscoelastic anisotropy without relying on iterative finite element solvers. Validation using human brain MRE datasets demonstrated that the extracted anisotropic parameters closely reflected known fiber architecture, affirming both the accuracy and robustness of the proposed framework. With the continued refinement of inversion algorithms and integration of multimodal imaging, these noninvasive approaches are becoming increasingly powerful and reliable tools for characterizing brain anisotropy.

Similar to findings from invasive testing, studies using MRE and USE have consistently reported frequency-dependent mechanical behavior in brain tissue, specifically the phenomenon of frequency-stiffening [133,138,157–159]. This trend reflects the viscoelastic nature of brain tissue, wherein higher loading frequencies constrain the time available for internal structural processes such as fluid redistribution, resulting in increased resistance to deformation and thus elevated apparent shear stiffness [255]. However, results on age-related effects exhibit substantial inter-study variability. During early development, particularly in neonates, brain stiffness has been shown to increase with age, reflecting active neurodevelopmental processes such as extracellular matrix maturation and changes in the neural stem cell microenvironment [205,207,213]. In contrast, adult aging is generally associated with a progressive decline in brain stiffness. For example, Sack and their colleagues observed a pronounced age-related softening, reporting a reduction in stiffness of approximately 0.75 % to 0.8 % per year [155,157]. Their findings were supported by McIlvain, et al. [154] and Klemmer Chandía, et al. [215] in their brain aging analyses using MRE and USE, respectively. The softening of brain tissue in adults has been attributed to increased water content—particularly within the glymphatic system—and loss of structural integrity in gray matter [256]. Notably, Parker, et al. [256] reported region-specific water-related stiffness changes in adult human brain, where grey matter stiffness decreases inversely to the square of the water fraction, whereas white matter followed an inverse two-thirds power law. However, some MRE studies have found no significant correlation between age and brain stiffness [135,158,159]. These inconsistencies may be driven by differences in imaging resolution, anatomical specificity, subject demographics, or methodological variations.

Gender-related differences in brain mechanical properties have also been explored. Some studies reported that female brains exhibit higher stiffness compared to male brains [155,157,159], while other investigations using USE found no significant discrepancy between sexes [209,213]. Moreover, the distinction between healthy and pathological brain tissue has been examined across various neurological conditions. Altered mechanical properties have been observed in cases of brain tumors [153,165,206,216,227], AD [168], epilepsy [172], PD [169], dementia [170] and normal pressure hydrocephalus [171,211].

An interesting observation from noninvasive testing methods is the finding that white matter appears consistently stiffer than gray matter in both MRE and USE measurements. In contrast, invasive testing methods show mixed trends in brain shear stiffness, as shown in Fig. 4a. To provide a comparative overview, we compile the shear stiffness values obtained from both invasive and noninvasive approaches, alongside the instantaneous shear stiffness values for reference, as shown in Fig. 9. Noninvasive measurements generally yield higher shear stiffness values compared to invasive methods (Fig. 9a), and these values tend to fall within the range of instantaneous shear stiffness (Fig. 9b). This outcome is within expectation and can be attributed to several factors. Invasive methods such as AMT, OST, or IND typically rely on post-conditioning data for parameter calibration. These values are naturally lower than preconditioning responses due to potential microstructural reorganization or redistribution of interstitial fluid, as discussed in Section 3.1. In this context, preconditioning data may more closely resemble *in vivo* mechanical behavior [126]. Additionally, tissue degradation in post-mortem samples further contributes to the lower shear stiffness reported in *ex vivo* studies. This contrast between invasive and noninvasive results ties into the broader discussion of *in vivo* versus *ex vivo* (or *in vitro*) mechanical characterization, which is an ongoing debate explored in numerous studies [21,43,45,262].

However, inter-study comparisons of human brain mechanics are extremely limited due to ethical considerations that make invasive *in vivo* testing on human subjects both difficult and controversial. A rare example is the pilot study by Schiavone, et al. [47], who introduced a light-based aspiration device for post-operative *in vivo* elasticity measurements. However, this method was restricted to shallow cortical indentation (1–3 mm) of cortex and suffered from measurements artifacts due to poor synchronization between applied pressure and imaging-based deformation tracking. Conversely, the reliability of intra-study comparison is also limited by methodological inconsistencies, including difference in sample characteristics (e.g., subject variation, anatomical location, sample dimension), testing conditions (e.g., apparatus, temperature, humidity, loading rate), and data interpretation approaches (e.g., model assumptions, calibration techniques). Noninvasive results are further affected by factors such as

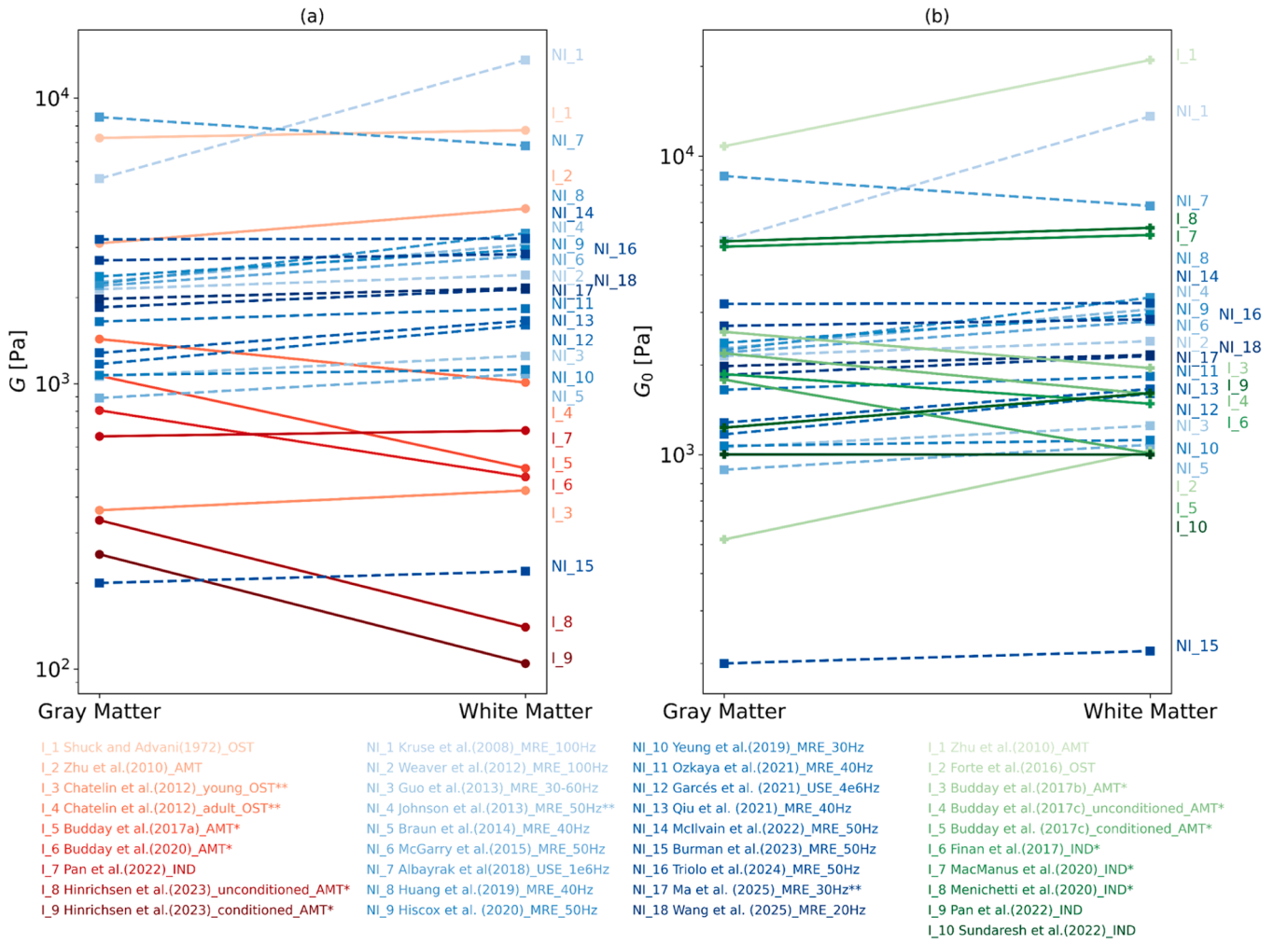

Fig. 9. Comparison of gray matter and white matter shear properties from both invasive and non-**invasive studies**. Data compiled from Tables 2 and 3. (a) Shear modulus (G) from invasive and noninvasive measurements; (b). Instantaneous shear modulus (G_0) from invasive studies compared to shear modulus from noninvasive studies. For studies reporting multiple regions within gray or white matter (marked with *), modulus values are averaged across regions. The magnitude of complex modulus was calculated for studies only reporting loss and storage modulus (marked with **). In the study by Zhu, et al. [25], shear modulus was derived using the standard linear elastic relationship $G = E/(2(1+\nu))$, assuming incompressibility. In study by Budday, et al. [30], the shear modulus was chosen from simultaneous fit using a modified one-term Ogden model. In the study by Chatelin, et al. [120], the stiffness value measured under lowest frequency was selected. Note: The values presented in this figure are drawn from studies employing diverse experimental setups, measurement modalities, and tissue conditions. As such, direct quantitative comparisons should be interpreted with caution.

actuation frequency, operator expertise, imaging quality, and data post-processing. As such, it remains a major challenge to determine which testing methods best reflects the actual mechanical behavior of human brain tissue or quantify the discrepancy between *in vivo* and *ex vivo* results presuming the former as a golden standard. An alternative approach is to use the animal brains for comparative analyses. Table 4 provides a summary of selected animal studies to offer insights into the differences between *in vivo* and *ex vivo* testing conditions. Although animal studies provide valuable insights and controlled environments for experimentation, caution must be exercised when extrapolating their results to human brain mechanics, particularly in the context of clinical relevance and model calibration.

Another important consideration when comparing *in vivo* and *ex vivo* brain experiments is the presence of physiological perfusion and pulsatile dynamics *in vivo* states, which are largely absent or markedly altered in *ex* vivo conditions [265]. This transition to a non-physiological environment may significantly change the mechanical behavior of brain tissue. Several studies have demonstrated that arterial pulsation plays a non-negligible role in modulating brain tissue mechanics. For example, Hirsch, et al. [266] showed that the central cerebrum undergoes harmonic expansion in response to arterial pulsation, with intracranial volumetric strain exhibiting sensitivity to venous pressure modulated by abdominal muscle contractions. Schrank, et al. [259] further advanced this understanding by employing cardiac-gated steady-state MRE to measure viscoelastic variations during the cardiac cycle. Their findings indicated that brain tissue becomes softer and more viscous during systole stage, with stiffness decreasing by 6.6 ± 1.9 % and the phase angle of the complex modulus increasing by 0.5 ± 1.9 %. Notably, the magnitude of this softening effect diminished slightly with age, at a rate around 0.1 ± 0.05 % per year. More recently, Meyer, et al. [267] introduced a noninvasive time-harmonic elastography technique capable of real-time monitoring the brain stiffness synchronized with arterial pulsation. Using this method, they observed global stiffness fluctuations across the brain in phase with the cardiac cycle. Specifically, the brain stiffness in healthy volunteers increased from minimum values during cerebral diastole to peak values during systole, with changes on the order of approximately 10 %. These findings highlight the importance of considering the absence of perfusion and pulsation in *ex vivo* measurements, as their omission may lead to systematic mischaracterization of physiological brain stiffness.

Table 4
Summary of animal brain studies conducted *in vivo, in situ, in vitro*, and *ex vivo*. PMI: post-mortem interval. IND: indentation, OST: oscillatory shear test, MRE: magnetic resonance elastography, USE: ultrasound elastography.

Literature	Animals	Methods					Findings
		in vivo	*in situ*	*in vitro*	*ex vivo*	PMI	
Fallenstein, et al. [199]	Monkey	OST		OST		2–5h	No significant difference between loss tangent *in vivo* and *in vitro*.
Gefen, et al. [263]	Porcine	IND	IND	IND		6h	Long-term time constant of relaxation significantly decreased form *in vivo* to *in situ* modes; Preconditioning decreased the shear moduli, with a more pronounced effect *in situ* and *in vitro*.
Vappou, et al. [235]	Rat	MRE			MRE	0.5–24h	Significant increase in shear storage modulus of about 100 % was found to occur just after death; Insignificant difference between shear loss moduli *in vivo* and *ex vivo* (0.5 h), and a decrease of about 50 % was found to occur after 24 h.
Prevost, et al. [86]	Porcine	IND	IND	IND		6–7h	The indentation response was significantly stiffer *in situ* than *in vivo* by a factor of 1.5–2; The indentation response *in vitro* was more compliant than *in situ*, with peak forces 20 % lower *in vitro*.
Urbanczyk, et al. [264]	Porcine	USE	USE	USE		4–5h	Shear modulus *in situ* and *in vitro* were 37 % and 22 % higher than *in vivo* moduli; Brain stiffness decreases with increased temperature (23 %) and external confinement (22–37 %).
Guertler, et al. [236]	Porcine	MRE			MRE	2h	Brain tissue *in vivo* appears stiffer than *ex vivo* at frequencies of 100 Hz and 125 Hz; Brain mechanical difference between *in vivo* and *ex vivo* becomes smaller at lower frequencies.
Liu, et al. [210]	Rabbit	USE			USE	1h	Shear modulus from *in vivo* measurements is about 47 % higher than *ex vivo* measurements; The change in *ex vivo* elastic properties within 60-min post-mortem is negligible.

4. Summary, challenges, and perspectives

As the most functionally complex and vital organ in the human body, the brain exhibits highly intricate and unique mechanical behaviors. Understanding these properties is essential not only for deepening our knowledge of fundamental brain physiology but also for informing clinical applications such as surgical planning, trauma modeling, and disease diagnosis. However, accurately characterizing brain mechanics remains exceptionally challenging due to their biphasic composition, extreme softness and fragility, and the structural heterogeneity arising from its diverse cellular populations and anatomically distinct subregions. In this review, we systematically introduced the most commonly used mechanical testing techniques applied to brain tissue, including both invasive approaches (AFM, IND, AMT, and OST) and noninvasive modalities (MRE and USE). Each of these techniques offers specific advantages and faces particular limitations, and their applicability is often dictated by distinct spatial and temporal requirements, as well as the experimental context. For example, AFM and IND are well-suited for probing localized mechanical properties at multiple resolutions, ranging from the cellular or subcellular to the tissue level, but their testing accuracies are sensitive to the geometry of the indenter tip and the mechanical models for characterization. AMT and OST provide versatile platforms for assessing regional mechanical properties and capturing nonlinear, anisotropic behaviors, yet often require complex sample preparations and are susceptible to boundary effects induced by tissue fixation. On the other hand, MRE and USE enable noninvasive, *in vivo* mapping of brain mechanics with broad spatial coverage, supporting large-cohort studies and regional analyses. These techniques offer substantial penetration depth and near full-brain coverage, however, they are generally limited to small deformations and rely on simplifying model assumptions, such as linear viscoelasticity and homogeneity. Notably, such assumptions also apply to many invasive methods and should be considered when interpreting any modality's results. By summarizing these techniques, we aim to provide a practical reference for researchers and clinicians in selecting the appropriate tools for investigating brain biomechanics across different application domains.

Recognizing the limitations of animal models due to species-specific differences, we further reviewed existing publications focused on examining the mechanical properties of human brain tissue. These studies were presented separately according to invasive and noninvasive approaches. We systematically summarized and compared the reported material properties, testing conditions, and parameter calibration strategies across all the studies reviewed. Invasive methods revealed a broad spectrum of mechanical properties, with various shear-related moduli values spanning several orders of magnitude. This variability is largely attributed to differences in tissue preparation, environmental testing conditions (e.g., temperature and humidity), and preconditioning effects, as well as post-mortem degradation in *ex vivo* samples. Noninvasive methods, in contrast, facilitated population-level assessments in terms of age, gender, and pathological conditions. These studies also revealed more consistent trends, such as higher stiffness observed in white matter relative to gray matter, although their spatial resolution and interpretability remain constrained by model-based assumptions. Furthermore, we found that the choice of constitutive modeling frameworks—ranging from linear elastic and hyperelastic to viscoelastic and poroelastic—also influences how mechanical properties are interpreted and reported. Based on our review and analysis, we suggest the following perspectives as potential considerations for advancing future studies on human brain tissue mechanical experiments:

4.1. Standardized and clearly reported testing conditions are critical

In mechanical testing of brain tissue, it is imperative to report sampling information and experimental settings with clarity and precision. This includes, but is not limited to, (1) subject-related details: age, gender, and any relevant pathological conditions; (2) critical sampling parameters for invasive testing: post-mortem interval, anatomical locations and orientation of the extracted tissue, preservation method, specimen's geometry and dimensions, humidity control, and testing temperature; (3) loading conditions: testing apparatus, preconditioning, loading rate or frequency, the deformation ranges, and method of data acquisition; (4) model assumption: compressibility, mechanical simplifications, and the choice of constitutive models. All of these factors can influence the measured outcomes of brain tissue. Comprehensive and transparent reporting of this information not only enhances the reproducibility of experimental findings but also facilitates meaningful intra- and inter-study comparisons, offering valuable guidance for future research in the field.

4.2. Noninvasive methods are promising but cannot fully replace invasive techniques

Noninvasive techniques such as MRE and USE provide powerful capabilities for measuring brain mechanical properties *in vivo*. These methods enable large-scale studies and longitudinal assessments without the need for tissue extraction. However, their accuracy is highly

sensitive to the imaging resolution, operator experience, and efficiency of shear wave excitation mechanisms. Both MRE and USE operate within the small-strain regime, limiting their ability to capture the nonlinear mechanical responses that arise under large deformations. Such large-strain behavior is particularly important for calibrating constitutive models used in computational brain biomechanics, including traumatic brain injury [8], brain development [268], neurosurgical brain shift [269], and implant–tissue interactions [270]—where brain tissue experiences significant deformation across a wide range of spatial and temporal scales. Additionally, the calibration of mechanical parameters often relies on simplifying assumptions and predefined mechanical models, which may not fully capture the brain's complex mechanical responses. Invasive methods, though facing ethical constraints in human studies, remain indispensable for obtaining high-fidelity data, particularly in cases requiring fine-scale or multi-modal testing. Moreover, the invasive methods enable direct measurement of continuous force-displacement or stress-strain relationships under controlled loading conditions, offering critical insights into brain mechanical behavior and serving as a foundation for robust material model development. Albeit with current limitations, elastography-based noninvasive methods still hold great promise in transforming the measurement paradigm. With ongoing advancements in imaging techniques and inversion algorithms—particularly those leveraging machine learning (ML) [151,184,185]—noninvasive methods such as MRE and USE are expected to become increasingly accurate, efficient, and clinically viable, thereby narrowing the gap that currently exists between practicality and precision in brain biomechanics. However, it is important to note that current neural network-based inversion methods still face challenges related to generalizability, interpretability, and uncertainty estimation. For instance, while approaches like ElastoNet demonstrate improved performance and include uncertainty quantification mechanisms [271], broader concerns around deep learning reliability in medical imaging—such as poorly calibrated predictions and "black-box" behavior—remain prevalent [272]. Addressing these limitations is essential for ensuring the reliability and credibility of both scientific research and clinical applications.

4.3. *Multiscale and multimodal testing should be encouraged to capture the full mechanical landscape*

Brain tissue exhibits distinct mechanical behaviors across spatial and temporal scales. Techniques such as AFM enable the probing of nano- or microscale stiffness heterogeneity, while AMT provide insight into bulk tissue responses. Integrating data from multiple modalities (e.g., AFM, IND, AMT, MRE) across different scales allows for a more comprehensive understanding of how microstructure features influence overall tissue mechanics, thereby improving the fidelity of biomechanical models [115,273]. To date, no single constitutive model with a unified parameter set can fully capture the complex mechanical responses of brain tissue under all loading scenarios. Each deformation mode—whether tension, compression, or shear—reveals unique aspects of the tissue's behavior. Therefore, incorporating multimodal experimental data into mechanical characterization is crucial for enhancing the robustness, generalizability, and predictive accuracy of constitutive models. Such integrative approaches are essential for building a more complete and realistic representation of brain tissue mechanics.

4.4. *Inverse modeling with FEM offers a more accurate and physically reliable characterization of material parameters*

Given the complex deformation patterns and boundary conditions involved in brain mechanics, inverse parameter identification methods, especially those using FEM, are essential for accurately extracting material properties [274]. These approaches allow researchers to go beyond simple curve fitting and simulate the actual testing environment, effectively reducing artifacts introduced by the boundary effects, sample geometry inconsistencies, or deformation caused by gravitational force [25,94]. Conventional FEM-based inverse identification often presumes a specific material model, such as hyperelastic, viscoelastic, poroelastic, or combined forms, followed by iterative optimization of the model parameters. This is done by minimizing the discrepancy between simulated mechanical responses (deformation or stress) and experimental observations [275]. While this strategy generally yields more reliable parameter calibration than direct fitting of experimental data, it is often computationally expensive and time-consuming regarding FEM modeling. Moreover, the reliance on predefined material model forms inherently constrains the discovery of novel constitutive behaviors or unanticipated mechanical features present in experimental data. Emerging approaches based on ML, including data-driven inverse modeling and automated parameter discovery framework, have shown promise in overcoming these limitations [276–278].

4.5. *While precision matters, relative trends often suffice for clinical applications*

Brain tissue is composed of a diverse array of living cells, each contributing to its structurally and functionally heterogeneous nature. Given its dynamic and evolving properties—shaped by factors like age, microstructural remodeling, and disease progression—achieving a universally "accurate" mechanical parameter is often unrealistic. For many clinical applications, such as disease diagnosis or monitoring, it is more meaningful to assess relative changes in tissue stiffness, spatial gradients, and temporal trends, or propose a safe physiological range, rather than relying solely on absolute material constants. As a result, *in vivo* techniques like USE are more frequently applied in clinical practice than in fundamental research. However, accurate and standardized testing protocols are also needed considering the wide variation in reported mechanical parameters (often spanning several orders of magnitude), especially in invasive testing.

Looking forward, we hope this review will serve as a valuable resource for advancing the field of brain biomechanics. We encourage future research to bridge the gap between *in vivo* and *ex vivo* findings, standardize testing protocols, and develop more physiologically relevant models that capture the complex, nonlinear, and time-dependent behavior of human brain tissue.

CRediT authorship contribution statement

Jixin Hou: Writing – original draft, Methodology, Investigation, Conceptualization. **Kun Jiang:** Writing – original draft, Conceptualization. **Arunachalam Ramanathan:** Writing – review & editing. **Abhishek Saji Kumar:** Writing – review & editing. **Wei Zhang:** Writing – review & editing. **Lin Zhao:** Writing – review & editing. **Taotao Wu:** Writing – review & editing. **Ramana Pidaparti:** Writing – review & editing. **Dajiang Zhu:** Writing – review & editing. **Gang Li:** Writing – review & editing. **Kenan Song:** Writing – review & editing, Conceptualization. **Tianming Liu:** Writing – review & editing. **Mir Jalil Razavi:** Writing – review & editing. **Ellen Kuhl:** Writing – review & editing. **Xianqiao Wang:** Writing – review & editing, Writing – original draft, Supervision, Funding acquisition, Conceptualization.

Declaration of competing interest

The authors declare that they have no known competing financial interests or personal relationships that could have appeared to influence the work reported in this paper.

Acknowledgement

JH, KJ, TL, and XW acknowledges the support from the National Science Foundation (IIS-2011369) and National Institutes of Health (1R01NS135574-01). KS acknowledges the support from Women and

Philanthropy Foundation (N/A), Arizona Biomedical Research Centre (award # RFGA2022-010-07), 2023 Mayo Clinic and Arizona State University Alliance for Health Care Collaborative Research Seed Grant (N/A), and the NSF Faculty Early Career Development Program (CAREER) award (2145895). GL acknowledges the support from the National Institutes of Health (EB037388), MJR acknowledges the support from the National Science Foundation (CMMI: 2123061).

Data Availability Statement

No data was used for the research described in this manuscript.

References

[1] T. Zhang, M.J. Razavi, X. Li, H. Chen, T. Liu, X. Wang, Mechanism of consistent gyrus formation: an experimental and computational study, Sci. Rep. 6 (1) (2016) 37272, https://doi.org/10.1038/srep37272.
[2] M.J. Razavi, T. Zhang, H. Chen, Y. Li, S. Platt, Y. Zhao, L. Guo, X. Hu, X. Wang, T. Liu, Radial structure scaffolds convolution patterns of developing cerebral cortex, Front. Comput. Neurosci. 11 (2017), https://doi.org/10.3389/fncom.2017.00076.
[3] P. Chavoshnejad, X. Li, S. Zhang, W. Dai, L. Vasung, T. Liu, T. Zhang, X. Wang, M. J. Razavi, Role of axonal fibers in the cortical folding patterns: a tale of variability and regularity, Brain Multiphys. 2 (2021) 100029, https://doi.org/10.1016/j.brain.2021.100029.
[4] M.J. Razavi, T. Liu, X. Wang, Mechanism exploration of 3-hinge gyral formation and pattern recognition, Cereb. Cortex. Commun. 2 (3) (2021), https://doi.org/10.1093/texcom/tgab044 tgab044.
[5] P. Chavoshnejad, L. Chen, X. Yu, J. Hou, N. Filla, D. Zhu, T. Liu, G. Li, M. J. Razavi, X. Wang, An integrated finite element method and machine learning algorithm for brain morphology prediction, Cereb. Cortex. 33 (15) (2023) 9354–9366, https://doi.org/10.1093/cercor/bhad208.
[6] A. Solhtalab, A.H. Foroughi, L. Pierotich, M.J. Razavi, Stress landscape of folding brain serves as a map for axonal pathfinding, Nat. Commun. 16 (1) (2025) 1187, https://doi.org/10.1038/s41467-025-56362-3.
[7] S. Ji, M. Ghajari, H. Mao, R.H. Kraft, M. Hajiaghamemar, M.B. Panzer, R. Willinger, M.D. Gilchrist, S. Kleiven, J.D. Stitzel, Use of brain biomechanical models for monitoring impact exposure in contact sports, Ann. Biomed. Eng. (2022), https://doi.org/10.1007/s10439-022-02999-w.
[8] T. Wu, J.A. Rifkin, A. Rayfield, M.B. Panzer, D.F. Meaney, An interdisciplinary computational model for predicting traumatic brain injury: linking biomechanics and functional neural networks, Neuroimage 251 (2022) 119002, https://doi.org/10.1016/j.neuroimage.2022.119002.
[9] J. Weickenmeier, E. Kuhl, A. Goriely, Multiphysics of prionlike diseases: progression and atrophy, Phys. Rev. Lett. 121 (15) (2018) 158101, https://doi.org/10.1103/PhysRevLett.121.158101.
[10] Y. Blinkouskaya, J. Weickenmeier, Brain shape changes associated with cerebral atrophy in healthy aging and alzheimer's disease, Front. Mech. Eng. 64 (2021).
[11] T. Tallinen, J.Y. Chung, J.S. Biggins, L. Mahadevan, Gyrification from constrained cortical expansion, Proc. Natl. Acad. Sci. 111 (35) (2014) 12667–12672.
[12] M.Jalil Razavi, T. Zhang, T. Liu, X. Wang, Cortical folding pattern and its consistency induced by biological growth, Sci. Rep. 5 (1) (2015) 14477, https://doi.org/10.1038/srep14477.
[13] T. Tallinen, J.Y. Chung, F. Rousseau, N. Girard, J. Lefèvre, L. Mahadevan, On the growth and form of cortical convolutions, Nat. Phys. 12 (6) (2016) 588–593, https://doi.org/10.1038/nphys3632.
[14] T.C. Harris, R. de Rooij, E. Kuhl, The shrinking brain: cerebral atrophy following traumatic brain injury, Ann. Biomed. Eng. 47 (9) (2019) 1941–1959, https://doi.org/10.1007/s10439-018-02148-2.
[15] T. Wu, M. Hajiaghamemar, J.S. Giudice, A. Alshareef, S.S. Margulies, M. B. Panzer, Evaluation of tissue-level brain injury metrics using species-specific simulations, J. Neurotrauma 38 (13) (2021) 1879–1888, https://doi.org/10.1089/neu.2020.7445.
[16] C. Zhang, L. Bartels, A. Clansey, J. Kloiber, D. Bondi, P. van Donkelaar, L. Wu, A. Rauscher, S. Ji, A computational pipeline towards large-scale and multiscale modeling of traumatic axonal injury, Comput. Biol. Med. 108109 (2024), https://doi.org/10.1016/j.compbiomed.2024.108109.
[17] A. Schäfer, J. Weickenmeier, E. Kuhl, The interplay of biochemical and biomechanical degeneration in Alzheimer's disease, Comput. Methods Appl. Mech. Eng. 352 (2019) 369–388, https://doi.org/10.1016/j.cma.2019.04.028.
[18] K. Miller, G.R. Joldes, G. Bourantas, S.K. Warfield, D.E. Hyde, R. Kikinis, A. Wittek, Biomechanical modeling and computer simulation of the brain during neurosurgery, Int. J. Numer. Method. Biomed. Eng. 35 (10) (2019) e3250, https://doi.org/10.1002/cnm.3250.
[19] C. Pan, Z. Huang, J. Zhou, X. Li, Brain stiffness in epilepsy's patients by indentation test, Mater. Today Commun. 30 (2022) 103227, https://doi.org/10.1016/j.mtcomm.2022.103227.
[20] A. Coelho, N. Sousa, Magnetic resonance elastography of the ageing brain in normal and demented populations: a systematic review, Hum. Brain Mapp. 43 (13) (2022) 4207–4218, https://doi.org/10.1002/hbm.25891.
[21] S. Budday, T.C. Ovaert, G.A. Holzapfel, P. Steinmann, E. Kuhl, Fifty shades of brain: a review on the mechanical testing and modeling of brain tissue, Arch. Comput. Methods Eng. 27 (4) (2020) 1187–1230, https://doi.org/10.1007/s11831-019-09352-w.
[22] K. Miller, K. Chinzei, Mechanical properties of brain tissue in tension, J. Biomech. 35 (4) (2002) 483–490, https://doi.org/10.1016/s0021-9290(01)00234-2.
[23] S. Budday, R. Nay, R. de Rooij, P. Steinmann, T. Wyrobek, T.C. Ovaert, E. Kuhl, Mechanical properties of gray and white matter brain tissue by indentation, J. Mech. Behav. Biomed. Mater. 46 (2015) 318–330, https://doi.org/10.1016/j.jmbbm.2015.02.024.
[24] G. Franceschini, D. Bigoni, P. Regitnig, G.A. Holzapfel, Brain tissue deforms similarly to filled elastomers and follows consolidation theory, J. Mech. Phys. Solids. 54 (12) (2006) 2592–2620, https://doi.org/10.1016/j.jmps.2006.05.004.
[25] F. Zhu, X. Jin, F. Guan, L. Zhang, H. Mao, K.H. Yang, A.I. King, Identifying the properties of ultra-soft materials using a new methodology of combined specimen-specific finite element model and optimization techniques, Mater. Des. 31 (10) (2010) 4704–4712, https://doi.org/10.1016/j.matdes.2010.05.023.
[26] J. Hinrichsen, N. Reiter, L. Bräuer, F. Paulsen, S. Kaessmair, S. Budday, Inverse identification of region-specific hyperelastic material parameters for human brain tissue, Biomech. Model. Mechanobiol. 22 (5) (2023) 1729–1749, https://doi.org/10.1007/s10237-023-01739-w.
[27] P.K. Viji Babu, M. Radmacher, Mechanics of brain tissues studied by atomic force microscopy: a perspective, Front. Neurosci. 13 (2019), https://doi.org/10.3389/fnins.2019.00600.
[28] A. Menichetti, D.B. MacManus, M.D. Gilchrist, B. Depreitere, J. Vander Sloten, N. Famaey, Regional characterization of the dynamic mechanical properties of human brain tissue by microindentation, Int. J. Eng. Sci. 155 (2020) 103355, https://doi.org/10.1016/j.ijengsci.2020.103355.
[29] F. Boudjema, B. Khelidj, M. Lounis, Dynamical properties of the brain tissue under oscillatory shear stresses at large strain range, J. Phys.: Conf. Ser. 790 (1) (2017) 012002, https://doi.org/10.1088/1742-6596/790/1/012002.
[30] S. Budday, G. Sommer, C. Birkl, C. Langkammer, J. Haybaeck, J. Kohnert, M. Bauer, F. Paulsen, P. Steinmann, E. Kuhl, Mechanical characterization of human brain tissue, Acta Biomater. 48 (2017) 319–340, https://doi.org/10.1016/j.actbio.2016.10.036.
[31] X. Wang, J. Lefèvre, A. Bohi, M.A. Harrach, M. Dinomais, F. Rousseau, The influence of biophysical parameters in a biomechanical model of cortical folding patterns, Sci. Rep. 11 (1) (2021) 7686, https://doi.org/10.1038/s41598-021-87124-y.
[32] P. Chavoshnejad, L. Vallejo, S. Zhang, Y. Guo, W. Dai, T. Zhang, M.J. Razavi, Mechanical hierarchy in the formation and modulation of cortical folding patterns, Sci. Rep. 13 (1) (2023) 13177, https://doi.org/10.1038/s41598-023-40086-9.
[33] D.B. MacManus, A. Menichetti, B. Depreitere, N. Famaey, J. Vander Sloten, M. Gilchrist, Towards animal surrogates for characterising large strain dynamic mechanical properties of human brain tissue, Brain Multiphys. 1 (2020) 100018, https://doi.org/10.1016/j.brain.2020.100018.
[34] D.B. MacManus, B. Pierrat, J.G. Murphy, M.D. Gilchrist, Region and species dependent mechanical properties of adolescent and young adult brain tissue, Sci. Rep. 7 (1) (2017) 13729, https://doi.org/10.1038/s41598-017-13727-z.
[35] G. Bertalan, J. Becker, H. Tzschätzsch, A. Morr, H. Herthum, M. Shahryari, R. D. Greenhalgh, J. Guo, L. Schröder, C. Alzheimer, S. Budday, K. Franze, J. Braun, I. Sack, Mechanical behavior of the hippocampus and corpus callosum: an attempt to reconcile ex vivo with *in vivo* and micro with macro properties, J. Mech. Behav. Biomed. Mater. 138 (2023) 105613, https://doi.org/10.1016/j.jmbbm.2022.105613.
[36] B. Rashid, M. Destrade, M.D. Gilchrist, Influence of preservation temperature on the measured mechanical properties of brain tissue, J. Biomech. 46 (7) (2013) 1276–1281, https://doi.org/10.1016/j.jbiomech.2013.02.014.
[37] G.M. Boiczyk, N. Pearson, V.B. Kote, A. Sundaramurthy, D.R. Subramaniam, J. E. Rubio, G. Unnikrishnan, J. Reifman, K.L. Monson, Rate- and region-dependent mechanical properties of Göttingen minipig brain tissue in simple shear and unconfined compression, J. Biomech. Eng. 145 (6) (2023), https://doi.org/10.1115/1.4056480.
[38] J. Weickenmeier, R. de Rooij, S. Budday, P. Steinmann, T.C. Ovaert, E. Kuhl, Brain stiffness increases with myelin content, Acta Biomater. 42 (2016) 265–272, https://doi.org/10.1016/j.actbio.2016.07.040.
[39] W. Li, D.E.T. Shepherd, D.M. Espino, Dynamic mechanical characterization and viscoelastic modeling of bovine brain tissue, J. Mech. Behav. Biomed. Mater. 114 (2021) 104204, https://doi.org/10.1016/j.jmbbm.2020.104204.
[40] S.V. Mangrulkar, S.V. Dabhekar, P. Neje, N. Parkarwar, A. Turankar, B. G. Taksande, M.J. Umekar, K.T. Nakhate, *In vivo* animal models development and their limitations for brain research, in: A. Alexander (Ed.), Application of Nanocarriers in Brain Delivery of Therapeutics, Springer Nature Singapore, Singapore, 2024, pp. 315–339.
[41] M.T. Prange, S.S. Margulies, Regional, directional, and age-dependent properties of the brain undergoing large deformation, J. Biomech. Eng. 124 (2) (2002) 244–252, https://doi.org/10.1115/1.1449907.
[42] A.E. Forte, S.M. Gentleman, D. Dini, On the characterization of the heterogeneous mechanical response of human brain tissue, Biomech. Model. Mechanobiol. 16 (2016) 907–920, https://doi.org/10.1007/s10237-016-0860-8.
[43] J. Bergs, A.S. Morr, R.V. Silva, C. Infante-Duarte, I. Sack, The networking brain: how extracellular matrix, cellular networks, and vasculature shape the *In vivo* mechanical properties of the brain, Adv. Sci. 11 (31) (2024) 2402338, https://doi.org/10.1002/advs.202402338.
[44] P.V. Bayly, A. Alshareef, A.K. Knutsen, K. Upadhyay, R.J. Okamoto, A. Carass, J. A. Butman, D.L. Pham, J.L. Prince, K. Ramesh, MR imaging of human brain mechanics in vivo: new measurements to facilitate the development of

computational models of brain injury, Ann. Biomed. Eng. 49 (2021) 2677–2692, https://doi.org/10.1007/s10439-021-02820-0.
[45] S. Chatelin, A. Constantinesco, R. Willinger, Fifty years of brain tissue mechanical testing: from *in vitro* to *in vivo* investigations, Biorheology 47 (2010) 255–276, https://doi.org/10.3233/BIR-2010-0576.
[46] H. Ozawa, T. Matsumoto, T. Ohashi, M. Sato, S. Kokubun, Comparison of spinal cord gray matter and white matter softness: measurement by pipette aspiration method, J. Neurosurg.: Spine 95 (2) (2001) 221–224, https://doi.org/10.3171/spi.2001.95.2.0221.
[47] P. Schiavone, F. Chassat, T. Boudou, E. Promayon, F. Valdivia, Y. Payan, *In vivo* measurement of human brain elasticity using a light aspiration device, Med. Image Anal. 13 (4) (2009) 673–678, https://doi.org/10.1016/j.media.2009.04.001.
[48] A.S. Mijailovic, S. Galarza, S. Raayai-Ardakani, N.P. Birch, J.D. Schiffman, A. J. Crosby, T. Cohen, S.R. Peyton, K.J. Van Vliet, Localized characterization of brain tissue mechanical properties by needle induced cavitation rheology and volume controlled cavity expansion, J. Mech. Behav. Biomed. Mater. 114 (2021) 104168, https://doi.org/10.1016/j.jmbbm.2020.104168.
[49] C.E. Dougan, Z. Song, H. Fu, A.J. Crosby, S. Cai, S.R. Peyton, Cavitation induced fracture of intact brain tissue, Biophys. J. 121 (14) (2022) 2721–2729, https://doi.org/10.1016/j.bpj.2022.06.016.
[50] C.E. Dougan, H. Fu, A.J. Crosby, S.R. Peyton, Needle-induced cavitation: a method to probe the local mechanics of brain tissue, J. Mech. Behav. Biomed. Mater. 160 (2024) 106698, https://doi.org/10.1016/j.jmbbm.2024.106698.
[51] P. Binner, I. Starshynov, G. Tejeda, A. McFall, C. Molloy, G. Ciccone, M. Walker, M. Vassalli, A.B. Tobin, D. Faccio, Optical, contact-free assessment of brain tissue stiffness and neurodegeneration, Biomed. Opt. Express. 16 (2) (2025) 447–459, https://doi.org/10.1364/BOE.545580.
[52] A. Bejgam, S. Rao, H.J. Pandya, Engineering approaches for characterizing soft tissue mechanical properties: a review, Clin. Biomech. 69 (2019) 127–140, https://doi.org/10.1016/j.clinbiomech.2019.07.016.
[53] E. Song, Y. Huang, N. Huang, Y. Mei, X. Yu, J.A. Rogers, Recent advances in microsystem approaches for mechanical characterization of soft biological tissues, Microsyst. Nanoeng. 8 (1) (2022) 77, https://doi.org/10.1038/s41378-022-00412-z.
[54] K. Navindaran, J.S. Kang, K. Moon, Techniques for characterizing mechanical properties of soft tissues, J. Mech. Behav. Biomed. Mater. 138 (2023) 105575, https://doi.org/10.1016/j.jmbbm.2022.105575.
[55] T.M. Bahwini, Y. Zhong, C. Gu, Z. Nasa, D. Oetomo, Investigating the mechanical properties of biological brain cells with atomic force microscopy, J. Med. Device 12 (4) (2018), https://doi.org/10.1115/1.4040995.
[56] E. Lobanova, D. Whiten, F.S. Ruggeri, C.G. Taylor, A. Kouli, Z. Xia, D. Emin, Y. P. Zhang, J.Y.L. Lam, C.H. Williams-Gray, D. Klenerman, Imaging protein aggregates in the serum and cerebrospinal fluid in Parkinson's disease, Brain 145 (2) (2021) 632–643, https://doi.org/10.1093/brain/awab306.
[57] D.T. She, M.H. Nai, C.T. Lim, Atomic force microscopy in the characterization and clinical evaluation of neurological disorders: current and emerging technologies, Med-X 2 (1) (2024) 8, https://doi.org/10.1007/s44258-024-00022-6.
[58] E.P. Canovic, B. Qing, A.S. Mijailovic, A. Jagielska, M.J. Whitfield, E. Kelly, D. Turner, M. Sahin, K.J. Van Vliet, Characterizing multiscale mechanical properties of brain tissue using atomic force microscopy, impact indentation, and rheometry, J. Vis. Exp. (115) (2016), https://doi.org/10.3791/54201.
[59] W. Runke, Q. Suo, J. Huijing, Y. Fuhua, Y. Guang-Zhong, F. Yuan, Multiscale measurement of brain tissue and cell biomechanics using a mouse model, Biophys. Rep. 0 (0) (2025), https://doi.org/10.52601/bpr.2024.240049.
[60] A.S. Morr, M. Nowicki, G. Bertalan, R. Vieira Silva, C. Infante Duarte, S.P. Koch, P. Boehm-Sturm, U. Krügel, J. Braun, B. Steiner, J.A. Käs, T. Fuhs, I. Sack, Mechanical properties of murine hippocampal subregions investigated by atomic force microscopy and *in vivo* magnetic resonance elastography, Sci. Rep. 12 (1) (2022) 16723, https://doi.org/10.1038/s41598-022-21105-7.
[61] M.M. Urbanski, M.B. Brendel, C.V. Melendez-Vasquez, Acute and chronic demyelinated CNS lesions exhibit opposite elastic properties, Sci. Rep. 9 (1) (2019) 999, https://doi.org/10.1038/s41598-018-37745-7.
[62] J. Najera, M.R. Rosenberger, M. Datta, Atomic force microscopy methods to measure tumor mechanical properties, Cancers. (Basel) 15 (13) (2023) 3285, https://doi.org/10.3390/cancers15133285.
[63] M. d. S. do Nascimento Amorim, Á.R.Silva França, R. Santos-Oliveira, J. Rodrigues Sanches, T. Marinho Melo, B. Araújo Serra Pinto, L.R.S. Barbosa, L. M.R. Alencar, Atomic force microscopy applied to the study of tauopathies, ACS. Chem. Neurosci. 15 (4) (2024) 699–715, https://doi.org/10.1021/acschemneuro.3c00819.
[64] S. De, D.R. Whiten, F.S. Ruggeri, C. Hughes, M. Rodrigues, D.I. Sideris, C. G. Taylor, F.A. Aprile, S. Muyldermans, T.P.J. Knowles, M. Vendruscolo, C. Bryant, K. Blennow, I. Skoog, S. Kern, H. Zetterberg, D. Klenerman, Soluble aggregates present in cerebrospinal fluid change in size and mechanism of toxicity during Alzheimer's disease progression, Acta Neuropathol. Commun. 7 (1) (2019) 120, https://doi.org/10.1186/s40478-019-0777-4.
[65] C.L. Essmann, D. Martinez-Martinez, R. Pryor, K.-Y. Leung, K.B. Krishnan, P. P. Lui, N.D.E. Greene, A.E.X. Brown, V.M. Pawar, M.A. Srinivasan, F. Cabreiro, Mechanical properties measured by atomic force microscopy define health biomarkers in ageing C. elegans, Nat. Commun. 11 (1) (2020) 1043, https://doi.org/10.1038/s41467-020-14785-0.
[66] B.S. Elkin, E.U. Azeloglu, K.D. Costa, B. Morrison Iii, Mechanical heterogeneity of the rat hippocampus measured by atomic force microscope indentation, J. Neurotrauma 24 (5) (2007) 812–822, https://doi.org/10.1089/neu.2006.0169.
[67] Y.-C. Chuang, A. Alcantara, G. Fabris, J. Abderezaei, T.-A. Lu, C.V. Melendez-Vasquez, M. Kurt, Myelination dictates axonal viscoelasticity, Eur. J. Neurosci. 57 (8) (2023) 1225–1240, https://doi.org/10.1111/ejn.15954.
[68] A.J. Thompson, E.K. Pillai, I.B. Dimov, S.K. Foster, C.E. Holt, K. Franze, Rapid changes in tissue mechanics regulate cell behaviour in the developing embryonic brain, Elife 8 (2019) e39356, https://doi.org/10.7554/eLife.39356.
[69] D.C. Lin, D.I. Shreiber, E.K. Dimitriadis, F. Horkay, Spherical indentation of soft matter beyond the hertzian regime: numerical and experimental validation of hyperelastic models, Biomech. Model. Mechanobiol. 8 (5) (2009) 345–358, https://doi.org/10.1007/s10237-008-0139-9.
[70] A. Jamal, A. Bernardini, D. Dini, Microscale characterisation of the time-dependent mechanical behaviour of brain white matter, J. Mech. Behav. Biomed. Mater. 125 (2022) 104917, https://doi.org/10.1016/j.jmbbm.2021.104917.
[71] J. Faber, J. Hinrichsen, A. Greiner, N. Reiter, S. Budday, Tissue-scale biomechanical testing of brain Tissue for the calibration of nonlinear material models, Curr. Protoc. 2 (2022), https://doi.org/10.1002/cpz1.381.
[72] B.S. Elkin, A. Ilankova, B. Morrison III, Dynamic, regional mechanical properties of the porcine brain: indentation in the coronal plane, J. Biomech. Eng. 133 (7) (2011), https://doi.org/10.1115/1.4004494.
[73] D.B. MacManus, B. Pierrat, J.G. Murphy, M.D. Gilchrist, Mechanical characterization of the P56 mouse brain under large-deformation dynamic indentation, Sci. Rep. 6 (1) (2016) 21569, https://doi.org/10.1038/srep21569.
[74] J. Weickenmeier, R. de Rooij, S. Budday, T.C. Ovaert, E. Kuhl, The mechanical importance of myelination in the central nervous system, J. Mech. Behav. Biomed. Mater. 76 (2017) 119–124, https://doi.org/10.1016/j.jmbbm.2017.04.017.
[75] N. Bailly, E. Wagnac, Y. Petit, Regional mechanical properties of spinal cord gray and white matter in transverse section, J. Mech. Behav. Biomed. Mater. 163 (2025) 106898, https://doi.org/10.1016/j.jmbbm.2025.106898.
[76] D.C. Stewart, A. Rubiano, K. Dyson, C.S. Simmons, Mechanical characterization of human brain tumors from patients and comparison to potential surgical phantoms, PLoS. One 12 (6) (2017) e0177561, https://doi.org/10.1371/journal.pone.0177561.
[77] I. Skambath, J. Kren, P. Kuppler, S. Buschschlueter, M.M. Bonsanto, An attempt to identify brain tumour tissue in neurosurgery by mechanical indentation measurements, Acta Neurochir. (Wien) 166 (1) (2024) 343, https://doi.org/10.1007/s00701-024-06218-4.
[78] N. Antonovaite, L.A. Hulshof, C.F.M. Huffels, E.M. Hol, W.J. Wadman, D. Iannuzzi, Mechanical alterations of the hippocampus in the APP/PS1 Alzheimer's disease mouse model, J. Mech. Behav. Biomed. Mater. 122 (2021) 104697, https://doi.org/10.1016/j.jmbbm.2021.104697.
[79] L. Qian, Y. Sun, Q. Tong, J. Tian, Z. Ren, H. Zhao, Indentation response in porcine brain under electric fields, Soft. Matter. 15 (4) (2019) 623–632, https://doi.org/10.1039/C8SM01272E.
[80] J.D. Finan, B.S. Elkin, E.M. Pearson, I.L. Kalbian, B. Morrison, Viscoelastic properties of the rat brain in the sagittal plane: effects of anatomical structure and age, Ann. Biomed. Eng. 40 (1) (2012) 70–78, https://doi.org/10.1007/s10439-011-0394-2.
[81] B.S. Elkin, B. Morrison, Viscoelastic properties of the P17 and adult rat brain from indentation in the coronal plane, J. Biomech. Eng. 135 (11) (2013), https://doi.org/10.1115/1.4025386.
[82] S.N. Sundaresh, J.D. Finan, B.S. Elkin, C. Lee, J. Xiao, B. Morrison, Viscoelastic characterization of porcine brain tissue mechanical properties under indentation loading, Brain Multiphys. 2 (2021) 100041, https://doi.org/10.1016/j.brain.2021.100041.
[83] M.T. Abba, S.R. Kalidindi, Protocols for studying the time-dependent mechanical response of viscoelastic materials using spherical indentation stress-strain curves, Mech. Time-Depend. Mater. 26 (1) (2022) 1–20, https://doi.org/10.1007/s11043-020-09472-y.
[84] S. Qiu, W. Jiang, M.S. Alam, S. Chen, C. Lai, T. Wang, X. Li, J. Liu, M. Gao, Y. Tang, X. Li, J. Zeng, Y. Feng, Viscoelastic characterization of injured brain tissue after controlled cortical impact (CCI) using a mouse model, J. Neurosci. Methods 330 (2020) 108463, https://doi.org/10.1016/j.jneumeth.2019.108463.
[85] A. Sridharan, S.D. Rajan, J. Muthuswamy, Long-term changes in the material properties of brain tissue at the implant–tissue interface, J. Neural Eng. 10 (6) (2013) 066001, https://doi.org/10.1088/1741-2560/10/6/066001.
[86] T.P. Prevost, G. Jin, M.A. de Moya, H.B. Alam, S. Suresh, S. Socrate, Dynamic mechanical response of brain tissue in indentation *in vivo, in situ* and *in vitro*, Acta Biomaterilia 7 (12) (2011) 4090–4101, https://doi.org/10.1016/j.actbio.2011.06.032.
[87] J. Weickenmeier, M. Kurt, E. Ozkaya, R. de Rooij, T.C. Ovaert, R.L. Ehman, K. Butts Pauly, E. Kuhl, Brain stiffens post mortem, J. Mech. Behav. Biomed. Mater. 84 (2018) 88–98, https://doi.org/10.1016/j.jmbbm.2018.04.009.
[88] Y. Feng, C.-H. Lee, L. Sun, S. Ji, X. Zhao, Characterizing white matter tissue in large strain via asymmetric indentation and inverse finite element modeling, J. Mech. Behav. Biomed. Mater. 65 (2017) 490–501, https://doi.org/10.1016/j.jmbbm.2016.09.020.
[89] Y. Feng, R.J. Okamoto, R. Namani, G.M. Genin, P.V. Bayly, Measurements of mechanical anisotropy in brain tissue and implications for transversely isotropic material models of white matter, J. Mech. Behav. Biomed. Mater. 23 (2013) 117–132, https://doi.org/10.1016/j.jmbbm.2013.04.007.
[90] W. Li, D.E.T. Shepherd, D.M. Espino, Frequency dependent viscoelastic properties of porcine brain tissue, J. Mech. Behav. Biomed. Mater. 102 (2020) 103460, https://doi.org/10.1016/j.jmbbm.2019.103460.

[91] L. Qian, H. Zhao, Y. Guo, Y. Li, M. Zhou, L. Yang, Z. Wang, Y. Sun, Influence of strain rate on indentation response of porcine brain, J. Mech. Behav. Biomed. Mater. 82 (2018) 210–217, https://doi.org/10.1016/j.jmbbm.2018.03.031.
[92] R.M. Delaine-Smith, S. Burney, F.R. Balkwill, M.M. Knight, Experimental validation of a flat punch indentation methodology calibrated against unconfined compression tests for determination of soft tissue biomechanics, J. Mech. Behav. Biomed. Mater. 60 (2016) 401–415, https://doi.org/10.1016/j.jmbbm.2016.02.019.
[93] A. Garo, M. Hrapko, J.A.W. van Dommelen, G.W.M. Peters, Towards a reliable characterisation of the mechanical behaviour of brain tissue: the effects of post-mortem time and sample preparation, Biorheology 44 (2007) 51–58, https://doi.org/10.1177/0006355X200704400100.
[94] A. Greiner, N. Reiter, F. Paulsen, G.A. Holzapfel, P. Steinmann, E. Comellas, S. Budday, Poro-viscoelastic effects during biomechanical testing of Human brain tissue, Front. Mech. Eng. 7 (2021), https://doi.org/10.3389/fmech.2021.708350.
[95] A.V. Basilio, D. Zeng, L.A. Pichay, S.A. Maas, S.N. Sundaresh, J.D. Finan, B. S. Elkin, G.M. McKhann, G.A. Ateshian, B. Morrison, Region-dependent mechanical properties of Human brain tissue under large deformations using inverse finite element modeling, Ann. Biomed. Eng. 52 (3) (2024) 600–610, https://doi.org/10.1007/s10439-023-03407-7.
[96] S. Budday, Exploring human brain mechanics by combining experiments, modeling, and simulation, Brain Multiphys. 5 (2023) 100076, https://doi.org/10.1016/j.brain.2023.100076.
[97] X. Jin, F. Zhu, H. Mao, M. Shen, K.H. Yang, A comprehensive experimental study on material properties of human brain tissue, J. Biomech. 46 (16) (2013) 2795–2801, https://doi.org/10.1016/j.jbiomech.2013.09.001.
[98] M.C. Murphy, J. Huston III, C.R. Jack Jr., K.J. Glaser, M.L. Senjem, J. Chen, A. Manduca, J.P. Felmlee, R.L. Ehman, Measuring the characteristic topography of brain stiffness with magnetic resonance elastography, PLoS. One 8 (12) (2013) e81668, https://doi.org/10.1371/journal.pone.0081668.
[99] H. Tzschätzsch, B. Kreft, F. Schrank, J. Bergs, J. Braun, I. Sack, *In vivo* time-harmonic ultrasound elastography of the human brain detects acute cerebral stiffness changes induced by intracranial pressure variations, Sci. Rep. 8 (1) (2018) 17888, https://doi.org/10.1038/s41598-018-36191-9.
[100] B. Rashid, M. Destrade, M.D. Gilchrist, Inhomogeneous deformation of brain tissue during tension tests, Comput. Mater. Sci. 64 (2012) 295–300, https://doi.org/10.1016/j.commatsci.2012.05.030.
[101] B. Rashid, M. Destrade, M.D. Gilchrist, Hyperelastic and viscoelastic properties of brain tissue in tension, ASME 2012 Int. Mech. Eng. Congr. Expo. (2012) 921–929.
[102] B. Rashid, M. Destrade, M.D. Gilchrist, Mechanical characterization of brain tissue in tension at dynamic strain rates, J. Mech. Behav. Biomed. Mater. 33 (2014) 43–54, https://doi.org/10.1016/j.jmbbm.2012.07.015.
[103] S. Cheng, L.E. Bilston, Unconfined compression of white matter, J. Biomech. 40 (1) (2007) 117–124, https://doi.org/10.1016/j.jbiomech.2005.11.004.
[104] L. Su, B. Qi, J. Yin, X. Qin, G.M. Genin, S. Liu, T.J. Lu, Compressive response of white matter in the brain at low strain rates, Int. J. Mech. Sci. 277 (2024) 109415, https://doi.org/10.1016/j.ijmecsci.2024.109415.
[105] H.W. Haslach, L.N. Leahy, P. Riley, R. Gullapalli, S. Xu, A.H. Hsieh, Solid–extracellular fluid interaction and damage in the mechanical response of rat brain tissue under confined compression, J. Mech. Behav. Biomed. Mater. 29 (2014) 138–150, https://doi.org/10.1016/j.jmbbm.2013.08.027.
[106] K. Miller, Method of testing very soft biological tissues in compression, J. Biomech. 38 (1) (2005) 153–158, https://doi.org/10.1016/j.jbiomech.2004.03.004.
[107] B. Rashid, M. Destrade, M.D. Gilchrist, Temperature effects on brain tissue in compression, J. Mech. Behav. Biomed. Mater. 14 (2012) 113–118, https://doi.org/10.1016/j.jmbbm.2012.04.005.
[108] B. Rashid, M. Destrade, M.D. Gilchrist, Mechanical characterization of brain tissue in simple shear at dynamic strain rates, J. Mech. Behav. Biomed. Mater. 28 (2013) 71–85, https://doi.org/10.1016/j.jmbbm.2013.07.017.
[109] M. Destrade, M.D. Gilchrist, J.G. Murphy, B. Rashid, G. Saccomandi, Extreme softness of brain matter in simple shear, Int. J. Non. Linear. Mech. 75 (2015) 54–58, https://doi.org/10.1016/j.ijnonlinmec.2015.02.014.
[110] V. Balbi, A. Trotta, M. Destrade, A.N. Annaidh, Poynting effect of brain matter in torsion, Soft. Matter. 15 (25) (2019) 5147–5153, https://doi.org/10.1039/c9sm00131j.
[111] E. Kuhl, A. Goriely, I too I2: a new class of hyperelastic isotropic incompressible models based solely on the second invariant, J. Mech. Phys. Solids. 188 (2024) 105670, https://doi.org/10.1016/j.jmps.2024.105670.
[112] F. Eskandari, M. Shafieian, M.M. Aghdam, K. Laksari, Tension strain-softening and compression strain-stiffening behavior of brain white matter, Ann. Biomed. Eng. 49 (1) (2021) 276–286, https://doi.org/10.1007/s10439-020-02541-w.
[113] S. Nicolle, M. Lounis, R. Willinger, in: Shear properties of brain tissue over a frequency range relevant for automotive impact situations: new experimental results, 48th Stapp Car Crash Conference, SAE Technical Paper, 2004.
[114] M. Hrapko, J.A.W. van Dommelen, G.W.M. Peters, J.S.H.M. Wismans, Characterisation of the mechanical behaviour of brain tissue in compression and shear, Biorheology 45 (2008) 663–676, https://doi.org/10.3233/BIR-2008-0512.
[115] S. Budday, M. Sarem, L. Starck, G. Sommer, J. Pfefferle, N. Phunchago, E. Kuhl, F. Paulsen, P. Steinmann, V.P. Shastri, G.A. Holzapfel, Towards microstructure-informed material models for human brain tissue, Acta Biomater. 104 (2020) 53–65, https://doi.org/10.1016/j.actbio.2019.12.030.
[116] K. Linka, S.R.S. Pierre, E. Kuhl, Automated model discovery for human brain using constitutive artificial neural networks, Acta Biomater. 160 (2023) 134–151, https://doi.org/10.1016/j.actbio.2023.01.055.
[117] J. Hou, N. Filla, X. Chen, M.J. Razavi, D. Zhu, T. Liu, X. Wang, Exploring hyperelastic material model discovery for human brain cortex: multivariate analysis *vs.* artificial neural network approaches, J. Mech. Behav. Biomed. Mater. 165 (2025) 106934, https://doi.org/10.1016/j.jmbbm.2025.106934.
[118] K.M. Labus, C.M. Puttlitz, An anisotropic hyperelastic constitutive model of brain white matter in biaxial tension and structural–mechanical relationships, J. Mech. Behav. Biomed. Mater. 62 (2016) 195–208, https://doi.org/10.1016/j.jmbbm.2016.05.003.
[119] K.M. Labus, C.M. Puttlitz, Viscoelasticity of brain corpus callosum in biaxial tension, J. Mech. Phys. Solids. 96 (2016) 591–604, https://doi.org/10.1016/j.jmps.2016.08.010.
[120] S. Chatelin, J. Vappou, S. Roth, J.-S. Raul, R. Willinger, Towards child *versus* adult brain mechanical properties, J. Mech. Behav. Biomed. Mater. 6 (2012) 166–173, https://doi.org/10.1016/j.jmbbm.2011.09.013.
[121] G. Li, J. Zhang, K. Wang, M. Wang, C. Gao, C. Ma, Experimental research of mechanical behavior of porcine brain tissue under rotational shear stress, J. Mech. Behav. Biomed. Mater. 57 (2016) 224–234, https://doi.org/10.1016/j.jmbbm.2015.12.002.
[122] B. Xue, X. Wen, R. Kuwar, D. Sun, N. Zhang, Age-dependent viscoelastic characterization of rat brain cortex, Brain Multiphys. 3 (2022), https://doi.org/10.1016/j.brain.2022.100056.
[123] L.Z. Shuck, S.H. Advani, Rheological response of Human brain tissue in shear, J. Basic Eng. 94 (4) (1972) 905–911, https://doi.org/10.1115/1.3425588.
[124] B. Qing, E.P. Canovic, A.S. Mijailovic, A. Jagielska, M.J. Whitfield, A.L. Lowe, E. H. Kelly, D. Turner, M. Sahin, K.J. Van Vliet, Probing mechanical properties of brain in a tuberous sclerosis model of autism, J. Biomech. Eng. 141 (3) (2019), https://doi.org/10.1115/1.4040945.
[125] K.B. Arbogast, S.S. Margulies, Material characterization of the brainstem from oscillatory shear tests, J. Biomech. 31 (9) (1998) 801–807, https://doi.org/10.1016/S0021-9290(98)00068-2.
[126] S. Budday, G. Sommer, G. Holzapfel, P. Steinmann, E. Kuhl, Viscoelastic parameter identification of human brain tissue, J. Mech. Behav. Biomed. Mater. 74 (2017) 463–476, https://doi.org/10.1016/j.jmbbm.2017.07.014.
[127] D.B. MacManus, M. Ghajari, Material properties of human brain tissue suitable for modelling traumatic brain injury, Brain Multiphys. 3 (2022) 100059, https://doi.org/10.1016/j.brain.2022.100059.
[128] K.K. Darvish, J.R. Crandall, Nonlinear viscoelastic effects in oscillatory shear deformation of brain tissue, Med. Eng. Phys. 23 (9) (2001) 633–645, https://doi.org/10.1016/S1350-4533(01)00101-1.
[129] M. Hrapko, J. Van Dommelen, G. Peters, J. Wismans, The mechanical behaviour of brain tissue: large strain response and constitutive modelling, Biorheology 43 (5) (2006) 623–636, https://doi.org/10.1177/0006355X2006043005004.
[130] W. Li, P. Zhang, Investigation of the mechanical characteristics of porcine brain tissue in complex environments, Acta Bioeng. Biomech. 26 (2) (2024), https://doi.org/10.37190/abb-02458-2024-03.
[131] R. Muthupillai, D.J. Lomas, P.J. Rossman, J.F. Greenleaf, A. Manduca, R. L. Ehman, Magnetic resonance elastography by direct visualization of propagating acoustic strain waves, Science (1979) 269 (5232) (1995) 1854–1857, https://doi.org/10.1126/science.7569924.
[132] C.L. Johnson, E.H. Telzer, Magnetic resonance elastography for examining developmental changes in the mechanical properties of the brain, Dev. Cogn. Neurosci. 33 (2018) 176–181, https://doi.org/10.1016/j.dcn.2017.08.010.
[133] X. Huang, H. Chafi, K.L. Matthews, O. Carmichael, T. Li, Q. Miao, S. Wang, G. Jia, Magnetic resonance elastography of the brain: a study of feasibility and reproducibility using an ergonomic pillow-like passive driver, Magn. Reson. ImAging 59 (2019) 68–76, https://doi.org/10.1016/j.mri.2019.03.009.
[134] A. Manduca, P.V. Bayly, R.L. Ehman, A. Kolipaka, T.J. Royston, I. Sack, R. Sinkus, B.E. Van Beers, MR elastography: principles, guidelines, and terminology, Magn. Reson. Med. 85 (5) (2021) 2377–2390, https://doi.org/10.1002/mrm.28627.
[135] S.A. Kruse, G.H. Rose, K.J. Glaser, A. Manduca, J.P. Felmlee, C.R. Jack, R. L. Ehman, Magnetic resonance elastography of the brain, Neuroimage 39 (1) (2008) 231–237, https://doi.org/10.1016/j.neuroimage.2007.08.030.
[136] M. Bigot, F. Chauveau, O. Beuf, S.A. Lambert, Magnetic resonance elastography of rodent brain, Front. Neurol. 9 (2018), https://doi.org/10.3389/fneur.2018.01010.
[137] J.-L. Gnanago, J.-F. Capsal, T. Gerges, P. Lombard, V. Semet, P.-J. Cottinet, M. Cabrera, S.A. Lambert, Actuators for MRE: new perspectives with flexible electroactive materials, Front. Phys. 9 (2021) 633848.
[138] S. Qiu, Z. He, R. Wang, R. Li, A. Zhang, F. Yan, Y. Feng, An electromagnetic actuator for brain magnetic resonance elastography with high frequency accuracy, NMR Biomed. 34 (12) (2021) e4592, https://doi.org/10.1002/nbm.4592.
[139] S. Qiu, Z. He, R. Wang, R. Li, W. Jin, L. Chen, J. Liu, F. Yan, G.Z. Yang, Y. Feng, Indirect shear wave excitation for brain magnetic resonance elastography with minimal cerebral blood flow alteration, IEEE Trans. Biomed. Eng. 71 (9) (2024) 2590–2598, https://doi.org/10.1109/tbme.2024.3381708.
[140] J.B. Weaver, A.J. Pattison, M.D. McGarry, I.M. Perreard, J.G. Swienckowski, C. J. Eskey, S.S. Lollis, K.D. Paulsen, Brain mechanical property measurement using MRE with intrinsic activation, Phys. Med. Biol. 57 (22) (2012) 7275, https://doi.org/10.1088/0031-9155/57/22/7275.
[141] A.A. Badachhape, R.J. Okamoto, R.S. Durham, B.D. Efron, S.J. Nadell, C. L. Johnson, P.V. Bayly, The relationship of three-dimensional Human skull motion to brain tissue deformation in magnetic resonance elastography studies, J. Biomech. Eng. 139 (5) (2017) 0510021–05100212, https://doi.org/10.1115/1.4036146.

[142] A. Zorgani, R. Souchon, A.-H. Dinh, J.-Y. Chapelon, J.-M. Ménager, S. Lounis, O. Rouvière, S. Catheline, Brain palpation from physiological vibrations using MRI, Proc. Natl. Acad. Sci. 112 (42) (2015) 12917–12921, https://doi.org/10.1073/pnas.1509895112.
[143] M.A. Troelstra, J.H. Runge, E. Burnhope, A. Polcaro, C. Guenthner, T. Schneider, R. Razavi, T.F. Ismail, J. Martorell, R. Sinkus, Shear wave cardiovascular MR elastography using intrinsic cardiac motion for transducer-free non-invasive evaluation of myocardial shear wave velocity, Sci. Rep. 11 (1) (2021) 1403, https://doi.org/10.1038/s41598-020-79231-z.
[144] Y. Feng, M.C. Murphy, E. Hojo, F. Li, N. Roberts, Magnetic resonance elastography in the study of neurodegenerative diseases, J. Magn. Reson. Imaging 59 (1) (2024) 82–96, https://doi.org/10.1002/jmri.28747.
[145] M.D.J. McGarry, C.L. Johnson, B.P. Sutton, J.G. Georgiadis, E.E.W. Van Houten, A.J. Pattison, J.B. Weaver, K.D. Paulsen, Suitability of poroelastic and viscoelastic mechanical models for high and low frequency MR elastography, Med. Phys. 42 (2) (2015) 947–957, https://doi.org/10.1118/1.4905048.
[146] L.V. Hiscox, C.L. Johnson, E. Barnhill, M.D.J. McGarry, J. Huston, E.J.R. van Beek, J.M. Starr, N. Roberts, Magnetic resonance elastography (MRE) of the human brain: technique, findings and clinical applications, Phys. Med. Biol. 61 (24) (2016) R401, https://doi.org/10.1088/0031-9155/61/24/R401.
[147] W. Zeng, S.W. Gordon-Wylie, L. Tan, L. Solamen, M.D.J. McGarry, J.B. Weaver, K. D. Paulsen, Nonlinear inversion MR elastography with low-frequency actuation, IEEe Trans. Med. ImAging 39 (5) (2020) 1775–1784, https://doi.org/10.1109/tmi.2019.2958212.
[148] M. Burman Ingeberg, E. Van Houten, J.J.M. Zwanenburg, Estimating the viscoelastic properties of the human brain at 7 T MRI using intrinsic MRE and nonlinear inversion, Hum. Brain Mapp. 44 (18) (2023) 6575–6591, https://doi.org/10.1002/hbm.26524.
[149] R. Wang, Y. Chen, F. Yan, G.-Z. Yang, Y. Feng, A 3D fast MR elastography sequence with interleaved multislab acquisition and hadamard encoding, Magn. Reson. Med. 93 (3) (2025) 1163–1175, https://doi.org/10.1002/mrm.30342.
[150] C. Santarelli, M. Carfagni, L. Alparone, A. Arienzo, F. Argenti, Multimodal fusion of tomographic sequences of medical images: MRE spatially enhanced by MRI, Comput. Methods Programs Biomed. 223 (2022) 106964, https://doi.org/10.1016/j.cmpb.2022.106964.
[151] S. Ma, R. Wang, S. Qiu, R. Li, Q. Yue, Q. Sun, L. Chen, F. Yan, G.Z. Yang, Y. Feng, MR elastography with optimization-based phase unwrapping and traveling wave expansion-based neural network (TWENN), IEEe Trans. Med. ImAging 42 (9) (2023) 2631–2642, https://doi.org/10.1109/TMI.2023.3261346.
[152] I. Sack, Magnetic resonance elastography from fundamental soft-tissue mechanics to diagnostic imaging, Nat. Rev. Phys. 5 (1) (2023) 25–42, https://doi.org/10.1038/s42254-022-00543-2.
[153] L. Xu, Y. Lin, J.C. Han, Z.N. Xi, H. Shen, P.Y. Gao, Magnetic resonance elastography of brain tumors: preliminary results, Acta Radiol. 48 (3) (2007) 327–330, https://doi.org/10.1080/02841850701199967.
[154] G. McIlvain, J.M. Schneider, M.A. Matyi, M.D.J. McGarry, Z. Qi, J.M. Spielberg, C. L. Johnson, Mapping brain mechanical property maturation from childhood to adulthood, Neuroimage 263 (2022) 119590, https://doi.org/10.1016/j.neuroimage.2022.119590.
[155] I. Sack, K.-J. Streitberger, D. Krefting, F. Paul, J. Braun, The influence of physiological aging and atrophy on brain viscoelastic properties in humans, PLoS. One 6 (9) (2011) e23451, https://doi.org/10.1371/journal.pone.0023451.
[156] C.L. Johnson, H. Schwarb, D. J. M. M, A.T. Anderson, G.R. Huesmann, B. P. Sutton, N.J. Cohen, Viscoelasticity of subcortical gray matter structures, Hum. Brain Mapp. 37 (12) (2016) 4221–4233, https://doi.org/10.1002/hbm.23314.
[157] I. Sack, B. Beierbach, J. Wuerfel, D. Klatt, U. Hamhaber, S. Papazoglou, P. Martus, J. Braun, The impact of aging and gender on brain viscoelasticity, Neuroimage 46 (3) (2009) 652–657, https://doi.org/10.1016/j.neuroimage.2009.02.040.
[158] J. Yeung, L. Jugé, A. Hatt, L.E. Bilston, Paediatric brain tissue properties measured with magnetic resonance elastography, Biomech. Model. Mechanobiol. 18 (5) (2019) 1497–1505, https://doi.org/10.1007/s10237-019-01157-x.
[159] E. Ozkaya, G. Fabris, F. Macruz, Z.M. Suar, J. Abderezaei, B. Su, K. Laksari, L. Wu, D.B. Camarillo, K.B. Pauly, M. Wintermark, M. Kurt, Viscoelasticity of children and adolescent brains through MR elastography, J. Mech. Behav. Biomed. Mater. 115 (2021) 104229, https://doi.org/10.1016/j.jmbbm.2020.104229.
[160] C.L. Johnson, M.D.J. McGarry, A.A. Gharibans, J.B. Weaver, K.D. Paulsen, H. Wang, W.C. Olivero, B.P. Sutton, J.G. Georgiadis, Local mechanical properties of white matter structures in the human brain, Neuroimage 79 (2013) 145–152, https://doi.org/10.1016/j.neuroimage.2013.04.089.
[161] J. Braun, J. Guo, R. Lützkendorf, J. Stadler, S. Papazoglou, S. Hirsch, I. Sack, J. Bernarding, High-resolution mechanical imaging of the human brain by three-dimensional multifrequency magnetic resonance elastography at 7T, Neuroimage 90 (2014) 308–314, https://doi.org/10.1016/j.neuroimage.2013.12.032.
[162] H. Schwarb, C.L. Johnson, M.D.J. McGarry, N.J. Cohen, Medial temporal lobe viscoelasticity and relational memory performance, Neuroimage 132 (2016) 534–541, https://doi.org/10.1016/j.neuroimage.2016.02.059.
[163] E. Triolo, O. Khegai, M. McGarry, T. Lam, J. Veraart, A. Alipour, P. Balchandani, M. Kurt, Characterizing brain mechanics through 7 tesla magnetic resonance elastography, Phys. Med. Biol. 69 (20) (2024) 205011, https://doi.org/10.1088/1361-6560/ad7fc9.
[164] P.V. Bayly, J.R. Garbow, Pre-clinical MR elastography: principles, techniques, and applications, J. Magn. Reson. 291 (2018) 73–83, https://doi.org/10.1016/j.jmr.2018.01.004.
[165] M. Simon, J. Guo, S. Papazoglou, H. Scholand-Engler, C. Erdmann, U. Melchert, M. Bonsanto, J. Braun, D. Petersen, I. Sack, J. Wuerfel, Non-invasive characterization of intracranial tumors by magnetic resonance elastography, New. J. Phys. 15 (8) (2013) 085024, https://doi.org/10.1088/1367-2630/15/8/085024.
[166] A. Bunevicius, K. Schregel, R. Sinkus, A. Golby, S. Patz, REVIEW: MR elastography of brain tumors, NeuroImage: Clin. 25 (2020) 102109, https://doi.org/10.1016/j.nicl.2019.102109.
[167] Y. Streibel, M.O. Breckwoldt, J. Hunger, C. Pan, M. Fischer, V. Turco, B. Boztepe, H. Fels-Palesandro, J.G. Scheck, V. Sturm, K. Karimian-Jazi, D.A. Agardy, G. Annio, R. Mustapha, S.S. Soni, A. Alasa, I. Weidenfeld, C.B. Rodell, W. Wick, S. Heiland, F. Winkler, M. Platten, M. Bendszus, R. Sinkus, K. Schregel, Tumor biomechanics as a novel imaging biomarker to assess response to immunotherapy in a murine glioma model, Sci. Rep. 14 (1) (2024) 15613, https://doi.org/10.1038/s41598-024-66519-7.
[168] M.C. Murphy, D.T. Jones, C.R. Jack, K.J. Glaser, M.L. Senjem, A. Manduca, J. P. Felmlee, R.E. Carter, R.L. Ehman, J. Huston, Regional brain stiffness changes across the Alzheimer's disease spectrum, NeuroImage: Clin. 10 (2016) 283–290, https://doi.org/10.1016/j.nicl.2015.12.007.
[169] A. Lipp, C. Skowronek, A. Fehlner, K.-J. Streitberger, J. Braun, I. Sack, Progressive supranuclear palsy and idiopathic Parkinson's disease are associated with local reduction of *in vivo* brain viscoelasticity, Eur. Radiol. 28 (2018) 3347–3354, https://doi.org/10.1007/s00330-017-5269-y.
[170] J. Huston III, M.C. Murphy, B.F. Boeve, N. Fattahi, A. Arani, K.J. Glaser, A. Manduca, D.T. Jones, R.L. Ehman, Magnetic resonance elastography of frontotemporal dementia, J. Magn. Reson. Imaging 43 (2) (2016) 474–478, https://doi.org/10.1002/jmri.24977.
[171] P. Karki, M.C. Murphy, P.M. Cogswell, M.L. Senjem, J. Graff-Radford, B.D. Elder, A. Perry, C.S. Graffeo, F.B. Meyer, C.R. Jack, Prediction of surgical outcomes in normal pressure hydrocephalus by MR elastography, Am. J. Neuroradiol. 45 (3) (2024) 328–334.
[172] G.R. Huesmann, H. Schwarb, D.R. Smith, R.T. Pohlig, A.T. Anderson, M.D. J. McGarry, K.D. Paulsen, T.M. Wszalek, B.P. Sutton, C.L. Johnson, Hippocampal stiffness in mesial temporal lobe epilepsy measured with MR elastography: preliminary comparison with healthy participants, NeuroImage: Clin. 27 (2020) 102313, https://doi.org/10.1016/j.nicl.2020.102313.
[173] D.R. Smith, C.A. Guertler, R.J. Okamoto, A.J. Romano, P.V. Bayly, C.L. Johnson, Multi-excitation magnetic resonance elastography of the brain: wave propagation in anisotropic white matter, J. Biomech. Eng. 142 (7) (2020), https://doi.org/10.1115/1.4046199.
[174] D.R. Smith, D.A. Caban-Rivera, M.D.J. McGarry, L.T. Williams, G. McIlvain, R. J. Okamoto, E.E.W. Van Houten, P.V. Bayly, K.D. Paulsen, C.L. Johnson, Anisotropic mechanical properties in the healthy human brain estimated with multi-excitation transversely isotropic MR elastography, Brain Multiphys. 3 (2022) 100051, https://doi.org/10.1016/j.brain.2022.100051.
[175] S. Wang, C.A. Guertler, R.J. Okamoto, C.L. Johnson, M.D.J. McGarry, P.V. Bayly, Mechanical stiffness and anisotropy measured by MRE during brain development in the minipig, Neuroimage 277 (2023) 120234, https://doi.org/10.1016/j.neuroimage.2023.120234.
[176] S. Ma, Z. He, R. Wang, A. Zhang, Q. Sun, J. Liu, F. Yan, M.S. Sacks, X.-Q. Feng, G.-Z. Yang, Y. Feng, Measurement of biomechanical properties of transversely isotropic biological tissue using traveling wave expansion, Med. Image Anal. 101 (2025) 103457, https://doi.org/10.1016/j.media.2025.103457.
[177] H. Herthum, S. Hetzer, B. Kreft, H. Tzschätzsch, M. Shahryari, T. Meyer, S. Görner, H. Neubauer, J. Guo, J. Braun, I. Sack, Cerebral tomoelastography based on multifrequency MR elastography in two and three dimensions, Front. Bioeng. Biotechnol. 10 (2022), https://doi.org/10.3389/fbioe.2022.1056131. Volume2022.
[178] A.M. Daugherty, H.D. Schwarb, M.D.J. McGarry, C.L. Johnson, N.J. Cohen, Magnetic resonance elastography of Human hippocampal subfields: cA3-dentate gyrus viscoelasticity predicts relational memory accuracy, J. Cogn. Neurosci. 32 (9) (2020) 1704–1713, https://doi.org/10.1162/jocn_a_01574.
[179] Y. Le, J. Chen, P.J. Rossman, B. Bolster Jr, S. Kannengiesser, A. Manduca, K. J. Glaser, Y. Sui, J. Huston III, Z. Yin, R.L. Ehman, Wavelet MRE: imaging propagating broadband acoustic waves with wavelet-based motion-encoding gradients, Magn. Reson. Med. 91 (5) (2024) 1923–1935, https://doi.org/10.1002/mrm.29972.
[180] H. Dong, N. Jin, S. Kannengiesser, B. Raterman, R.D. White, A. Kolipaka, Magnetic resonance elastography for estimating *in vivo* stiffness of the abdominal aorta using cardiac-gated spin-echo echo-planar imaging: a feasibility study, NMR Biomed. 34 (1) (2021) e4420, https://doi.org/10.1002/nbm.4420.
[181] L. Lilaj, H. Herthum, T. Meyer, M. Shahryari, G. Bertalan, A. Caiazzo, J. Braun, T. Fischer, S. Hirsch, I. Sack, Inversion-recovery MR elastography of the human brain for improved stiffness quantification near fluid-solid boundaries, Magn. Reson. Med. 86 (5) (2021) 2552–2561, https://doi.org/10.1002/mrm.28898.
[182] M. McGarry, E.V. Houten, C. Guertler, R. Okamoto, D. Smith, D. Sowinski, C. Johnson, P. Bayly, J. Weaver, K. Paulsen, A heterogenous, time harmonic, nearly incompressible transverse isotropic finite element brain simulation platform for MR elastography, Phys. Med. Biol. 66 (5) (2021) 055029, https://doi.org/10.1088/1361-6560/ab9a84.
[183] A.G. Chartrain, M. Kurt, A. Yao, R. Feng, K. Nael, J. Mocco, J.B. Bederson, P. Balchandani, R.K. Shrivastava, Utility of preoperative meningioma consistency measurement with magnetic resonance elastography (MRE): a review, Neurosurg. Rev. 42 (1) (2019) 1–7, https://doi.org/10.1007/s10143-017-0862-8.
[184] M.C. Murphy, A. Manduca, J.D. Trzasko, K.J. Glaser, J. Huston III, R.L. Ehman, Artificial neural networks for stiffness estimation in magnetic resonance elastography, Magn. Reson. Med. 80 (1) (2018) 351–360, https://doi.org/10.1002/mrm.27019.

[185] J.M. Scott, A. Arani, A. Manduca, K.P. McGee, J.D. Trzasko, J. Huston 3rd, R. L. Ehman, M.C. Murphy, Artificial neural networks for magnetic resonance elastography stiffness estimation in inhomogeneous materials, Med. Image Anal. 63 (2020) 101710, https://doi.org/10.1016/j.media.2020.101710.
[186] T. Yue, X. Jia, J. Petrosino, L. Sun, Z. Fan, J. Fine, R. Davis, S. Galster, J. Kuret, D. W. Scharre, M. Zhang, Computational integration of nanoscale physical biomarkers and cognitive assessments for Alzheimer's disease diagnosis and prognosis, Sci. Adv. 3 (7) (2017) e1700669, https://doi.org/10.1126/sciadv.1700669.
[187] D. Eberle, G. Fodelianaki, T. Kurth, A. Jagielska, S. Möllmert, E. Ulbricht, K. Wagner, A.V. Taubenberger, N. Träber, J.-C. Escolano, K.J. Van Vliet, J. Guck, Acquired demyelination but not genetic developmental defects in myelination leads to brain tissue stiffness changes, Brain Multiphys. 1 (2020) 100019, https://doi.org/10.1016/j.brain.2020.100019.
[188] W. Ong, N. Marinval, J. Lin, M.H. Nai, Y.-S. Chong, C. Pinese, S. Sajikumar, C. T. Lim, C. Ffrench-Constant, M.E. Bechler, S.Y. Chew, Biomimicking Fiber platform with tunable stiffness to study mechanotransduction reveals stiffness enhances oligodendrocyte differentiation but impedes myelination through YAP-dependent regulation, Small. 16 (37) (2020) 2003656, https://doi.org/10.1002/smll.202003656.
[189] M. Iwashita, T. Nomura, T. Suetsugu, F. Matsuzaki, S. Kojima, Y. Kosodo, Comparative analysis of brain stiffness among amniotes using glyoxal fixation and atomic force microscopy, Front. Cell Dev. Biol. 8 (2020), https://doi.org/10.3389/fcell.2020.574619.
[190] C.M. Hall, E. Moeendarbary, G.K. Sheridan, Mechanobiology of the brain in ageing and Alzheimer's disease, Eur. J. Neurosci. 53 (12) (2021) 3851–3878, https://doi.org/10.1111/ejn.14766.
[191] D.B. MacManus, J.G. Murphy, M.D. Gilchrist, Mechanical characterisation of brain tissue up to 35% strain at 1, 10, and 100/s using a custom-built micro-indentation apparatus, J. Mech. Behav. Biomed. Mater. 87 (2018) 256–266, https://doi.org/10.1016/j.jmbbm.2018.07.025.
[192] M.T. Prange, S.S. Margulies, Regional, directional, and age-dependent properties of the brain undergoing large deformation, J. Biomech. Eng. 124 (2) (2002) 244–252, https://doi.org/10.1115/1.1449907.
[193] B. Rashid, M. Destrade, M.D. Gilchrist, Determination of friction coefficient in unconfined compression of brain tissue, J. Mech. Behav. Biomed. Mater. 14 (2012) 163–171, https://doi.org/10.1016/j.jmbbm.2012.05.001.
[194] S. Budday, G. Sommer, J. Haybaeck, P. Steinmann, G.A. Holzapfel, E. Kuhl, Rheological characterization of human brain tissue, Acta Biomater. 60 (2017) 315–329, https://doi.org/10.1016/j.actbio.2017.06.024.
[195] M. Hosseini-Farid, A. Rezaei, A. Eslaminejad, M. Ramzanpour, M. Ziejewski, G. Karami, Instantaneous and equilibrium responses of the brain tissue by stress relaxation and quasi-linear viscoelasticity theory, Sci. Iran. 26 (2019) 2047–2056, https://doi.org/10.24200/sci.2019.21314, 4: Special Issue Dedicated to Professor Abolhassan Vafai.
[196] M. Hosseini-Farid, M. Ramzanpour, J. McLean, M. Ziejewski, G. Karami, A poro-hyper-viscoelastic rate-dependent constitutive modeling for the analysis of brain tissues, J. Mech. Behav. Biomed. Mater. 102 (2020) 103475, https://doi.org/10.1016/j.jmbbm.2019.103475.
[197] L. Su, M. Wang, J. Yin, F. Ti, J. Yang, C. Ma, S. Liu, T.J. Lu, Distinguishing poroelasticity and viscoelasticity of brain tissue with time scale, Acta Biomater. 155 (2023) 423–435, https://doi.org/10.1016/j.actbio.2022.11.009.
[198] N. Reiter, S. Auer, L. Hoffmann, L. Bräuer, F. Paulsen, S. Budday, Do human brain white matter and brain stem structures show direction-dependent mechanical behavior? Acta Biomater. (2025) https://doi.org/10.1016/j.actbio.2025.04.004.
[199] G. Fallenstein, V.D. Hulce, J.W. Melvin, Dynamic mechanical properties of human brain tissue, J. Biomech. 2 (3) (1969) 217–226, https://doi.org/10.1016/0021-9290(69)90079-7.
[200] S. Nicolle, M. Lounis, R. Willinger, Shear Properties of Brain Tissue Over a Frequency Range Relevant For Automotive Impact situations: New Experimental Results, SAE Technical Paper, 2004.
[201] J. Weickenmeier, M. Kurt, E. Ozkaya, M. Wintermark, K.B. Pauly, E. Kuhl, Magnetic resonance elastography of the brain: a comparison between pigs and humans, J. Mech. Behav. Biomed. Mater. 77 (2018) 702–710, https://doi.org/10.1016/j.jmbbm.2017.08.029.
[202] Z.S. Xu, R.J. Lee, S.S. Chu, A. Yao, M.K. Paun, S.P. Murphy, P.D. Mourad, Evidence of changes in brain tissue stiffness after ischemic stroke derived from ultrasound-based elastography, J. Ultrasound. Med. 32 (3) (2013) 485–494, https://doi.org/10.7863/jum.2013.32.3.485.
[203] Z.S. Xu, A. Yao, S.S. Chu, M.K. Paun, A.M. McClintic, S.P. Murphy, P.D. Mourad, Detection of mild traumatic brain injury in rodent models using shear wave elastography, J. Ultrasound. Med. 33 (10) (2014) 1763–1771, https://doi.org/10.7863/ultra.33.10.1763.
[204] Y. Jiang, G. Li, L.-X. Qian, S. Liang, M. Destrade, Y. Cao, Measuring the linear and nonlinear elastic properties of brain tissue with shear waves and inverse analysis, Biomech. Model. Mechanobiol. 14 (5) (2015) 1119–1128, https://doi.org/10.1007/s10237-015-0658-0.
[205] Y. Su, J. Ma, L. Du, J. Xia, Y. Wu, X. Jia, Y. Cai, Y. Li, J. Zhao, Q. Liu, Application of acoustic radiation force impulse imaging (ARFI) in quantitative evaluation of neonatal brain development, Clin Exp Obs. Gynecol 42 (6) (2015) 797–800.
[206] D. Chauvet, M. Imbault, L. Capelle, C. Demene, M. Mossad, C. Karachi, A.L. Boch, J.L. Gennisson, M. Tanter, *In vivo* measurement of brain tumor elasticity using intraoperative shear wave elastography, Ultraschall. Med. 37 (6) (2016) 584–590, https://doi.org/10.1055/s-0034-1399152.
[207] H.G. Kim, M.S. Park, J.-D. Lee, S.Y. Park, Ultrasound elastography of the neonatal brain: preliminary study, J. Ultrasound. Med. 36 (7) (2017) 1313–1319, https://doi.org/10.7863/ultra.16.06079.
[208] Y.-L. Liu, G.-Y. Li, P. He, Z.-Q. Mao, Y. Cao, Temperature-dependent elastic properties of brain tissues measured with the shear wave elastography method, J. Mech. Behav. Biomed. Mater. 65 (2017) 652–656, https://doi.org/10.1016/j.jmbbm.2016.09.026.
[209] E. Albayrak, T. Kasap, Evaluation of neonatal brain parenchyma using 2-dimensional shear wave elastography, J. Ultrasound. Med. 37 (4) (2018) 959–967, https://doi.org/10.1002/jum.14366.
[210] Y.-L. Liu, D. Liu, L. Xu, C. Su, G.-Y. Li, L.-X. Qian, Y. Cao, *In vivo* and ex vivo elastic properties of brain tissues measured with ultrasound elastography, J. Mech. Behav. Biomed. Mater. 83 (2018) 120–125, https://doi.org/10.1016/j.jmbbm.2018.04.017.
[211] T. Dirrichs, N. Meiser, A. Panek, S. Trepels-Kottek, T. Orlikowsky, C.K. Kuhl, S. Schrading, Transcranial shear wave elastography of neonatal and infant brains for quantitative evaluation of increased intracranial pressure, Invest. Radiol. 54 (11) (2019) 719–727, https://doi.org/10.1097/rli.0000000000000602.
[212] F.-Y. Lay, P.-Y. Chen, H.-F. Cheng, Y.-M. Kuo, C.-C. Huang, Ex vivo evaluation of mouse brain elasticity using high-frequency ultrasound elastography, IEEE Trans. Biomed. Eng. 66 (12) (2019) 3426–3435, https://doi.org/10.1109/TBME.2019.2905551.
[213] E. Garcés Iñigo, R. Llorens Salvador, R. Escrig, D. Hervás, M. Vento, L. Martí-Bonmatí, Quantitative evaluation of neonatal brain elasticity using shear wave elastography, J. Ultrasound. Med. 40 (4) (2021) 795–804, https://doi.org/10.1002/jum.15464.
[214] J. Blackwell, Mechanical evaluation of ovine brain tissue using rheometry and shear wave ultrasound elastography, 2023.
[215] S. Klemmer Chandía, J. Schattenfroh, S.T. Brinker, H. Tzschätzsch, I. Sack, T. Meyer, Multimodal assessment of brain stiffness variation in healthy subjects using magnetic resonance elastography and ultrasound time-harmonic elastography, Sci. Rep. 14 (1) (2024) 28580, https://doi.org/10.1038/s41598-024-79991-y.
[216] J. Yu, H. Guo, X. Qiao, L. Jiang, Y. Chen, J. Liu, C. Zhang, X. Su, H. Zhang, M. Wan, Transcranial ultrasound estimation of viscoelasticity and fluidity in brain tumors aided by transcranial shear waves, Ultrasonics. 138 (2024) 107262, https://doi.org/10.1016/j.ultras.2024.107262.
[217] R.M. Sigrist, J. Liau, A. El Kaffas, M.C. Chammas, J.K. Willmann, Ultrasound elastography: review of techniques and clinical applications, Theranostics. 7 (5) (2017) 1303, https://doi.org/10.7150/thno.18650.
[218] A.A. Oglat, T. Abukhalil, Ultrasound elastography: methods, clinical applications, and limitations: a review article, Appl. Sci. 14 (10) (2024) 4308, https://doi.org/10.1016/j.wneu.2022.10.108.
[219] J. Liao, H. Yang, J. Yu, X. Liang, Z. Chen, Progress in the application of ultrasound elastography for brain diseases, J. Ultrasound. Med. 39 (11) (2020) 2093–2104, https://doi.org/10.1002/jum.15317.
[220] D. deCampo, M. Hwang, Characterizing the neonatal brain with ultrasound elastography, Pediatr. Neurol. 86 (2018) 19–26, https://doi.org/10.1016/j.pediatrneurol.2018.06.005.
[221] J.L. Gennisson, T. Deffieux, M. Fink, M. Tanter, Ultrasound elastography: principles and techniques, Diagn. Interv. ImAging 94 (5) (2013) 487–495, https://doi.org/10.1016/j.diii.2013.01.022.
[222] C. Bruno, S. Minniti, A. Bucci, R.Pozzi Mucelli, ARFI: from basic principles to clinical applications in diffuse chronic disease—A review, Insights. ImAging 7 (5) (2016) 735–746, https://doi.org/10.1007/s13244-016-0514-5.
[223] N. Nitta, M. Yamakawa, H. Hachiya, T. Shiina, A review of physical and engineering factors potentially affecting shear wave elastography, J. Med. Ultrason. 48 (4) (2021) 403–414, https://doi.org/10.1007/s10396-021-01127-w.
[224] Y. Deng, N.C. Rouze, M.L. Palmeri, K.R. Nightingale, Ultrasonic Shear wave elasticity imaging sequencing and data processing using a verasonics research scanner, IEEe Trans. Ultrason. Ferroelectr. Freq. Control 64 (1) (2017) 164–176, https://doi.org/10.1109/tuffc.2016.2614944.
[225] K. Nightingale, Acoustic radiation force impulse (ARFI) imaging: a review, Curr. Med. ImAging Rev. 7 (4) (2011) 328–339, https://doi.org/10.2174/157340511798038657.
[226] M.L. Palmeri, D. Yufeng, N.C. Rouze, K.R. Nightingale, Dependence of shear wave spectral content on acoustic radiation force excitation duration and spatial beamwidth, 2014 IEEE Int. Ultrason. Symp. (2014) 1105–1108.
[227] H.W. Chan, C. Uff, A. Chakraborty, N. Dorward, J.C. Bamber, Clinical application of shear wave elastography for assisting brain tumor resection, Front. Oncol. 11 (2021) 619286, https://doi.org/10.3389/fonc.2021.619286.
[228] S.S. Shin, T.A.G.M. Huisman, M. Hwang, Ultrasound imaging for traumatic brain injury, J. Ultrasound. Med. 37 (8) (2018) 1857–1867, https://doi.org/10.1002/jum.14547.
[229] M. Hille, S. Kühn, G. Kempermann, T. Bonhoeffer, U. Lindenberger, From animal models to human individuality: integrative approaches to the study of brain plasticity, Neuron 112 (21) (2024) 3522–3541, https://doi.org/10.1016/j.neuron.2024.10.006.
[230] N. Kanwisher, Animal models of the human brain: successes, limitations, and alternatives, Curr. Opin. Neurobiol. 90 (2025) 102969, https://doi.org/10.1016/j.conb.2024.102969.
[231] N. Filla, J. Hou, T. Liu, S. Budday, X. Wang, Accuracy meets simplicity: a constitutive model for heterogenous brain tissue, J. Mech. Behav. Biomed. Mater. 150 (2024) 106271, https://doi.org/10.1016/j.jmbbm.2023.106271.
[232] J. Hou, X. Chen, T. Wu, E. Kuhl, X. Wang, Automated data-driven discovery of material models based on symbolic regression: a case study on the human brain

cortex, Acta Biomater. 188 (2024) 276–296, https://doi.org/10.1016/j.actbio.2024.09.005.
[233] J. Hou, Z. Wu, X. Chen, L. Wang, D. Zhu, T. Liu, G. Li, X. Wang, Role of data-driven regional growth model in shaping brain folding patterns, Soft. Matter. 21 (4) (2025) 729–749, https://doi.org/10.1039/D4SM01194E.
[234] J. Weickenmeier, M. Jucker, A. Goriely, E. Kuhl, A physics-based model explains the prion-like features of neurodegeneration in Alzheimer's disease, Parkinson's disease, and amyotrophic lateral sclerosis, J. Mech. Phys. Solids. 124 (2019) 264–281, https://doi.org/10.1016/j.jmps.2018.10.013.
[235] J. Vappou, E. Breton, P. Choquet, R. Willinger, A. Constantinesco, Assessment of *in vivo* and post-mortem mechanical behavior of brain tissue using magnetic resonance elastography, J. Biomech. 41 (14) (2008) 2954–2959, https://doi.org/10.1016/j.jbiomech.2008.07.034.
[236] C.A. Guertler, R.J. Okamoto, J.L. Schmidt, A.A. Badachhape, C.L. Johnson, P. V. Bayly, Mechanical properties of porcine brain tissue *in vivo* and ex vivo estimated by MR elastography, J. Biomech. 69 (2018) 10–18, https://doi.org/10.1016/j.jbiomech.2018.01.016.
[237] A. Greiner, N. Reiter, J. Hinrichsen, M. Kainz, G. Sommer, G. Holzapfel, P. Steinmann, E. Comellas, S. Budday, Model-driven exploration of poro-viscoelasticity in human brain tissue: be careful with the parameters!, Interface Focus. 14 (2024), https://doi.org/10.1098/rsfs.2024.0026.
[238] J.E. Galford, J.H. McElhaney, A viscoelastic study of scalp, brain, and dura, J. Biomech. 3 (2) (1970) 211–221, https://doi.org/10.1016/0021-9290(70)90007-2.
[239] J.H. McElhaney, J.W. Melvin, V.L. Roberts, H.D. Portnoy, Dynamic characteristics of the tissues of the head, in: R.M. Kenedi (Ed.), Perspectives in Biomedical Engineering, Palgrave Macmillan UK, London, 1973, pp. 215–222.
[240] B.R. Donnelly, J. Medige, Shear properties of Human brain tissue, J. Biomech. Eng. 119 (4) (1997) 423–432, https://doi.org/10.1115/1.2798289.
[241] J.D. Finan, S.N. Sundaresh, B.S. Elkin, G.M. McKhann, B. Morrison, Regional mechanical properties of human brain tissue for computational models of traumatic brain injury, Acta Biomater. 55 (2017) 333–339, https://doi.org/10.1016/j.actbio.2017.03.037.
[242] K. Park, G.E. Lonsberry, M. Gearing, A.I. Levey, J.P. Desai, Viscoelastic properties of Human autopsy brain tissues as biomarkers for Alzheimer's diseases, IEEE Trans. Biomed. Eng. 66 (6) (2019) 1705–1713, https://doi.org/10.1109/TBME.2018.2878555.
[243] A. Karimi, S.M. Rahmati, R. Razaghi, M. Hasani, Mechanical measurement of the human cerebellum under compressive loading, J. Med. Eng. Technol. 43 (1) (2019) 55–58, https://doi.org/10.1080/03091902.2019.1609609.
[244] M. Hrapko, J.A.W. van Dommelen, G.W.M. Peters, J.S.H.M. Wismans, The influence of test conditions on characterization of the mechanical properties of brain tissue, J. Biomech. Eng. 130 (3) (2008), https://doi.org/10.1115/1.2907746.
[245] M.S. Estes, J. McElhaney, Response of Brain Tissue of Compressive Loading, ASME, 1970.
[246] M.T. Prange, D.F. Meaney, S.S. Margulies, Defining brain mechanical properties: effects of region, direction, and species, 44th Stapp Car Crash Conf. (2000) 205–213.
[247] E.G. Takhounts, J.R. Crandall, K. Darvish, On the importance of nonlinearity of brain tissue under large deformations, in: 47th Stapp Car Crash Conference SAE Technical Paper, 2003.
[248] S.N. Sundaresh, J.D. Finan, B.S. Elkin, A.V. Basilio, G.M. McKhann, B. Morrison III, Region-dependent viscoelastic properties of human brain tissue under large deformations, Ann. Biomed. Eng. 50 (11) (2022) 1452–1460, https://doi.org/10.1007/s10439-022-02910-7.
[249] A. Romano, M. Scheel, S. Hirsch, J. Braun, I. Sack, *In vivo* waveguide elastography of white matter tracts in the human brain, Magn. Reson. Med. 68 (5) (2012) 1410–1422, https://doi.org/10.1002/mrm.24141.
[250] A.T. Anderson, E.E.W. Van Houten, M.D.J. McGarry, K.D. Paulsen, J.L. Holtrop, B. P. Sutton, J.G. Georgiadis, C.L. Johnson, Observation of direction-dependent mechanical properties in the human brain with multi-excitation MR elastography, J. Mech. Behav. Biomed. Mater. 59 (2016) 538–546, https://doi.org/10.1016/j.jmbbm.2016.03.005.
[251] D. Jyoti, M. McGarry, D.A. Caban-Rivera, E. Van Houten, C.L. Johnson, K. Paulsen, Transversely-isotropic brain *in vivo* MR elastography with anisotropic damping, J. Mech. Behav. Biomed. Mater. 141 (2023) 105744, https://doi.org/10.1016/j.jmbbm.2023.105744.
[252] A. Romano, J. Guo, T. Prokscha, T. Meyer, S. Hirsch, J. Braun, I. Sack, M. Scheel, *In vivo* waveguide elastography: effects of neurodegeneration in patients with amyotrophic lateral sclerosis, Magn. Reson. Med. 72 (6) (2014) 1755–1761, https://doi.org/10.1002/mrm.25067.
[253] P. Kalra, B. Raterman, X. Mo, A. Kolipaka, Magnetic resonance elastography of brain: comparison between anisotropic and isotropic stiffness and its correlation to age, Magn. Reson. Med. 82 (2) (2019) 671–679, https://doi.org/10.1002/mrm.27757.
[254] M. McGarry, E. Van Houten, D. Sowinski, D. Jyoti, D.R. Smith, D.A. Caban-Rivera, G. McIlvain, P. Bayly, C.L. Johnson, J. Weaver, K. Paulsen, Mapping heterogenous anisotropic tissue mechanical properties with transverse isotropic nonlinear inversion MR elastography, Med. Image Anal. 78 (2022) 102432, https://doi.org/10.1016/j.media.2022.102432.
[255] H. Lv, M. Kurt, N. Zeng, E. Ozkaya, F. Marcuz, L. Wu, K. Laksari, D.B. Camarillo, K.B. Pauly, Z. Wang, M. Wintermark, MR elastography frequency-dependent and independent parameters demonstrate accelerated decrease of brain stiffness in elder subjects, Eur. Radiol. 30 (12) (2020) 6614–6623, https://doi.org/10.1007/s00330-020-07054-7.
[256] K.J. Parker, I.E. Kabir, M.M. Doyley, A. Faiyaz, M.N. Uddin, G. Flores, G. Schifitto, Brain elastography in aging relates to fluid/solid trendlines, Phys. Med. Biol. 69 (11) (2024) 115037, https://doi.org/10.1088/1361-6560/ad4446.
[257] J. Guo, S. Hirsch, A. Fehlner, S. Papazoglou, M. Scheel, J. Braun, I. Sack, Towards an elastographic atlas of brain anatomy, PLoS. One 8 (8) (2013) e71807, https://doi.org/10.1371/journal.pone.0071807.
[258] L.V. Hiscox, C.L. Johnson, M.D.J. McGarry, M. Perrins, A. Littlejohn, E.J.R. van Beek, N. Roberts, J.M. Starr, High-resolution magnetic resonance elastography reveals differences in subcortical gray matter viscoelasticity between young and healthy older adults, Neurobiol. Aging 65 (2018) 158–167, https://doi.org/10.1016/j.neurobiolaging.2018.01.010.
[259] F. Schrank, C. Warmuth, H. Tzschätzsch, B. Kreft, S. Hirsch, J. Braun, T. Elgeti, I. Sack, Cardiac-gated steady-state multifrequency magnetic resonance elastography of the brain: effect of cerebral arterial pulsation on brain viscoelasticity, J. Cereb. Blood Flow Metab. 40 (5) (2020) 991–1001, https://doi.org/10.1177/0271678x19850936.
[260] L.V. Hiscox, M.D.J. McGarry, H. Schwarb, E.E.W. Van Houten, R.T. Pohlig, N. Roberts, G.R. Huesmann, A.Z. Burzynska, B.P. Sutton, C.H. Hillman, A. F. Kramer, N.J. Cohen, A.K. Barbey, K.D. Paulsen, C.L. Johnson, Standard-space atlas of the viscoelastic properties of the human brain, Hum. Brain Mapp. 41 (18) (2020) 5282–5300, https://doi.org/10.1002/hbm.25192.
[261] T. Takamura, U. Motosugi, Y. Sasaki, T. Kakegawa, K. Sato, K.J. Glaser, R. L. Ehman, H. Onishi, Influence of age on global and regional brain stiffness in young and middle-aged adults, J. Magn. Reson. Imaging 51 (3) (2020) 727–733, https://doi.org/10.1002/jmri.26881.
[262] K.A. Hamilton, V. Santhakumar, Current ex vivo and *in vitro* approaches to uncovering mechanisms of neurological dysfunction after traumatic brain injury, Curr. Opin. Biomed. Eng. 14 (2020) 18–24, https://doi.org/10.1016/j.cobme.2020.05.001.
[263] A. Gefen, S.S. Margulies, Are *in vivo* and *in situ* brain tissues mechanically similar? J. Biomech. 37 (9) (2004) 1339–1352, https://doi.org/10.1016/j.jbiomech.2003.12.032.
[264] C.A. Urbanczyk, M.L. Palmeri, C.R. Bass, Material characterization of *in Vivo* and *in Vitro* porcine brain using shear wave elasticity, Ultrasound. Med. Biol. 41 (3) (2015) 713–723, https://doi.org/10.1016/j.ultrasmedbio.2014.10.019.
[265] M.E. Wagshul, P.K. Eide, J.R. Madsen, The pulsating brain: a review of experimental and clinical studies of intracranial pulsatility, Fluids. Barriers. CNS. 8 (1) (2011) 5, https://doi.org/10.1186/2045-8118-8-5.
[266] S. Hirsch, D. Klatt, F. Freimann, M. Scheel, J. Braun, I. Sack, *In vivo* measurement of volumetric strain in the human brain induced by arterial pulsation and harmonic waves, Magn. Reson. Med. 70 (3) (2013) 671–683, https://doi.org/10.1002/mrm.24499.
[267] T. Meyer, B. Kreft, J. Bergs, E. Antes, M.S. Anders, B. Wellge, J. Braun, M. Doyley, H. Tzschätzsch, I. Sack, Stiffness pulsation of the human brain detected by non-invasive time-harmonic elastography, Front. Bioeng. Biotechnol. 11 (2023), https://doi.org/10.3389/fbioe.2023.1140734. Volume2023.
[268] M. Darayi, M.E. Hoffman, J. Sayut, S. Wang, N. Demirci, J. Consolini, M. A. Holland, Computational models of cortical folding: a review of common approaches, J. Biomech. 139 (2022) 110851, https://doi.org/10.1016/j.jbiomech.2021.110851.
[269] G.R. Joldes, A. Wittek, K. Miller, Suite of finite element algorithms for accurate computation of soft tissue deformation for surgical simulation, Med. Image Anal. 13 (6) (2009) 912–919, https://doi.org/10.1016/j.media.2008.12.001.
[270] S.P. Lacour, G. Courtine, J. Guck, Materials and technologies for soft implantable neuroprostheses, Nat. Rev. Mater. 1 (10) (2016) 16063, https://doi.org/10.1038/natrevmats.2016.63.
[271] H. Bustin, T. Meyer, R. Reiter, J. Jordan, L. Walczak, H. Tzschätzsch, I. Sack, A. Hennemuth, ElastoNet: neural network-based multicomponent MR elastography wave inversion with uncertainty quantification, Med. Image Anal. 105 (2025) 103642, https://doi.org/10.1016/j.media.2025.103642.
[272] K. Zou, Z. Chen, X. Yuan, X. Shen, M. Wang, H. Fu, A review of uncertainty estimation and its application in medical imaging, Meta-Radiol. 1 (1) (2023) 100003, https://doi.org/10.1016/j.metrad.2023.100003.
[273] C. Zhang, L. Qian, H. Zhao, Elucidation of regional mechanical properties of brain tissues based on cell density, J. Bionic. Eng. 18 (3) (2021) 611–622, https://doi.org/10.1007/s42235-021-0047-6.
[274] P. Chavoshnejad, G.K. German, M.J. Razavi, Hyperelastic material properties of axonal fibers in brain white matter, Brain Multiphys. 2 (2021) 100035, https://doi.org/10.1016/j.brain.2021.100035.
[275] J.S. Giudice, A. Alshareef, T. Wu, A.K. Knutsen, L.V. Hiscox, C.L. Johnson, M. B. Panzer, Calibration of a heterogeneous brain model using a subject-specific inverse finite element approach, Front. Bioeng. Biotechnol. 9 (2021), https://doi.org/10.3389/fbioe.2021.664268. Volume2021.
[276] M. Flaschel, S. Kumar, L. De Lorenzis, Automated discovery of generalized standard material models with EUCLID, Comput. Methods Appl. Mech. Eng. 405 (2023) 115867, https://doi.org/10.1016/j.cma.2022.115867.
[277] S.R.S. Pierre, K. Linka, E. Kuhl, Principal-stretch-based constitutive neural networks autonomously discover a subclass of Ogden models for human brain tissue, Brain Multiphys. 4 (2023) 100066, https://doi.org/10.1016/j.brain.2023.100066.
[278] J. Hinrichsen, L. Feiler, N. Reiter, L. Bräuer, M. Schicht, F. Paulsen, S. Budday, Identifying composition-mechanics relations in human brain tissue based on neural-network-enhanced inverse parameter identification, Math. Mech. Solids. 29 (6) (2024) 1271–1292, https://doi.org/10.1177/10812865231206544.